CALIFORNIA INSTITUTE OF TECHNOLOGY

DYNAMICS LABORATORY

# DYNAMICS OF THIN-WALLED BEAMS OF OPEN SECTION

by

Wai Keung Tso

JUNE 1964

# DYNAMICS OF THIN-WALLED BEAMS OF OPEN SECTION

Thesis by

Wai Keung Tso

In Partial Fulfillment of the Requirements

For the Degree of

Doctor of Philosophy

California Institute of Technology

Pasadena, California

1964

# ACKNOWLEDGMENTS

The author wishes to thank Professor G. W. Housner for his patient guidance and assistance in the course of research and preparation of the thesis. Also, he wishes to thank Professor T. K. Caughey for his interest in the problem and his help on various portions of the thesis.

The author would like to acknowledge his appreciation of the fellowships from the U. S. Steel Foundation for the years 1961-1963, the many summer fellowships from the Woodrow Wilson Foundation, the tuition scholarships and graduate teaching assistantships from the California Institute of Technology, and the use of the vibrations laboratory established by a National Science Foundation grant to the Division of Engineering.

# ABSTRACT

A study of the coupled torsional and bending vibrations of thin-walled beams of asymmetric open section is made. The formal solution to Gere's theory for the case of a monosymmetric section under general loading conditions and boundary conditions is presented.

A higher order theory including the effect of shear strain induced by bending and warping of the beam is derived. Spectrum curves of the higher order theory are compared with those from the elementary theory for various boundary conditions for a special family of monosymmetric sections. A study is made to assess the effect of the shape of the cross section of the beam to the differences of the spectrum curves from the two theories. An experiment is performed on two specimens to determine their natural frequencies at different beam lengths and the experimental results are compared to those predicted from the two theories. It is concluded that when the beam is long, the elementary theory is adequate to predict the natural frequencies for torsion predominant modes, but is inadequate for bending predominant modes. For bending predominant modes, the higher order theory should be used. The higher order theory also serves as a guide for the range of validity of the elementary theory.

Certain nonlinear behavior of the beam is observed in the experiment. When the beam is excited at resonance at a higher mode, under special circumstances, there is a tendency for the beam to shift from the higher resonant mode to vibrate at its fundamental mode, resulting in a high order subharmonic oscillation. An analysis

is made to show the possibility of such behavior if the inherently nonlinear governing equations for coupled torsional and bending vibrations are used.

TABLE OF CONTENTS

# Chapter 1

# INTRODUCTION

For intricate structures such as spacecraft, beams of standard cross sections may not be the most efficient or convenient structural members to use. Thin-walled beams of open section are frequently employed for their structural efficiency. With the improvement of extrusion methods in metal forming, beams of different shapes of cross sections can be formed to order. Occasions often arise when nonsymmetrical cross sections are more convenient to use. However, it has long been known that a beam with nonsymmetrical cross section under loads will, in general, not only deflect but will twist also. Only under special loading along the flexure axis, a line joining the shear centers, will the beam deflect without twist. The concept of shear center is well known and is discussed in textbooks. Essentially, it is the point through which the resultant of the shear forces of the cross section passes. If the loading does not pass through the shear center, a torque is generated by the loading and the resultant of the reactions from the section. Such a torque will cause the twisting of the beam. Abundant literature exists on the subject of thin-walled beams and a fairly comprehensive list of references can be found in a survey paper by Nowinski[1].

When a thin-walled beam is subjected to dynamic excitation, the inertial loading due to the acceleration of the beam itself has to be taken into account. The resultant of such loading may be considered to pass through the centroid of the section. Unless the shear center of the section coincides with its centroid, both bending and

torsional vibrations will result. Due to the low torsional rigidity of thin-walled open sections, the problem of coupled bending and torsional vibrations is of particular interest. The coupling of bending and torsional vibrations can be shown by using d'Alembert's principle and substituting the inertial forces into the equations of equilibrium[2]. The equations for bending in the X and Y directions (principal directions of the section) and for nonuniform torsion along the Z direction of a beam for static loadings are

$$EI_{xx}\xi'''' = p_x \tag{I.1}$$

$$EI_{yy}\eta'''' = p_y \tag{I.2}$$

$$EI_{\omega\omega}\theta'''' - GI_d\theta'' = p_t \tag{I.3}$$

where $\xi, \eta$ are the displacements of the shear center C along the X, Y directions, and $\theta$ is the rotation of the section about C. The origin of the axes coincides with the centroid of the section and the shear center C has coordinates $a_x, a_y$ as shown in Figure 1. $p_x$, $p_y$ and $p_t$ are static loadings in the X, Y directions and the torque along Z direction. $I_{xx}$ is the moment of inertia about the Y axis and $I_{yy}$ is the moment of inertia about the X axis. $I_{\omega\omega}$ and $I_d$ are the warping constant and the torsion constant as defined in chapter 3, equation (III. 22).

For small rotations, the inertia forces of translation in the X and Y directions are $p_x = -\rho A\frac{\partial^2}{\partial t^2}(\xi + a_y\theta)$ and $p_y = -\rho A\frac{\partial^2}{\partial t^2}(\eta - a_x\theta)$, respectively, acting through the centroid O.

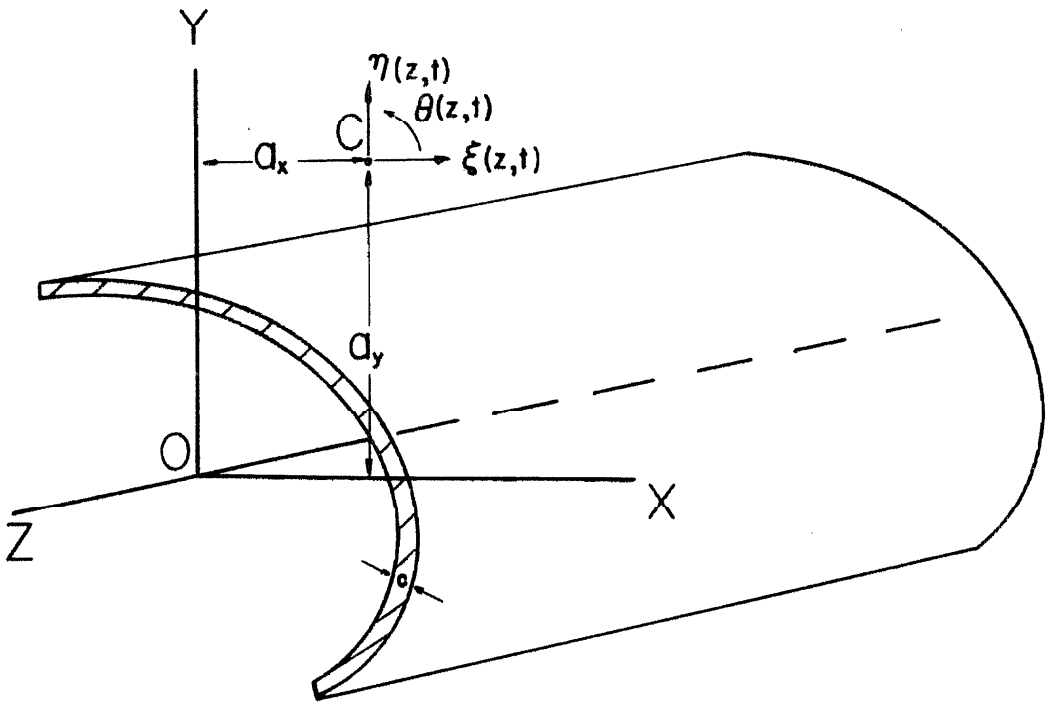


FIG. 1 THIN-WALLED BEAM OF ASYMMETRIC OPEN SECTION

Referring back to the shear center C, the inertial torque is $p_t = -\rho I_g \frac{\partial^2\theta}{\partial t^2} - \rho A a_y \frac{\partial^2}{\partial t^2}(\xi + a_y\theta) + \rho A a_x \frac{\partial^2}{\partial t^2}(\eta - a_x\theta)$ where $I_g$ is the polar moment of inertia about the centroid O. Substituting the expressions for $p_x$, $p_y$ and $p_t$ into equations (I.1), (I.2) and (I.3), there is obtained

$$EI_{xx}\xi'''' + \rho A\ddot{\xi} + \rho A a_y\ddot{\theta} = 0 \qquad (I.4)$$

$$EI_{yy}\eta'''' + \rho A\ddot{\eta} - \rho A a_x\ddot{\theta} = 0 \qquad (I.5)$$

$$EI_{\omega\omega}\theta'''' - GI_d\theta'' + \rho I_p\ddot{\theta} + \rho A a_y\ddot{\xi} - \rho A a_x\ddot{\eta} = 0 \qquad (I.6)$$

where $I_p$ is the polar moment of inertia about the shear center C and $\dot{\xi} \equiv \frac{\partial\xi}{\partial t}$, $\xi' \equiv \frac{\partial\xi}{\partial z}$, etc. Equations (I.4), (I.5) and (I.6) were derived by Gere[3]. It is seen that the bending and torsional equations are dynamically coupled.

A similar set of equations were obtained by Vlasov[4],

$$EI_{xx}\xi'''' - \rho I_{xx}\ddot{\xi}'' + \rho A\ddot{\xi} + \rho A a_y\ddot{\theta} = 0 \qquad (I.7)$$

$$EI_{yy}\eta'''' - \rho I_{yy}\ddot{\eta}'' + \rho A\ddot{\eta} - \rho A a_x\ddot{\theta} = 0 \qquad (I.8)$$

$$EI_{\omega\omega}\theta'''' - \rho I_{\omega\omega}\ddot{\theta}'' - GI_d\theta'' + \rho I_p\ddot{\theta} + \rho A a_y\ddot{\xi} - \rho A a_x\ddot{\eta} = 0 \qquad (I.9)$$

The difference between Vlasov's equations and Gere's equations is the inclusion of the axial inertia terms $\rho I_{xx}\ddot{\xi}''$, $\rho I_{yy}\ddot{\eta}''$ and $\rho I_{\omega\omega}\ddot{\theta}''$.

It is interesting to note that for a section having two axes of symmetry, the shear center coincides with the centroid of the section and $a_x = a_y = 0$. In this case, the equations (I.4), (I.5) and (I.6) are

uncoupled. The bending equations of (I. 4) and (I. 5) reduce to Euler-Bernoulli equations for bending and the equations (I. 7) and (I. 8) reduce to Rayleigh's equations for bending. Studies in the theory of bending show that under most circumstances, the axial inertia effect is indeed negligible. Hence, for further comparison, Gere's equations are taken as the basic elementary theory for coupled vibrations of thin-walled elastic beams.

The present study is an extension of the elementary theory for coupled vibrations of thin-walled open sections. In chapter 2, a formal solution to Gere's theory is given under general loading conditions and general boundary conditions. The range of validity of the elementary theory is sought next and this is done both theoretically and experimentally. A higher order theory including the shear strain effect induced by bending and warping is constructed in chapter 3. Spectrum curves of the elementary theory and the higher order theory are compared under various boundary conditions in chapter 4. In chapter 5, a study is made of the influence of the various sectional parameters on the mode shapes and frequencies of the coupled vibrations. Experimental verification on two test specimens is given in chapter 6. An analysis of some possible nonlinear behavior of the beam together with experimental observations is given in chapter 7.

It is hoped that this study will provide a guide to engineers and designers on the range of validity of the elementary theory of coupled bending and torsional vibrations of beams of thin-walled open sections.

It will enable them to make better predictions of the dynamic behavior and points out the existence of possible dangerous subharmonic oscillations of such beams.

# Chapter 2

# FORMAL SOLUTION TO GERE'S THEORY OF COUPLED VIBRATIONS

## 1. Introduction

In this chapter, a formal solution to Gere's theory of coupled bending and torsional vibrations is presented. Only beams with a monosymmetric cross section are considered. The shear center lies on the axis of symmetry and if the axis of symmetry of the section is taken to be the Y axis, then $a_x = 0$. According to Gere's theory, only one displacement coordinate $\xi(z, t)$ is coupled with the rotation coordinate $\theta(z, t)$; while the other displacement coordinate $\eta(z, t)$ is uncoupled. Thus, it is only necessary to consider the interaction of equations (I. 4) and (I. 6). The choice of this special case retains all the essential features of the coupled bending and torsional mechanisms and the analysis can be extended to the general case without much effort. In this analysis, the two coupled equations in $\xi$ and $\theta$ are treated as one single matrix equation. In this matrix formulation, each mode is represented by a vector function. A vector function is a vector in which each individual element is a function of some independent variable. The idea of a mode being represented by a vector function is a logical extension of the idea of a mode being represented by a function in the case of a continuous system described by one dependent variable; or the idea of a mode being represented by a vector in the case of a discrete system of N degrees of freedom. An orthogonal relationship is derived for the non-degenerate mode in section 2. With this relationship, the response of the beam under any

general loading with homogeneous boundary conditions is solved in section 3. For nonhomogeneous boundary conditions, the technique of Mindlin and Goodman[5] can be used. This technique divides the solution of the problem into two parts. The first part of the solution is constructed so that it satisfies the nonhomogeneous boundary conditions; but does not necessarily satisfy the differential equation. The second part of the solution satisfies the homogeneous boundary conditions. It is so determined that the sum of the two parts will satisfy both the differential equation and the nonhomogeneous boundary conditions. An example is worked out in section 4 to illustrate this procedure. Hence, the formal solution of Gere's theory is obtained for general loadings and general boundary conditions.

## 2. Orthogonality Relationship of Non-degenerate Modes

From Gere's theory, the pair of coupled homogeneous equations to be considered are

$$EI_{xx}\xi'''' + \rho A\ddot{\xi} + \rho Aa_y\ddot{\theta} = 0 \tag{II.1}$$

$$\rho Aa_y\ddot{\xi} + EI_{\omega\omega}\theta'''' - GI_d\theta'' + \rho I_p\ddot{\theta} = 0 \tag{II.2}$$

with homogeneous boundary conditions. The homogeneous boundary conditions encountered in common practice are fixed ends, pinned ends, and free ends. By fixed end, it is meant that there is no displacement, no slope, no rotation and complete restraint of warping at the end. By pinned end, it is meant that there is no displacement, no bending moment, no rotation and no restraint of warping. By

free end, it is meant that there is no bending moment, no shear force, no restraint of warping and no torque. Mathematically, such boundary conditions can be expressed as follows:

$$\text{Fixed end:} \quad \xi = 0; \quad \xi' = 0; \quad \theta = 0; \quad \theta' = 0$$

$$\text{Pinned end:} \quad \xi = 0; \quad \xi'' = 0; \quad \theta = 0; \quad \theta'' = 0 \qquad \text{(II. 3)}$$

$$\text{Free end:} \quad \xi'' = 0; \quad \xi''' = 0; \quad \theta'' = 0; \quad \theta''' - \frac{G}{E}\frac{I_d}{I_{\omega\omega}}\theta' = 0$$

To reduce the equations to nondimensional form, the radius of gyration $r$ is taken as the characteristic length. Let

$$r = (I_{xx}/A)^{1/2}; \quad z = r\bar{z}; \quad \xi = r\bar{\xi}; \quad a_y = r\bar{a}_y;$$

$$\bar{I}_d = c^2/(3r^2); \quad I_p = Ar^2\bar{I}_p; \quad \text{and} \quad I_{\omega\omega} = Ar^4\bar{I}_{\omega\omega}$$

Equations (II. 1) and (II. 2) can be written as one matrix equation with various nondimensional parameters.

$$\rho \begin{bmatrix} 1 & \bar{a}_y \\ \bar{a}_y & \bar{I}_p \end{bmatrix} \begin{Bmatrix} \ddot{\bar{\xi}} \\ \ddot{\theta} \end{Bmatrix} + \begin{bmatrix} \frac{E}{r^2} D_4 & 0 \\ 0 & \frac{E}{r^2}\bar{I}_{\omega\omega} D_4 - \frac{G}{r^2}\bar{I}_d D_2 \end{bmatrix} \begin{Bmatrix} \bar{\xi} \\ \theta \end{Bmatrix} = \begin{Bmatrix} 0 \\ 0 \end{Bmatrix} \qquad \text{(II. 4)}$$

where $D_4 = \partial^4/\partial\bar{z}^4$ ; $D_2 = \partial^2/\partial\bar{z}^2$. For sinusoidal vibrations, the form of the solution is taken to be

$$\begin{Bmatrix} \bar{\xi}(\bar{z}, t) \\ \theta(\bar{z}, t) \end{Bmatrix} = \sin \lambda_n t \begin{Bmatrix} \Xi_n(\bar{z}) \\ \Theta_n(\bar{z}) \end{Bmatrix} \qquad \text{(II. 5)}$$

Substituting (II. 5) into (II. 4), there is obtained

$$-\lambda_n^2\rho\begin{bmatrix}1 & \bar{a}_y\\ \bar{a}_y & \bar{I}_p\end{bmatrix}\begin{Bmatrix}\Xi_n\\ \Theta_n\end{Bmatrix}+\begin{bmatrix}\frac{E}{r^2}D_4 & 0\\ 0 & \frac{E}{r^2}\bar{I}_{\omega\omega}D_4-\frac{G}{r^2}\bar{I}_dD_2\end{bmatrix}\begin{Bmatrix}\Xi_n\\ \Theta_n\end{Bmatrix}=\begin{Bmatrix}0\\ 0\end{Bmatrix} \tag{II. 6}$$

Premultiplying (II. 6) by $\begin{Bmatrix}\Xi_m\\ \Theta_m\end{Bmatrix}^T$, the transpose of $\begin{Bmatrix}\Xi_m\\ \Theta_m\end{Bmatrix}$, and integrating along the beam from zero to $\ell/r$, (II. 6) becomes

$$\int_0^{\ell/r}\left\{\Xi_m,\Theta_m\right\}\begin{bmatrix}\frac{E}{r^2}D_4 & 0\\ 0 & \frac{E}{r^2}\bar{I}_{\omega\omega}D_4-\frac{G}{r^2}\bar{I}_dD_2\end{bmatrix}\begin{Bmatrix}\Xi_n\\ \Theta_n\end{Bmatrix}d\bar{z}$$

$$=\rho\lambda_n^2\int_0^{\ell/r}\left\{\Xi_m,\Theta_m\right\}\begin{bmatrix}1 & \bar{a}_y\\ \bar{a}_y & \bar{I}_p\end{bmatrix}\begin{Bmatrix}\Xi_n\\ \Theta_n\end{Bmatrix}d\bar{z} \tag{II. 7}$$

Interchanging the indices m and n in equation (II. 7), there is obtained:

$$\int_0^{\ell/r}\left\{\Xi_n,\Theta_n\right\}\begin{bmatrix}\frac{E}{r^2}D_4 & 0\\ 0 & \frac{E}{r^2}\bar{I}_{\omega\omega}D_4-\frac{G}{r^2}\bar{I}_dD_2\end{bmatrix}\begin{Bmatrix}\Xi_m\\ \Theta_m\end{Bmatrix}d\bar{z}$$

$$=\rho\lambda_m^2\int_0^{\ell/r}\left\{\Xi_n,\Theta_n\right\}\begin{bmatrix}1 & \bar{a}_y\\ \bar{a}_y & \bar{I}_p\end{bmatrix}\begin{Bmatrix}\Xi_m\\ \Theta_m\end{Bmatrix}d\bar{z} \tag{II. 8}$$

Subtracting (II. 8) from (II. 7), the following equation is obtained:

$$\int_0^{\ell/r} \left\{\Xi_m, \Theta_m\right\} \begin{bmatrix} \frac{E}{r^2} D_4 & 0 \\ 0 & \frac{E}{r^2}\bar{I}_{\omega\omega} D_4 - \frac{G}{r^2}\bar{I}_d D_2 \end{bmatrix} \begin{Bmatrix} \Xi_n \\ \Theta_n \end{Bmatrix} d\bar{z}$$

$$- \int_0^{\ell/r} \left\{\Xi_n, \Theta_n\right\} \begin{bmatrix} \frac{E}{r^2} D_4 & 0 \\ 0 & \frac{E}{r^2}\bar{I}_{\omega\omega} D_4 - \frac{G}{r^2}\bar{I}_d D_2 \end{bmatrix} \begin{Bmatrix} \Xi_m \\ \Theta_m \end{Bmatrix} d\bar{z}$$

$$= \rho(\lambda_n^2 - \lambda_m^2) \int_0^{\ell/r} \left\{\Xi_n, \Theta_n\right\} \begin{bmatrix} 1 & \bar{a}_y \\ \bar{a}_y & \bar{I}_p \end{bmatrix} \begin{Bmatrix} \Xi_m \\ \Theta_m \end{Bmatrix} d\bar{z} \quad \text{(II. 9)}$$

Noting that both $D_4$ and $D_2$ are self-adjoint operators, the first integral on the left-hand side of equation (II. 9) can be integrated by parts to reduce the left-hand side to the following expression:

$$\text{L. H. S.} = \frac{E}{r^2}\left(\Xi_m \frac{d^3\Xi_n}{d\bar{z}^3} - \frac{d^3\Xi_m}{d\bar{z}^3}\Xi_n - \frac{d\Xi_m}{d\bar{z}}\frac{d^2\Xi_n}{d\bar{z}^2} + \frac{d^2\Xi_m}{d\bar{z}^2}\frac{d\Xi_n}{d\bar{z}}\right)\Bigg|_0^{\ell/r}$$

$$+ \frac{E}{r^2}\bar{I}_{\omega\omega}\left(\frac{d^2\Theta_m}{d\bar{z}^2}\frac{d\Theta_n}{d\bar{z}} - \frac{d^2\Theta_n}{d\bar{z}^2}\frac{d\Theta_m}{d\bar{z}}\right)\Bigg|_0^{\ell/r}$$

$$+ \left[\left(\frac{E}{r^2}\bar{I}_{\omega\omega}\frac{d^3\Theta_n}{d\bar{z}^3} - \frac{G}{r^2}\bar{I}_d\frac{d\Theta_n}{d\bar{z}}\right)\Theta_m\right]\Bigg|_0^{\ell/r}$$

$$- \left[\left(\frac{E}{r^2}\bar{I}_{\omega\omega}\frac{d^3\Theta_m}{d\bar{z}^3} - \frac{G}{r^2}\bar{I}_d\frac{d\Theta_m}{d\bar{z}}\right)\Theta_n\right]\Bigg|_0^{\ell/r} \quad \text{(II. 10)}$$

For the homogeneous boundary conditions as shown in (II. 3) the expression (II. 10) is zero. Equation (II. 9) becomes

$$\rho(\lambda_n^2 - \lambda_m^2)\int_0^{\ell/r}\left\{\Xi_m, \Theta_m\right\}\begin{bmatrix} 1 & \bar{a}_y \\ \bar{a}_y & \bar{I}_p \end{bmatrix}\begin{Bmatrix}\Xi_n \\ \Theta_n\end{Bmatrix} d\bar{z} = 0$$

For non-degenerate modes, $\lambda_n^2 \neq \lambda_m^2$ for $m \neq n$. Therefore,

$$\int_0^{\ell/r}\left\{\Xi_m, \Theta_m\right\}\begin{bmatrix} 1 & \bar{a}_y \\ \bar{a}_y & \bar{I}_p \end{bmatrix}\begin{Bmatrix}\Xi_n \\ \Theta_n\end{Bmatrix} d\bar{z} = 0 \quad m \neq n \qquad \text{(II.11)}$$

The vector function can be normalized such that

$$\int_0^{\ell/r}\left\{\Xi_m, \Theta_m\right\}\begin{bmatrix} 1 & \bar{a}_y \\ \bar{a}_y & \bar{I}_p \end{bmatrix}\begin{Bmatrix}\Xi_m \\ \Theta_m\end{Bmatrix} d\bar{z} = 1$$

Assuming the vector function is normalized, the orthogonality relationship is given by

$$\int_0^{\ell/r}\left\{\Xi_m, \Theta_m\right\}\begin{bmatrix} 1 & \bar{a}_y \\ \bar{a}_y & \bar{I}_p \end{bmatrix}\begin{Bmatrix}\Xi_n \\ \Theta_n\end{Bmatrix} d\bar{z} = \delta_{mn} \qquad \text{(II.12)}$$

where $\delta_{mn}$ is the Kronecker delta. Noting the relationship $\bar{I}_p = \bar{I}_g + \bar{a}_y^2$, equation (II.12) can be written as

$$\int_0^{\ell/r}\left[(\Xi_m + \bar{a}_y\Theta_m)(\Xi_n + \bar{a}_y\Theta_n) + \bar{I}_g\Theta_m\Theta_n\right] d\bar{z} = \delta_{mn} \qquad \text{(II.13)}$$

It is interesting to note that $(\Xi_n + \bar{a}_y\Theta_n)$ is precisely the displacement of the centroid of the section for the $n^{th}$ mode. Thus, if new coordinates are chosen such that the behavior of the beam is specified by the displacements of its centroidal axis $\Xi_g(\bar{z})$, and the rotation of

the sections about the shear center $\Theta(\bar{z})$, the orthogonality relationship will have similar form as in the Timoshenko beam theory[6], namely,

$$\int_0^{\ell/r} \left[ (\Xi_g)_m (\Xi_g)_n + \bar{I}_g \Theta_m \Theta_n \right] d\bar{z} = \delta_{mn}$$

3. Formal Solution for General Loadings with Homogeneous Boundary Conditions

The case of a general loading $\begin{Bmatrix} p(\bar{z}, t) \\ q(\bar{z}, t) \end{Bmatrix}$ on the system is considered next. From (II. 4), there is obtained

$$\rho \begin{bmatrix} 1 & \bar{a}_y \\ \bar{a}_y & \bar{I}_p \end{bmatrix} \begin{Bmatrix} \ddot{\bar{\xi}} \\ \ddot{\theta} \end{Bmatrix} + \begin{bmatrix} \frac{E}{r^2} D_4 & 0 \\ 0 & \frac{E}{r^2} \bar{I}_{\omega\omega} D_4 - \frac{G}{r^2} \bar{I}_d D_2 \end{bmatrix} \begin{Bmatrix} \bar{\xi} \\ \theta \end{Bmatrix}$$

$$= \begin{Bmatrix} p(\bar{z}, t) \\ q(\bar{z}, t) \end{Bmatrix} \qquad \text{(II. 14)}$$

Assume the solution takes a form

$$\begin{Bmatrix} \bar{\xi} \\ \theta \end{Bmatrix} = \sum_{n=1}^{\infty} T_n(t) \begin{Bmatrix} \Xi_n(\bar{z}) \\ \Theta_n(\bar{z}) \end{Bmatrix} \qquad \text{(II. 15)}$$

Substituting (II. 15) into (II. 14) and making use of (II. 6), there is obtained

$$\sum_{n=1}^{\infty} \begin{bmatrix} 1 & \bar{a}_y \\ \bar{a}_y & \bar{I}_p \end{bmatrix} \begin{Bmatrix} \Xi_n \\ \Theta_n \end{Bmatrix} \ddot{T}_n(t) + \sum_{n=1}^{\infty} \rho \lambda_n^2 \begin{bmatrix} 1 & \bar{a}_y \\ \bar{a}_y & \bar{I}_p \end{bmatrix} \begin{Bmatrix} \Xi_n \\ \Theta_n \end{Bmatrix} T_n(t) = \begin{Bmatrix} p \\ q \end{Bmatrix}$$

(II. 16)

Premultiplying (II.16) by $\begin{Bmatrix} \Xi_m \\ \Theta_m \end{Bmatrix}^T$, integrating along the beam from zero to $\ell/r$, and using the orthogonal relationship (II.12), equation (II.16) becomes

$$\ddot{T}_m(t) + \lambda_m^2 T_m(t) = \int_0^{\ell/r} \left\{ \Xi_m, \Theta_m \right\} \begin{Bmatrix} p(\bar{z}, t) \\ q(\bar{z}, t) \end{Bmatrix} d\bar{z} = Q_m(t) \tag{II.17}$$

where $m = 1, 2, 3, \ldots$ . Solving, there is obtained

$$T_m(t) = A_m \cos \lambda_m t + B_m \sin \lambda_m t + \frac{1}{\lambda_m} \int_0^t Q_m(\tau) \sin \lambda_m (t-\tau)\, d\tau \tag{II.18}$$

where $A_m$ and $B_m$ are arbitrary constants determined from the initial conditions. Let the initial conditions be:

$$\begin{Bmatrix} \bar{\xi}(0, \bar{z}) \\ \theta(0, \bar{z}) \end{Bmatrix} = \begin{Bmatrix} \bar{\xi}_o(\bar{z}) \\ \theta_o(\bar{z}) \end{Bmatrix} = \sum_{n=1}^{\infty} R_n \begin{Bmatrix} \Xi_n \\ \Theta_n \end{Bmatrix}$$

$$\begin{Bmatrix} \dot{\bar{\xi}}(0, \bar{z}) \\ \dot{\theta}(0, \bar{z}) \end{Bmatrix} = \begin{Bmatrix} \bar{\xi}_1(\bar{z}) \\ \theta_1(\bar{z}) \end{Bmatrix} = \sum_{n=1}^{\infty} S_n \begin{Bmatrix} \Xi_n \\ \Theta_n \end{Bmatrix} \tag{II.19}$$

The coefficients $R_n$ and $S_n$ can be determined by using the orthogonal relationship and are defined by

$$R_m = \int_0^{\ell/r} \begin{Bmatrix} \Xi_m \\ \Theta_m \end{Bmatrix}^T \begin{bmatrix} 1 & \bar{a}_y \\ \bar{a}_y & \bar{I}_p \end{bmatrix} \begin{Bmatrix} \bar{\xi}_o \\ \theta_o \end{Bmatrix} d\bar{z}$$

$$S_m = \int_0^{\ell/r} \begin{Bmatrix} \Xi_m \\ \Theta_m \end{Bmatrix}^T \begin{bmatrix} 1 & \bar{a}_y \\ \bar{a}_y & \bar{I}_p \end{bmatrix} \begin{Bmatrix} \bar{\xi}_1 \\ \theta_1 \end{Bmatrix} d\bar{z} \tag{II.20}$$

Using (II.15) and (II.19), equation (II.18) can be written as

$$T_m(t) = R_m \cos \lambda_m t + \frac{S_m}{\lambda_m} \sin \lambda_m t + \frac{1}{\lambda_m} \int_0^t Q_m(\tau) \sin \lambda_m (t - \tau)\, d\tau \qquad \text{(II.21)}$$

Equations (II.15), (II.20) and (II.21) give the formal solution for the case of arbitrary loading on the beam.

4. Solution for Nonhomogeneous Boundary Conditions

When the constraints at the supports of the beam are time dependent, the boundary conditions of the problem are nonhomogeneous. In this case, the solution is considered to be composed of two parts: the first part of the solution is constructed so that it satisfies the time dependent boundary conditions, but not the differential equation. The second part of the solution is required to satisfy the homogeneous boundary conditions, and also a modified nonhomogeneous differential equation. To illustrate the technique, the case of a beam fixed at one end and pinned at the other end with the end constraints being time dependent is considered. Without external loading along the beam, the differential equation is

$$\rho \begin{bmatrix} 1 & \bar{a}_y \\ \bar{a}_y & \bar{I}_p \end{bmatrix} \begin{Bmatrix} \ddot{\bar{\xi}} \\ \ddot{\theta} \end{Bmatrix} + \begin{bmatrix} \frac{E}{r^2} D_4 & 0 \\ 0 & \frac{E}{r^2} \bar{I}_{\omega\omega} D_4 - \frac{G}{r^2} \bar{I}_d D_2 \end{bmatrix} \begin{Bmatrix} \bar{\xi} \\ \theta \end{Bmatrix} = \begin{Bmatrix} 0 \\ 0 \end{Bmatrix} \qquad \text{(II.22)}$$

The time dependent boundary conditions are taken to be

$$\begin{Bmatrix} \bar{\xi}(0,t) \\ \theta(0,t) \end{Bmatrix} = \begin{Bmatrix} f_1(t) \\ F_1(t) \end{Bmatrix} \quad ; \quad D_1 \begin{Bmatrix} \bar{\xi}(0,t) \\ \theta(0,t) \end{Bmatrix} = \begin{Bmatrix} f_2(t) \\ F_2(t) \end{Bmatrix}$$

$$\begin{Bmatrix} \bar{\xi}(\frac{\ell}{r},t) \\ \theta(\frac{\ell}{r},t) \end{Bmatrix} = \begin{Bmatrix} f_3(t) \\ F_3(t) \end{Bmatrix} \quad ; \quad D_2 \begin{Bmatrix} \bar{\xi}(\frac{\ell}{r},t) \\ \theta(\frac{\ell}{r},t) \end{Bmatrix} = \begin{Bmatrix} f_4(t) \\ F_4(t) \end{Bmatrix} \qquad \text{(II. 23)}$$

where $D_1$ and $D_2$ are spatial operators defined by $D_1 = \partial/\partial\bar{z}$; $D_2 = \partial^2/\partial\bar{z}^2$; and $f_i(t)$, $F_i(t)$, $i = 1, 2, 3, 4$, are given functions of time. Consider the solution consists of two parts:

$$\begin{Bmatrix} \bar{\xi} \\ \theta \end{Bmatrix} = \begin{Bmatrix} \bar{\xi} \\ \theta \end{Bmatrix}_I + \begin{Bmatrix} \bar{\xi} \\ \theta \end{Bmatrix}_{II} \qquad \text{(II. 24)}$$

and let

$$\begin{Bmatrix} \bar{\xi} \\ \theta \end{Bmatrix}_I = \sum_{i=1}^{4} \begin{bmatrix} g_i(\bar{z}) & 0 \\ 0 & G_i(\bar{z}) \end{bmatrix} \begin{Bmatrix} f_i(t) \\ F_i(t) \end{Bmatrix} \qquad \text{(II. 25)}$$

$\begin{Bmatrix} \bar{\xi} \\ \theta \end{Bmatrix}_I$ is so constructed as to satisfy the nonhomogeneous boundary conditions. Substituting equation (II. 25) into the boundary conditions of (II. 23) and arranging the result in matrix form, there is obtained

$$
\begin{bmatrix}
g_1(0) & 0 & g_2(0) & 0 & g_3(0) & 0 & g_4(0) & 0 \\
0 & G_1(0) & 0 & G_2(0) & 0 & G_3(0) & 0 & G_4(0) \\
D_1g_1(0) & 0 & D_1g_2(0) & 0 & D_1g_3(0) & 0 & D_1g_4(0) & 0 \\
0 & D_1G_1(0) & 0 & D_1G_2(0) & 0 & D_1G_3(0) & 0 & D_1G_4(0) \\
g_1(\frac{\ell}{r}) & 0 & g_2(\frac{\ell}{r}) & 0 & g_3(\frac{\ell}{r}) & 0 & g_4(\frac{\ell}{r}) & 0 \\
0 & G_1(\frac{\ell}{r}) & 0 & G_2(\frac{\ell}{r}) & 0 & G_3(\frac{\ell}{r}) & 0 & G_4(\frac{\ell}{r}) \\
D_2g_1(\frac{\ell}{r}) & 0 & D_2g_2(\frac{\ell}{r}) & 0 & D_2g_3(\frac{\ell}{r}) & 0 & D_2g_4(\frac{\ell}{r}) & 0 \\
0 & D_2G_1(\frac{\ell}{r}) & 0 & D_2G_2(\frac{\ell}{r}) & 0 & D_2G_3(\frac{\ell}{r}) & 0 & D_2G_4(\frac{\ell}{r})
\end{bmatrix}
\begin{Bmatrix}
f_1(t) \\ F_1(t) \\ f_2(t) \\ F_2(t) \\ f_3(t) \\ F_3(t) \\ f_4(t) \\ F_4(t)
\end{Bmatrix}
=
\begin{Bmatrix}
f_1(t) \\ F_1(t) \\ f_2(t) \\ F_2(t) \\ f_3(t) \\ F_3(t) \\ f_4(t) \\ F_4(t)
\end{Bmatrix}
\qquad \text{(II. 26)}
$$

In shorthand notation, we can represent equation (II. 26) as

$$\left[G - I\right]\left\{f\right\} = \left\{0\right\} \tag{II. 26a}$$

where $\left[I\right]$ is the identity matrix.

From matrix theory, for a non-trivial solution of $\left\{f\right\}$, the matrix $\left[G - I\right]$ must be singular. However, $\left\{f\right\}$ varies with time in general and $\left[G - I\right]$ is independent of time. In order to satisfy equation (II. 26a) at all time, it is necessary to have

$$\left[G - I\right] = \left[0\right] = \text{null matrix} \tag{II. 27}$$

The functions $g_i(\bar{z})$ and $G_i(\bar{z})$ are so chosen that equations (II. 26a) or (II. 27) are satisfied. For the specific case considered, it can be shown that

$$\begin{aligned}
g_1(\bar{z}) = G_1(\bar{z}) &= 1 - \frac{3}{2}\left(\frac{r}{\ell}\right)^2 \bar{z}^2 + \frac{1}{2}\left(\frac{r}{\ell}\right)^3 \bar{z}^3 \\
g_2(\bar{z}) = G_2(\bar{z}) &= \bar{z} - \frac{3}{2}\left(\frac{r}{\ell}\right)\bar{z}^2 + \frac{1}{2}\left(\frac{r}{\ell}\right)^2 \bar{z}^3 \\
g_3(\bar{z}) = G_3(\bar{z}) &= \frac{3}{2}\left(\frac{r}{\ell}\right)^2 \bar{z}^2 - \frac{1}{2}\left(\frac{r}{\ell}\right)^3 \bar{z}^3 \\
g_4(\bar{z}) = G_4(\bar{z}) &= -\frac{1}{4}\bar{z}^2 + \frac{1}{4}\left(\frac{r}{\ell}\right)\bar{z}^3
\end{aligned} \tag{II. 28}$$

will satisfy (II. 27). The choice of $g_i(z)$ and $G_i(z)$ is not unique. In special cases where some $f_i(t)$ and $F_i(t)$ are zero, the corresponding $g_i(z)$ and $G_i(z)$ can be set to zero. Equation (II. 26a) is satisfied in this case, although $\left[G - I\right]$ will not be a null matrix.

Substituting (II. 24) into (II. 22), and using (II. 25), there is obtained

$$\rho \begin{bmatrix} 1 & \bar{a}_y \\ \bar{a}_y & \bar{I}_p \end{bmatrix} \begin{Bmatrix} \ddot{\bar{\xi}} \\ \ddot{\theta} \end{Bmatrix}_{II} + \begin{bmatrix} \frac{E}{r^2} D_4 & 0 \\ 0 & \frac{E}{r^2} \bar{I}_{\omega\omega} D_4 - \frac{G}{r^2} \bar{I}_d D_2 \end{bmatrix} \begin{Bmatrix} \bar{\xi} \\ \theta \end{Bmatrix}_{II}$$

$$= -\rho \sum_{i=1}^{4} \begin{bmatrix} 1 & \bar{a}_y \\ \bar{a}_y & \bar{I}_p \end{bmatrix} \begin{bmatrix} g_i(\bar{z}) & 0 \\ 0 & G_i(\bar{z}) \end{bmatrix} \begin{Bmatrix} \ddot{f}_i(t) \\ F_i(t) \end{Bmatrix}$$

$$- \sum_{i=1}^{4} \begin{bmatrix} \frac{E}{r^2} D_4 & 0 \\ 0 & \frac{E}{r^2} \bar{I}_{\omega\omega} D_4 - \frac{G}{r^2} \bar{I}_d D_2 \end{bmatrix} \begin{bmatrix} g_i(\bar{z}) & 0 \\ 0 & G_i(\bar{z}) \end{bmatrix} \begin{Bmatrix} f_i(t) \\ F_i(t) \end{Bmatrix}$$

(II. 29)

Since $f_i(t)$ and $F_i(t)$ are given functions of time and $g_i(\bar{z})$ and $G_i(\bar{z})$ are constructed, as indicated in equation (II. 28), the right-hand side of (II. 29) is a known function of $z$ and $t$ and can be represented by $\begin{Bmatrix} p(\bar{z}, t) \\ q(\bar{z}, t) \end{Bmatrix}$. Thus, the second part of the solution $\begin{Bmatrix} \bar{\xi} \\ \theta \end{Bmatrix}_{II}$ has to satisfy the nonhomogeneous equation

$$\rho \begin{bmatrix} 1 & \bar{a}_y \\ \bar{a}_y & \bar{I}_p \end{bmatrix} \begin{Bmatrix} \ddot{\bar{\xi}} \\ \ddot{\theta} \end{Bmatrix}_{II} + \begin{bmatrix} \frac{E}{r^2} D_4 & 0 \\ 0 & \frac{E}{r^2} \bar{I}_{\omega\omega} D_4 - \frac{G}{r^2} \bar{I}_d D_2 \end{bmatrix} \begin{Bmatrix} \bar{\xi} \\ \theta \end{Bmatrix}_{II}$$

$$= \begin{Bmatrix} p(\bar{z}, t) \\ q(\bar{z}, t) \end{Bmatrix}$$

and the homogeneous boundary conditions

$$\begin{Bmatrix} \bar{\xi}(0,t) \\ \theta(0,t) \end{Bmatrix}_{II} = \begin{Bmatrix} 0 \\ 0 \end{Bmatrix}; \qquad D_1 \begin{Bmatrix} \bar{\xi}(0,t) \\ \theta(0,t) \end{Bmatrix}_{II} = \begin{Bmatrix} 0 \\ 0 \end{Bmatrix}$$

$$\begin{Bmatrix} \bar{\xi}(\frac{\ell}{r},t) \\ \theta(\frac{\ell}{r},t) \end{Bmatrix}_{II} = \begin{Bmatrix} 0 \\ 0 \end{Bmatrix}; \qquad D_2 \begin{Bmatrix} \bar{\xi}(\frac{\ell}{r},t) \\ \theta(\frac{\ell}{r},t) \end{Bmatrix}_{II} = \begin{Bmatrix} 0 \\ 0 \end{Bmatrix}$$

This is exactly the problem solved in section 3, and the solution is given by equations (II. 15), (II. 20), and (II. 21). Thus, the complete solution of the case of nonhomogeneous boundary conditions is given by equations (II. 24), (II. 25), (II. 28) plus the solution to the problem of homogeneous boundary conditions under general loading as given in section 3.

Thus, making use of the orthogonal relationship, the formal solution to Gere's equations for coupled torsional and bending vibrations of thin-walled beam of open section is found under general loading conditions and general boundary conditions.

# Chapter 3

# DERIVATION OF HIGHER ORDER APPROXIMATE THEORY

## 1. Introduction

In chapter 2, the formal solution to Gere's theory is presented under very general loading conditions and general boundary conditions. In this chapter, a higher order approximate theory will be constructed in order to check the validity of Gere's theory analytically. In addition to the Euler-Bernoulli bending mechanism, the St. Venant torsion mechanism and the effect of restraint of warping, the effect of shear strain caused by bending and warping is also included in this higher order theory. As seen in chapter 1, Gere's equations reduce to the Euler-Bernoulli beam equations for bending in the case where the section of the beam has two axes of symmetry; and under the same condition, Vlasov's equations reduce to Rayleigh's beam equations. It will be seen that when the shear center coincides with the centroid of the section, the higher order theory reduces to the Timoshenko beam theory in bending.

The higher order theory is derived using the variational formulation, treating the thin-walled beam as a special case of a thin-walled prismatic shell. In this way, not only the governing differential equations, but also the proper boundary conditions are obtained. In addition, this approach has the advantage over the "strength of materials" approach that each assumption implied in the final equations is clearly stated. This approach was also used by Dzanelidze[7] to obtain Vlasov's equations for the thin-walled beam.

The governing equations are derived from Hamilton's Principle. Since only inertial loading is considered, Hamilton's Principle can be stated as[8]

$$\delta \int_{t_1}^{t_2} (T - V)\, dt = 0 \qquad \text{(III. 1)}$$

where

T = kinetic energy of the system

V = potential energy (strain energy) of the system

In section 2, the expressions for strain energy and kinetic energy are derived. The governing equations and boundary conditions are presented in section 3. Finally, various elementary theories are given in section 4 as special cases of the derived theory.

## 2. Expressions for Strain Energy and Kinetic Energy

The thin-walled beam of open section is treated as a thin-walled prismatic shell. The shell generator is parallel to the Z axis. Let the origin of the coordinate axes coincide with the centroid of the cross section and the axes OX, OY be the principal axes of the section. For a prismatic shell, the lines of principal curvature are lines parallel to the generator and lines perpendicular to the generator on the shell surface. We denote these orthogonal sets of lines z and s respectively as shown in Figure 2.

From Love's first approximation in thin shell theory[9], the strain energy density U is given by

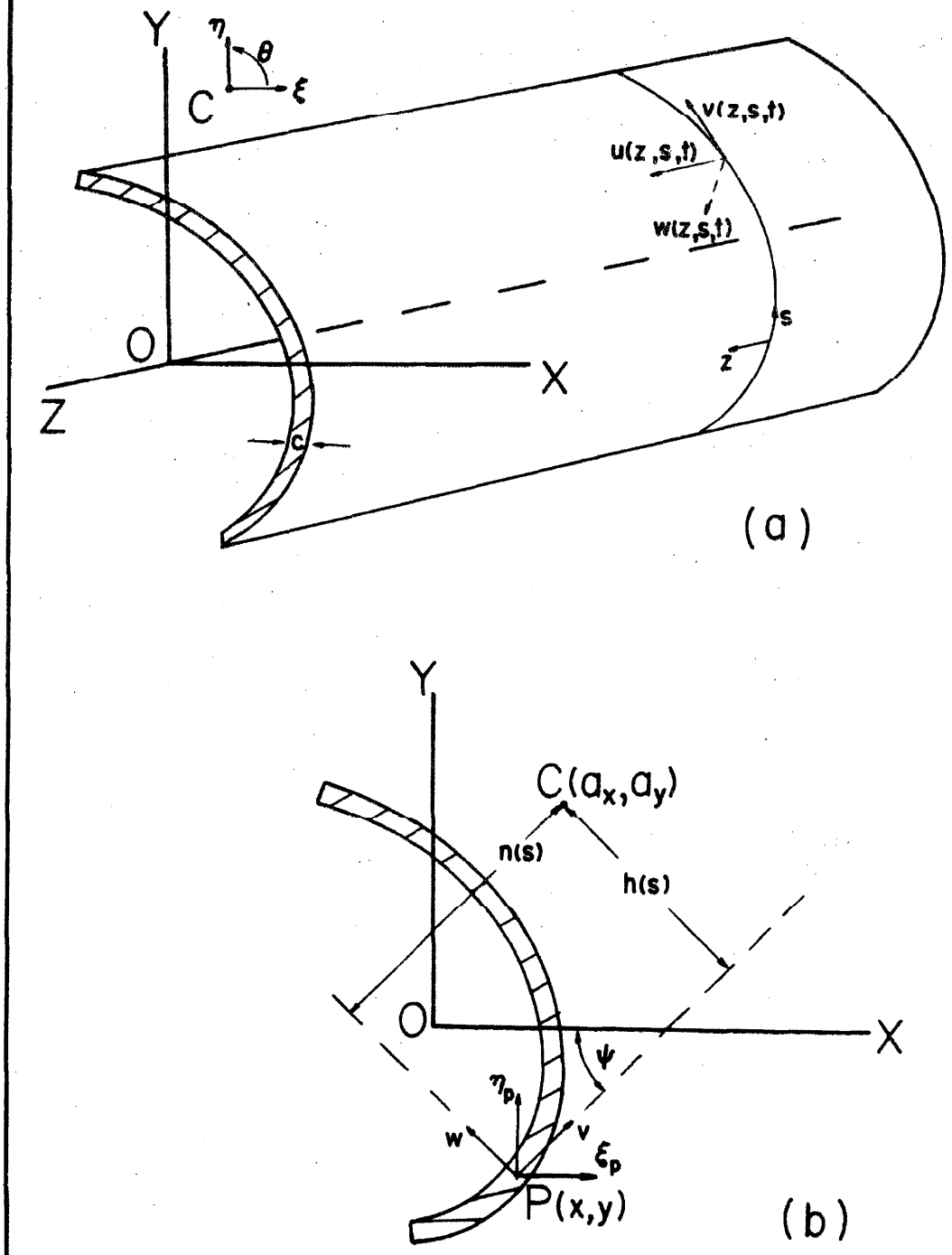


FIG. 2 THIN-WALLED BEAM AS SPECIAL PRISMATIC SHELL

$$U = U_{\epsilon} + U_{K}$$

$$= \frac{Ec}{2(1-\nu^2)} \left[ (\epsilon_z + \epsilon_s)^2 - 2(1-\nu)(\epsilon_z \epsilon_s - \frac{1}{4}\gamma_{zs}^2) \right]$$

$$+ \frac{Ec^3}{24(1-\nu^2)} \left[ (\kappa_z + \kappa_s)^2 - 2(1-\nu)(\kappa_z \kappa_s - \tau^2) \right] \qquad \text{(III. 2)}$$

where

$\epsilon_z$ = strain in z direction

$\epsilon_s$ = strain in s direction

$\gamma_{zs}$ = shear strain in the z-s plane

$\kappa_z$ = change of curvature in z direction

$\kappa_s$ = change of curvature in s direction

$\tau$ = twist in the z-s plane

The first term in (III. 2) denotes the strain energy due to stretching and the second term denotes the strain energy due to bending. The underlying assumptions of (III. 2) is that the state of stress is approximately plane, i.e., the effect of transverse shear stress and transverse normal stress acting on surfaces parallel to the middle surface of the shell, may be neglected in the strain energy density[10].

For prismatic shells, the strains and curvatures are related to the displacements u, v, w by the following expressions[9]:

$$\epsilon_z = \frac{\partial u}{\partial z} \; ; \quad \epsilon_s = \frac{\partial v}{\partial s} - \frac{v}{R} \; ; \quad \gamma_{zs} = \frac{\partial u}{\partial s} + \frac{\partial v}{\partial z}$$

(III. 3)

$$\kappa_z = \frac{\partial^2 w}{\partial z^2} \; ; \quad \kappa_s = \frac{\partial^2 w}{\partial s^2} + \frac{\partial}{\partial s}\left(\frac{v}{R}\right) \; ; \quad = \frac{\partial^2 w}{\partial s \partial z} + \frac{\partial}{\partial z}\left(\frac{v}{R}\right)$$

where

u = longitudinal displacement along the z direction

v = transverse displacement, directed along the tangent of the profile line of the cross section

w = transverse normal displacement

R = principal radius of curvature of the shell

Thus, once the displacements $u(s, z, t)$, $v(s, z, t)$ and $w(s, z, t)$ are specified, the state of strain and stress of the shell are completely determined.

The fundamental assumption in the theory of the thin-walled beam is that the section contour of the beam is undeformable. During deformation, the shape of the cross section at all sections of the beam does not change in its own plane. However, the section can be deformed out of its plane. Since a section cannot be deformed in its plane, the only possible motion of the section in its own plane is rigid body motion. The rigid body motion of the section can be described by three coordinates, two displacements $(\xi, \eta)$ of a point C and one rotation $(\theta)$ about the point C. The choice of point C is arbitrary, but it will be shown later that the algebra of the problem is greatly reduced if C is chosen as the shear center. Let the coordinates of point C be $(a_x, a_y)$. $\xi(z, t)$ and $\eta(z, t)$ are displace-

ments of the point C in the X and Y direction respectively, and they are independent of the variable s. Also, the rotation coordinate $\theta(z,t)$ is a function of z and t only, and the positive direction of $\theta$ is as shown in Figure 2.

Since $w(s,z,t)$ and $v(s,z,t)$ denote in-plane displacements perpendicular to the axis of the beam, they can be expressed in terms of $\xi$, $\eta$ and $\theta$. Let the displacements of a point P on the shell in the X and Y directions be $\xi_p$ and $\eta_p$ respectively. The displacements v, w at P are related to $\xi_p$ and $\eta_p$ by

$$\begin{Bmatrix} v(s,z,t) \\ w(s,z,t) \end{Bmatrix} = \begin{bmatrix} \cos\psi & \sin\psi \\ -\sin\psi & \cos\psi \end{bmatrix} \begin{Bmatrix} \xi_p \\ \eta_p \end{Bmatrix} \qquad \text{(III. 4)}$$

where $\psi(s)$ is the angle between the tangent of the profile line at P and the X axis. $\xi_p$ and $\eta_p$ are related to $\xi$ and $\eta$ by

$$\begin{Bmatrix} \xi_p \\ \eta_p \end{Bmatrix} = \begin{Bmatrix} \xi \\ \eta \end{Bmatrix} + \begin{bmatrix} \cos\theta & -\sin\theta \\ \sin\theta & \cos\theta \end{bmatrix} \begin{Bmatrix} x - a_x \\ y - a_y \end{Bmatrix} - \begin{Bmatrix} x - a_x \\ y - a_y \end{Bmatrix} \qquad \text{(III. 5)}$$

where (x, y) are the coordinates of point P.

For small rotations, it is justified to linearize the equations by using the approximations

$$\sin\theta \approx \theta \; ; \qquad \cos\theta \approx 1 \qquad \text{(III. 6)}$$

Substituting (III. 5) into (III. 4) and using (III. 6), there is obtained

$$v(s,z,t) = \xi(z,t)\cos\psi(s) + \eta(z,t)\sin\psi(s) + \theta(z,t)h(s)$$

$$w(s,z,t) = -\xi(z,t)\sin\psi(s) + \eta(z,t)\cos\psi(s) + \theta(z,t)n(s) \qquad \text{(III. 7)}$$

where $h(s) = (x - a_x)\sin\psi - (y - a_y)\cos\psi$

= perpendicular distance from point C to the tangent of of the profile line at point P

$n(s) = (x - a_x)\cos\psi + (y - a_y)\sin\psi$

= perpendicular distance from point C to the normal of the profile line at point P

It is convenient to treat each deformational coordinate as consisting of two parts: one part is the deformation calculated by neglecting the shear strain in the strain energy density expression (III. 2); and the second part gives the contribution due to the shear strain. Define

$$\begin{aligned} \xi(z,t) &= \xi_b(z,t) + \xi_s(z,t) \\ \eta(z,t) &= \eta_b(z,t) + \eta_s(z,t) \\ \theta(z,t) &= \theta_b(z,t) + \theta_s(z,t) \end{aligned} \qquad \text{(III. 8)}$$

where the subscript b denotes the part of solution which the shear strain has been neglected, and the subscript s denotes the contribution of the shear strain to the deformational coordinates. This choice of coordinates has the advantage that when the variables with subscripts s are equated to zero, the resulting equations reduce back to Vlasov's equations; and with minor modifications, to Gere's equations.

Similarly, $v$, $w$, and $u$ can be divided into their corresponding components.

$$v = v_b + v_s = (\xi_b \cos\psi + \eta_b \sin\psi + \theta_b h) + (\xi_s \cos\psi + \eta_s \sin\psi + \theta_s h)$$

$$w = w_b + w_s = (-\xi_b \sin\psi + \eta_b \cos\psi + \theta_b n) + (-\xi_s \sin\psi + \eta_s \cos\psi + \theta_s n)$$

$$u = u_b + u_s \qquad \text{(III. 9)}$$

$u_b$ can be determined in terms of $\xi_b$, $\eta_b$ and $\theta_b$ by noting that all quantities with the subscripts b are determined for zero shear strain. Splitting $\gamma_{zs}$ into $(\gamma_{zs})_b$ and $(\gamma_{zs})_s$, we have $(\gamma_{zs})_b = 0$. From (III. 3), $(\gamma_{zs})_b$ is defined by

$$(\gamma_{zs})_b = \frac{\partial u_b}{\partial s} + \frac{\partial v_b}{\partial z} = 0$$

Solving and making use of the relations $\sin\psi = \frac{dy}{ds}$, $\cos\psi = \frac{dx}{ds}$, $u_b(s, z, t)$ is determined.

$$u_b(s, z, t) = \zeta(z, t) - \xi_b'(z, t)x(s) - \eta_b'(z, t)y(s) - \theta_b'(z, t)\omega(s) \qquad \text{(III. 10)}$$

where $\zeta(z, t)$ is the longitudinal displacement at the point of the contour where $s = 0$, and

$$\omega(s) = \int_0^s h(\bar{s})\, d\bar{s}$$

We have no means of separating variables so that $u_s(s, z, t)$ is expressed as the sum of products of a function of $s$ and a function of $z$ and $t$. In order to reduce the governing equations to partial

differential equations of $z$ and $t$ only, it is necessary to make the assumption that $u_s(s, z, t)$ is small compared with $u_b$ and can be neglected. With this assumption, there is obtained from (III. 9) and (III. 10)

$$u = u_b = \zeta(z, t) - \xi_b'(z, t)x(s) - \eta_b'(z, t)y(s) - \theta_b'(z, t)\omega(s) \quad \text{(III. 11)}$$

Substituting the values of $u$, $v$, and $w$ in (III. 9) and (III. 11) into (III. 2), the results are:

$$\begin{aligned}
\epsilon_z &= \zeta' - \xi_b''x - \eta_b''y - \theta_b''\omega \\
\epsilon_s &= 0 \\
\gamma_{zs} &= \xi_s' \cos\psi + \eta_s' \sin\psi + \theta_s' h \\
\kappa_z &= -\xi'' \sin\psi + \eta'' \cos\psi + \theta'' n \\
\kappa_s &= 0 \\
\tau &= \theta'
\end{aligned} \quad \text{(III. 12)}$$

For a thin-walled beam where the thickness $c$ is small, the stretching effect is more important than the bending effect. Therefore $\kappa_z$ can be neglected in comparison to $\epsilon_z$ in the strain energy density calculation. Neglecting $\kappa_z$ and noting $\kappa_s = \epsilon_s = 0$, the strain energy density expression can be written as,

$$U = \frac{Ec}{2(1-\nu^2)}\left[\epsilon_z^2 + \frac{(1-\nu)}{2}\gamma_{zs}^2\right] + \frac{Ec^3}{12(1+\nu)}\tau^2 \quad \text{(III. 13)}$$

The strain energy of the whole beam is found by integrating the strain energy density throughout the beam. Using (III.12) and (III.13), there is obtained

$$V = \int_0^{\ell}\int_s \left\{ \frac{Ec}{2(1-\nu^2)} \left[ (\zeta' - \xi_b'' x - \eta_b'' y - \theta_b'' \omega)^2 \right.\right.$$

$$\left.\left. + \frac{1-\nu}{2} (\xi_s' \cos\psi + \eta_s' \sin\psi + \theta_s' h) \right] + \frac{Ec^3 \theta'^2}{12(1+\nu)} \right\} ds\, dz \qquad \text{(III.14)}$$

where the integral $\int_s ds$ represents the integration through out the whole contour of the beam.

The kinetic energy T of the whole beam is given by

$$T = \frac{1}{2}\int_0^{\ell}\int_s \rho c(\dot{u}^2 + \dot{v}^2 + \dot{w}^2)\, ds\, dz \qquad \text{(III.15)}$$

where $\rho$ = density of the material of the beam.

Using (III.7) and (III.11) to express u, v, and w in terms of $\zeta$, $\xi$, $\eta$ and $\theta$; and noting the relations

$$\begin{aligned} (x - a_x) &= n\cos\psi + h\sin\psi \\ (y - a_y) &= n\sin\psi - h\cos\psi \end{aligned} \qquad \text{(III.16)}$$

there is obtained

$$T = \frac{1}{2}\int_0^{\ell}\int_s \rho c \left\{ (\dot{\zeta}' - \dot{\xi}_b' x - \dot{\eta}_b' y - \dot{\theta}_b' \omega)^2 + \dot{\xi}^2 + \dot{\eta}^2 + \dot{\theta}^2(h^2 + n^2) \right.$$

$$\left. + 2\dot{\eta}\dot{\theta}(x - a_x) - 2\dot{\xi}\dot{\theta}(y - a_y) \right\} dz\, ds \qquad \text{(III.17)}$$

## 3. Derivation of the Differential Equations and Boundary Conditions

To simplify the algebra, it is convenient to make the following integrals zero.

$$\int_s xc\,ds = \int_s yc\,ds = \int_s xyc\,ds = 0 \tag{III.18}$$

$$\int_s x\omega c\,ds = \int_s y\omega c\,ds = 0 \tag{III.19}$$

$$\int_s \omega c\,ds = 0 \tag{III.20}$$

The three integrals in (III.18) are zero when the origin of the coordinate system is located at the centroid of the section and also the axes OX and OY are principal axes. Equation (III.19) can be satisfied by choosing point C to be the shear center of the section. Equation (III.20) is taken as the defining equation for the origin of the coordinate s on the contour of the section. It can be seen that for a monosymmetric section, the origin of the coordinate s is the point where the axis of symmetry intersects with the profile.

Substituting (III.14) and (III.17) into (III.1) and performing the variational procedure[11], seven equations are obtained for the seven deformational coordinates $\zeta$, $\xi_b$, $\xi_s$, $\eta_b$, $\eta_s$, $\theta_b$ and $\theta_s$.

$$E^*A\zeta'' - \rho A\ddot{\zeta} = 0 \tag{III.21a}$$

$$E^*I_{xx}\xi_b'''' - \rho I_{xx}\ddot{\xi}_b'' + \rho A(\ddot{\xi}_b + \ddot{\xi}_s) + \rho A a_y(\ddot{\theta}_b + \ddot{\theta}_s) = 0 \tag{III.21b}$$

$$G(I_{cc}\xi_s'' + I_{sc}\eta_s'' + I_{hc}\theta_s'') - \rho A a_y(\ddot{\theta}_b + \ddot{\theta}_s) - \rho A(\ddot{\xi}_b + \ddot{\xi}_s) = 0 \quad \text{(III. 21c)}$$

$$E^* I_{yy}\eta_b'''' - \rho I_{yy}\ddot{\eta}_b'' + \rho A(\ddot{\eta}_b + \ddot{\eta}_s) - \rho A a_x(\ddot{\theta}_b + \ddot{\theta}_s) = 0 \quad \text{(III. 21d)}$$

$$G(I_{sc}\xi_s'' + I_{ss}\eta_s'' + I_{hs}\theta_s'') - \rho A(\ddot{\eta}_b + \ddot{\eta}_s) + \rho A a_x(\ddot{\theta}_b + \ddot{\theta}_s) = 0 \quad \text{(III. 21e)}$$

$$E^* I_{\omega\omega}\theta_b'''' - \rho I_{\omega\omega}\ddot{\theta}_b'' + \rho I_p \ddot{\theta} + \rho A a_y(\ddot{\xi}_b + \ddot{\xi}_s) - \rho A a_x(\ddot{\eta}_b + \ddot{\eta}_s) - GI_d(\theta_b'' + \theta_s'') = 0 \quad \text{(III. 21f)}$$

$$G(I_{hc}\xi_s'' + I_{hs}\eta_s'' + I_{hh}\theta_s'') - \rho I_p(\ddot{\theta}_b + \ddot{\theta}_s) - \rho A a_y(\ddot{\xi}_b + \ddot{\xi}_s) + \rho A a_x(\ddot{\eta}_b + \ddot{\eta}_s) + GI_d(\theta_b'' + \theta_s'') = 0 \quad \text{(III. 21g)}$$

where

$$E^* = \frac{E}{1 - \nu^2} \; ;$$

$$I_{xx} = \int_s x^2 c \, ds \; ; \quad I_{yy} = \int_s y^2 c \, ds \; ; \quad I_{\omega\omega} = \int \omega^2 c \, ds \; ;$$

$$I_p = \int_s (h^2 + n^2) c \, ds; \quad I_{hc} = \int_s h(\cos\psi) c \, ds; \quad I_{hs} = \int_s h(\sin\psi) c \, ds;$$

$$I_{hh} = \int_s h^2 c \, ds; \quad I_{sc} = \int_s c \sin\psi \cos\psi \, ds; \quad I_{ss} = \int_s (\sin^2\psi) c \, ds;$$

$$I_{cc} = \int_s (\cos^2\psi) c \, ds; \quad I_d = \int_s \frac{c^3}{3} ds$$

(III. 22)

The associated boundary conditions are

$$\zeta' \delta\zeta \Big|_0^\ell = 0$$

$$\xi_b'' \delta\xi_b' \Big|_0^\ell = 0; \quad (I_{cc}\xi_s' + I_{sc}\eta_s' + I_{hc}\theta_s')\delta\xi \Big|_0^\ell = 0$$

$$\eta_b'' \delta\eta_b' \Big|_0^\ell = 0; \quad (I_{sc}\xi_s' + I_{ss}\eta_s' + I_{hs}\theta_s')\delta\eta \Big|_0^\ell = 0$$

$$\theta_b'' \delta\theta_b' \Big|_0^\ell = 0; \quad (I_{hc}\xi_s' + I_{hs}\eta_s' + I_{hh}\theta_s' + I_d\theta')\delta\theta \Big|_0^\ell = 0 \qquad \text{(III. 23)}$$

The set of equations in (III. 21) is a set of coupled partial differential equations in the variables z and t with constant coefficients. The first equation in (III. 21) for the longitudinal displacement $\zeta$ is a simple wave equation and is uncoupled from the rest of the set. It will be omitted in further discussions. There are two coupling mechanisms involved in the coupling of the remaining six equations. First, there is the shear strain contribution coupling between $\theta_b$ and $\theta_s$, $\xi_b$ and $\xi_s$ and $\eta_b$ and $\eta_s$. This coupling mechanism is similar to the Timoshenko beam theory coupling between bending and shear. Secondly, there is the dynamic coupling due to the nonsymmetrical property of the section. Hence, the set of equations (III. 21) can be considered as a "generalized Timoshenko theory" for thin-walled beams of open sections. It takes into account not only bending and shearing, but also torsional deformations.

It is worthwhile to summarize all the assumptions involved.

1. The section of the beam should be thin compared to the minimum

radius of curvature of the section.

2. The section contour is undeformable. This assumption is realized for inertial loads and many types of distributed loads. For concentrated loads, special diaphragms placed under the loads would be required to make this condition approximately satisfied.

3. The rotation of the section is small so that the theory may be linearized.

4. The shear strain contribution to the axial displacement is small compared to the axial displacement computed when the shear strain is neglected.

## 4. Reduction of the Generalized Theory to Elementary Theories

By neglecting certain parameters, the set of equations (III. 21) can be reduced to Vlasov's equations and Gere's equations for coupled bending and torsional vibration on one hand, and to Timoshenko beam equation for bending on the other.

If the effect of shear strain is neglected, $\xi_s$, $\eta_s$ and $\theta_s$ are zero and $\xi = \xi_b$, $\eta = \eta_b$ and $\theta = \theta_b$. Also, equation (III. 21c), (III. 21e) and (III. 21g) will not exist because they are the results of variation on the variables $\xi_s$, $\eta_s$ and $\theta_s$. Putting these modifications in (III. 21), Vlasov's equations are obtained as given in (I. 7), (I. 8) and (I. 9).

Further, if the mixed derivative terms, which are the results of including the axial inertia terms, are neglected from Vlasov's equations, Gere's equations are obtained as shown by equations (I. 4), (I. 5) and (I. 6).

On the other hand, if the section of the beam has one axis of symmetry, say the Y axis, then it can be shown from (III. 22) that $I_{sc}$, $I_{hs}$, and $a_x$ are zero. In this case, the two equations (III. 21d) and (III. 21e) for $\eta_b$ and $\eta_s$ become uncoupled from the rest of the set and reduce to the Timoshenko beam equations for bending in the Y direction, namely,

$$E^* I_{yy} \eta_b'''' - \rho I_{yy} \ddot{\eta}_b'' + \rho A(\ddot{\eta}_b + \ddot{\eta}_s) = 0$$

$$GI_{ss} \eta_s'' - \rho A(\ddot{\eta}_b + \ddot{\eta}_s) = 0 \qquad \text{(III. 24)}$$

Writing $I_{ss} = k'A$ where $k'$ is the shear correction coefficient, equations (III. 24) are in the same form as given by Anderson[12]. The remaining four equations for $\xi_b$, $\xi_s$, $\theta_b$ and $\theta_s$ are:

$$E^* I_{xx} \xi_b'''' - \rho I_{xx} \ddot{\xi}_b'' + \rho A(\ddot{\xi}_b + \ddot{\xi}_s) + \rho A a_y(\ddot{\theta}_b + \ddot{\theta}_s) = 0$$

$$G(I_{cc} \xi_s'' + I_{hc} \theta_s'') - \rho A a_y(\ddot{\theta}_b + \ddot{\theta}_s) - \rho A(\ddot{\xi}_b + \ddot{\xi}_s) = 0$$

$$E^* I_{\omega\omega} \theta_b'''' - GI_d(\theta_b'' + \theta_s'') - \rho I_{\omega\omega} \ddot{\theta}_b'' + \rho I_p(\ddot{\theta}_b + \ddot{\theta}_s) + \rho A a_y(\ddot{\xi}_b + \ddot{\xi}_s) = 0$$

$$G(I_{hc} \xi_s'' + I_{hh} \theta_s'') - \rho I_p(\ddot{\theta}_b + \ddot{\theta}_s) - \rho A a_y(\ddot{\xi}_b + \ddot{\xi}_s) + GI_d(\theta_b'' + \theta_s'') = 0 \qquad \text{(III. 25)}$$

For a section with two axes of symmetry, $I_{hc}$ and $a_y$ are also zero. Then, equations (III. 25) are further uncoupled into

$$E^*I_{xx}\xi_b'''' - \rho I_{xx}\ddot{\xi}_b'' + \rho A(\ddot{\xi}_b + \ddot{\xi}_s) = 0$$

$$GI_{cc}\xi_s'' - \rho A(\ddot{\xi}_b + \ddot{\xi}_s) = 0 \qquad \text{(III. 26)}$$

and

$$E^*I_{\omega\omega}\theta_b'''' - GI_d(\theta_b'' + \theta_s'') - \rho I_{\omega\omega}\ddot{\theta}_b'' + \rho I_p(\ddot{\theta}_b + \ddot{\theta}_s) = 0$$

$$GI_{hh}\theta_s'' - \rho I_p(\ddot{\theta}_b + \ddot{\theta}_s) + GI_d(\theta_b'' + \theta_s'') = 0 \qquad \text{(III. 27)}$$

Under such conditions, the bending and torsional vibrations are completely uncoupled. Equations (III. 26) are the Timoshenko beam equations for bending and equations (III. 27) are equations of torsion including the effect of warping and shear strain caused by warping in addition to St. Venant's torsion mechanism. It is a higher order theory than that which leads to the equations of Gere[13]. However, generally speaking, the primary mechanism is St. Venant's torsion and the effect of warping is a secondary effect. The shear strain caused by the warping will be a third order effect. Unless the warping effect is prominent, such a third order effect will not be important. In solid sections subjected to torsion, the warping effect is important and it has been shown by Barr[14] that the shear strain correction becomes significant under such circumstances.

# Chapter 4

# COMPARISON BETWEEN THE HIGHER ORDER THEORY AND GERE'S THEORY

## 1. Introduction

In this chapter, the theory developed in chapter 3 is compared with the elementary theory; namely the equations derived by Gere. The natural frequencies predicted by the two theories are taken as the criteria for comparison because natural frequencies are among the most important characteristics in a system in a dynamic environment. The geometric factors that can affect the natural frequencies of a thin-walled beam of open section include the length of the beam, the shape of its cross section and the method of support. Of all possible shapes, only sections with one axis of symmetry are considered in this chapter. The vibrations under such a condition are only "doubly coupled"; i.e., the torsional vibration is coupled with the bending vibration in one direction only. The special family of shapes chosen for computing the spectrum curves is that of a split circular ring. By varying the angle subtended by the two radii joining the center of the section to the edges of the ring, a family of sections having one axis of symmetry is obtained. Only the coupled bending and torsional equations are considered while the uncoupled bending equations are ignored.

In section 2, a scheme to calculate the natural frequencies of the beam under coupled vibrations is given. The actual calculations were performed on the IBM 7090 electronic digital computer at the

California Institute of Technology Computing Center. Spectrum curves for various boundary conditions for two chosen sections are presented in graphical form. Also, spectrum curves for a family of sections under simply supported conditions are given. In section 3, some observations are made on the spectrum curves.

## 2. Theoretical Calculations of the Natural Frequencies

According to the theory developed in chapter 3, the governing equations for a thin-walled beam with monosymmetric section under inertial loading are given by (III. 25).

$$
\begin{aligned}
&E^{*}I_{xx}\xi_b'''' - \rho I_{xx}\ddot{\xi}_b'' + \rho A(\ddot{\xi}_b + \ddot{\xi}_s) + \rho A a_y(\ddot{\theta}_b + \ddot{\theta}_s) = 0 \\
&G(I_{cc}\xi_s'' + I_{hc}\theta_s'') - \rho A(\ddot{\xi}_b + \ddot{\xi}_s) - \rho A a_y(\ddot{\theta}_b + \ddot{\theta}_s) = 0 \\
&E^{*}I_{\omega\omega}\theta_b'''' - \rho I_{\omega\omega}\ddot{\theta}_b'' + \rho I_p\ddot{\theta} + \rho A a_y\ddot{\xi} - GI_d\theta'' = 0 \\
&G(I_{hc}\xi_s'' + I_{hh}\theta_s'') - \rho I_p\ddot{\theta} - \rho A a_y\ddot{\xi} + GI_d\theta'' = 0
\end{aligned}
\qquad \text{(IV. 1)}
$$

The associated boundary conditions are:

$$
\begin{aligned}
&\xi_b''\delta\xi_b'\Big|_0^{\ell} = 0 \quad ; \qquad (I_{cc}\xi_s' + I_{hc}\theta_s')\delta\xi\Big|_0^{\ell} = 0 \\
&\theta_b''\delta\theta_b'\Big|_0^{\ell} = 0 \quad ; \qquad (I_{hc}\xi_s' + I_{hh}\theta_s' + I_d\theta')\delta\theta\Big|_0^{\ell} = 0
\end{aligned}
\qquad \text{(IV. 2)}
$$

Define

$$Ar^2 = I_{xx};\quad r\bar{a}_y = a_y;\quad r\bar{\xi}_b = \xi_b;\quad r\bar{\xi}_s = \xi_s;\quad r\bar{z} = z$$

$$A\bar{I}_{cc} = I_{cc};\quad Ar\bar{I}_{hc} = I_{hc};\quad Ar^2\bar{I}_{hh} = I_{hh} \tag{IV. 3}$$

$$Ar^2\bar{I}_p = I_p;\quad Ar^4\bar{I}_{\omega\omega} = I_{\omega\omega};\quad Ar^2\bar{I}_d = I_d$$

Equation (IV. 1) can be written in a non-dimensional form.

$$\frac{E^*}{\rho r^2}\frac{\partial^4\bar{\xi}_b}{\partial\bar{z}^4} - \frac{\partial^4\bar{\xi}_b}{\partial t^2\partial\bar{z}^2} + \frac{\partial^2\bar{\xi}}{\partial t^2} + \bar{a}_y\frac{\partial^2\theta}{\partial t^2} = 0$$

$$\frac{G}{\rho r^2}\left(\bar{I}_{cc}\frac{\partial^2\bar{\xi}_s}{\partial\bar{z}^2} + \bar{I}_{hc}\frac{\partial^2\theta_s}{\partial\bar{z}^2}\right) - \frac{\partial^2\bar{\xi}}{\partial t^2} - \bar{a}_y\frac{\partial^2\theta}{\partial t^2} = 0$$

$$\frac{E^*}{\rho r^2}\bar{I}_{\omega\omega}\frac{\partial^4\theta_b}{\partial\bar{z}^4} - \bar{I}_{\omega\omega}\frac{\partial^4\theta_b}{\partial t^2\partial\bar{z}^2} + \bar{I}_p\frac{\partial^2\theta}{\partial t^2} + \bar{a}_y\frac{\partial^2\bar{\xi}}{\partial t^2} - \frac{G}{\rho r^2}\bar{I}_d\frac{\partial^2\theta}{\partial\bar{z}^2} = 0 \tag{IV. 4}$$

$$\frac{G}{\rho r^2}\left(\bar{I}_{hc}\frac{\partial^2\bar{\xi}_s}{\partial\bar{z}^2} + \bar{I}_{hh}\frac{\partial^2\theta_s}{\partial\bar{z}^2} + \bar{I}_d\frac{\partial^2\theta}{\partial\bar{z}^2}\right) - \bar{I}_p\frac{\partial^2\theta}{\partial t^2} - \bar{a}_y\frac{\partial^2\bar{\xi}}{\partial t^2} = 0$$

The boundary conditions of (IV. 2) become

$$\frac{\partial^2\bar{\xi}_b}{\partial\bar{z}^2}\delta\left(\frac{\partial\bar{\xi}_b}{\partial\bar{z}}\right)\Bigg|_0^{\ell/r} = 0;\quad \left(\bar{I}_{cc}\frac{\partial\bar{\xi}_s}{\partial\bar{z}} + \bar{I}_{hc}\frac{\partial\theta_s}{\partial\bar{z}}\right)\delta\bar{\xi}\Bigg|_0^{\ell/r} = 0$$

$$\frac{\partial^2\theta_b}{\partial\bar{z}^2}\delta\left(\frac{\partial\theta_b}{\partial\bar{z}}\right)\Bigg|_0^{\ell/r} = 0;\quad \left(\bar{I}_{hc}\frac{\partial\bar{\xi}_s}{\partial\bar{z}} + \bar{I}_{hh}\frac{\partial\theta_s}{\partial\bar{z}} + \bar{I}_d\frac{\partial\theta}{\partial\bar{z}}\right)\delta\theta\Bigg|_0^{\ell/r} = 0 \tag{IV. 5}$$

For free vibrations, the solutions can be expressed in the form

$$\begin{Bmatrix} \bar{\xi}_b \\ \bar{\xi}_s \\ \theta_b \\ \theta_s \end{Bmatrix} = \begin{Bmatrix} \Xi_b(\bar{z}) \\ \Xi_s(\bar{z}) \\ \Theta_b(\bar{z}) \\ \Theta_s(\bar{z}) \end{Bmatrix} \sin \lambda t \qquad \text{(IV. 6)}$$

Substituting (IV. 6) in (IV. 4) and writing $\bar{\lambda}^2 = \lambda^2 \rho r^2 / G$, equation (IV. 4) can be written in a matrix form as follows:

$$\begin{bmatrix} b_{11} & -\bar{\lambda}^2 & -\bar{a}_y\bar{\lambda}^2 & -\bar{a}_y\bar{\lambda}^2 \\ \bar{\lambda}^2 & b_{22} & \bar{a}_y\bar{\lambda}^2 & \bar{I}_{hc}D_2 + \bar{a}_y\bar{\lambda}^2 \\ -\bar{a}_y\bar{\lambda}^2 & -\bar{a}_y\bar{\lambda}^2 & b_{33} & -\bar{I}_d D_2 - \bar{I}_p\bar{\lambda}^2 \\ \bar{a}_y\bar{\lambda}^2 & \bar{I}_{hc}D_2 + \bar{a}_y\bar{\lambda}^2 & \bar{I}_d D_2 + \bar{I}_p\bar{\lambda}^2 & b_{44} \end{bmatrix} \begin{Bmatrix} \Xi_b \\ \Xi_s \\ \Theta_b \\ \Theta_s \end{Bmatrix} = \begin{Bmatrix} 0 \\ 0 \\ 0 \\ 0 \end{Bmatrix}$$

(IV. 7)

where

$$b_{11} = \frac{E^*}{G} D_4 + \bar{\lambda}^2 D_2 - \bar{\lambda}^2$$

$$b_{22} = \bar{I}_{cc} D_2 + \bar{\lambda}^2$$

$$b_{33} = \frac{E^*}{G} \bar{I}_{\omega\omega} D_4 + \bar{\lambda}^2 \bar{I}_{\omega\omega} D_2 - \bar{I}_d D_2 - \bar{\lambda}^2 \bar{I}_p \qquad \text{(IV. 8)}$$

$$b_{44} = \bar{I}_d D_2 + \bar{I}_{hh} D_2 + \bar{I}_p \bar{\lambda}^2$$

In order to solve the system of coupled ordinary differential equations,

it is convenient to eliminate all but one variable in (IV. 7). Eliminating $\Xi_s(\bar{z})$ and $\Theta_s(\bar{z})$ in (IV. 7), there is obtained

$$\begin{bmatrix} a_6D_6+\bar{\lambda}^2a_4D_4+\bar{\lambda}^2a_2D_2+\bar{\lambda}^4a_o & \bar{\lambda}^2b_4D_4+\bar{\lambda}^2b_2D_2+\bar{\lambda}^4b_o \\ c_6D_6+\bar{\lambda}^2c_4D_4+\bar{\lambda}^2c_2D_2+\bar{\lambda}^4c_o & \bar{\lambda}^2d_2D_2+\bar{\lambda}^4d_o \end{bmatrix} \begin{Bmatrix} \Xi_b \\ \Theta_b \end{Bmatrix} = \begin{Bmatrix} 0 \\ 0 \end{Bmatrix} \tag{IV. 9}$$

where

$$\begin{aligned}
a_6 &= \frac{E^*}{G}\bar{I}_{cc}\bar{I}_d \\
a_4 &= \bar{I}_d\left(\bar{I}_{cc}+\frac{E^*}{G}\right)+\frac{E^*}{G}(\bar{I}_{cc}\bar{I}_p-\bar{I}_{hc}\bar{a}_y) \\
a_2 &= \bar{I}_d(-\bar{I}_{cc}+\bar{\lambda}^2)+\bar{\lambda}^2\bar{I}_p\left(\bar{I}_{cc}+\frac{E^*}{G}\right)-\bar{\lambda}^2\bar{a}_y\left(\frac{E^*}{G}\bar{a}_y+\bar{I}_{hc}\right) \\
a_o &= -(\bar{I}_p-\bar{a}_y^2)(\bar{I}_{cc}-\bar{\lambda}^2) \\
b_4 &= \frac{E^*}{G}\bar{I}_{\omega\omega}(\bar{I}_{hc}-\bar{I}_{cc}\bar{a}_y) \\
b_2 &= \bar{\lambda}^2\bar{I}_{\omega\omega}(\bar{I}_{hc}-\bar{I}_{cc}\bar{a}_y)-\bar{I}_{hc}\bar{I}_d \\
b_o &= -\bar{I}_{hc}(\bar{I}_p-\bar{a}_y^2) \\
c_6 &= \frac{E^*}{G}(\bar{I}_{hc}^2-\bar{I}_{cc}\bar{I}_d-\bar{I}_{cc}\bar{I}_{hh}) \\
c_4 &= \bar{I}_{hc}\left(\bar{I}_{hc}+\frac{2E^*}{G}\bar{a}_y\right)-\bar{I}_{cc}(\bar{I}_d+\bar{I}_{hh})-\frac{E^*}{G}(\bar{I}_d+\bar{I}_{hh}+\bar{I}_{cc}\bar{I}_p) \\
c_2 &= (\bar{I}_{cc}-\bar{\lambda}^2)(\bar{I}_d-\bar{I}_{hh})+\bar{I}_{hc}(2\bar{a}_y\bar{\lambda}^2-\bar{I}_{hc})-\bar{\lambda}^2\bar{I}_{cc}\bar{I}_p \\
&\qquad -\frac{E^*}{G}\bar{\lambda}^2(\bar{I}_p-\bar{a}_y^2) \\
c_o &= (\bar{I}_p-\bar{a}_y^2)(\bar{I}_{cc}-\bar{\lambda}^2) \\
d_2 &= \bar{I}_{hc}\bar{I}_d+\bar{a}_y\bar{I}_{cc}\bar{I}_{hh}-\bar{a}_y\bar{I}_{hc}^2 \\
d_o &= \bar{I}_{hc}(\bar{I}_p-\bar{a}_y^2)
\end{aligned} \tag{IV. 10}$$

Eliminating $\Theta_b(\bar{z})$ from (IV. 9), a tenth order ordinary differential equation for $\Xi_b(\bar{z})$ is obtained in the form

$$\Big\{ c_6b_4D_{10}+\Big[c_6b_2-a_6d_2+\bar{\lambda}^2c_4b_4\Big]D_8+\bar{\lambda}^2\Big[c_6b_o+c_4b_2+c_2b_4-a_4d_2-a_6d_o\Big]D_6$$
$$+\bar{\lambda}^2\Big[c_2b_2+a_2d_2+\bar{\lambda}^2(c_4b_o+c_ob_4-a_4d_o)\Big]D_4$$
$$+\bar{\lambda}^4\Big[c_2b_o+c_ob_2-a_2d_o-a_od_2\Big]D_2\Big\}\,\Xi_b(\bar{z})=0 \qquad \text{(IV. 11)}$$

Solving (IV. 11), the solution for $\Xi_b(\bar{z})$ becomes

$$\Xi_b(\bar{z}) = K_1\sin\mu_1\bar{z} + K_2\sin\mu_2\bar{z} + K_3\sinh\mu_3\bar{z} + K_4\sinh\mu_4\bar{z}$$
$$+ K_5\cos\mu_1\bar{z} + K_6\cos\mu_2\bar{z} + K_7\cosh\mu_3\bar{z} + K_8\cosh\mu_4\bar{z}$$
$$+ K_9\bar{z} + K_{10} \qquad \text{(IV. 12)}$$

where $K_i$, $(i = 1, 2, \ldots, 10)$, are arbitrary constants to be determined from the boundary conditions, and $\mu_j$ $(j = 1, 2, 3, 4)$, are the roots of the characteristic polynomial

$$c_6b_4\mu^8 + (c_6b_2 - a_6d_2 + \bar{\lambda}^2c_4b_4)\mu^6 + \bar{\lambda}^2(c_6b_o + c_4b_2 + c_2b_4 - a_4d_2 - a_6d_o)\mu^4$$
$$+ \bar{\lambda}^2\Big[c_2b_2 + a_2d_2 + \bar{\lambda}^2(c_4b_o + c_ob_4 - a_4d_o)\Big]\mu^2$$
$$+ \bar{\lambda}^4(c_2b_o + c_ob_2 - a_2d_o - a_od_2) = 0 \qquad \text{(IV. 13)}$$

Since the rigid body motions of the system are not of interest, $K_9$ and $K_{10}$ can be set equal to zero.

Eliminating $\Xi_b(\bar{z})$ from (IV. 9), an equation identical to (IV. 11) is obtained for $\Theta_b(\bar{z})$. The solution for $\Theta_b$ will be similar to

(IV.12) with different arbitrary constants. However, the two sets of arbitrary constants are not independent. Their relationship can be found using the first equation of (IV.9). The solution for $\Theta_b(\bar{z})$ can then be expressed as

$$\Theta_b(\bar{z}) = K_1 e_1 \sin \mu_1 \bar{z} + K_2 e_2 \sin \mu_2 \bar{z} + K_3 e_3 \sinh \mu_3 \bar{z} + K_4 e_4 \sinh \mu_4 \bar{z}$$
$$+ K_5 e_1 \cos \mu_1 \bar{z} + K_6 e_2 \cos \mu_2 \bar{z} + K_7 e_3 \cosh \mu_3 \bar{z} + K_8 e_4 \cosh \mu_4 \bar{z} \qquad \text{(IV.14)}$$

where

$$e_1 = \frac{a_6\mu_1^6 - a_4\mu_1^4 + a_2\mu_1^2 - a_o}{b_4\mu_1^4 - b_2\mu_1^2 + b_o}$$
$$e_2 = \frac{a_6\mu_2^6 - a_4\mu_2^4 + a_2\mu_2^2 - a_o}{b_4\mu_2^4 - b_2\mu_2^2 + b_o}$$
$$e_3 = \frac{-a_6\mu_3^6 - a_4\mu_3^4 - a_2\mu_3^2 - a_o}{b_4\mu_3^4 + b_2\mu_3^2 + b_o} \qquad \text{(IV.15)}$$
$$e_4 = \frac{-a_6\mu_4^6 - a_4\mu_4^4 - a_2\mu_4^2 - a_o}{b_4\mu_4^4 + b_2\mu_4^2 + b_o}$$

Knowing $\Xi_b(\bar{z})$ and $\Theta_b(\bar{z})$, $\Theta_s(\bar{z})$ can be found.

$$\Theta_s(\bar{z}) = K_1 m_1 \sin \mu_1 \bar{z} + K_2 m_2 \sin \mu_2 \bar{z} + K_3 m_3 \sinh \mu_3 \bar{z} + K_4 m_4 \sinh \mu_4 \bar{z}$$
$$+ K_5 m_1 \cos \mu_1 \bar{z} + K_6 m_2 \cos \mu_2 \bar{z} + K_7 m_3 \cosh \mu_3 \bar{z} + K_8 m_4 \cosh \mu_4 \bar{z} \qquad \text{(IV.16)}$$

where

$$\begin{Bmatrix} m_1 \\ m_2 \end{Bmatrix} = \frac{1}{\bar{I}_{hc} - \bar{I}_{cc}\bar{a}_y} \left[ \bar{I}_{cc}\bar{a}_y \begin{Bmatrix} e_1 \\ e_2 \end{Bmatrix} - \frac{E^*}{G\bar{\lambda}^2} \bar{I}_{cc} \begin{Bmatrix} \mu_1^4 \\ \mu_2^4 \end{Bmatrix} \right.$$

$$\left. + \left( \frac{E^*}{G} + \bar{I}_{cc} \right) \begin{Bmatrix} \mu_1^2 \\ \mu_2^2 \end{Bmatrix} + \begin{Bmatrix} \bar{I}_{cc} - \bar{\lambda}^2 \\ \bar{I}_{cc} - \bar{\lambda}^2 \end{Bmatrix} \right]$$

(IV.17)

$$\begin{Bmatrix} m_3 \\ m_4 \end{Bmatrix} = \frac{1}{\bar{I}_{hc} - \bar{I}_{cc}\bar{a}_y} \left[ \bar{I}_{cc}\bar{a}_y \begin{Bmatrix} e_3 \\ e_4 \end{Bmatrix} - \frac{E^*}{G\bar{\lambda}^2} \bar{I}_{cc} \begin{Bmatrix} \mu_3^4 \\ \mu_4^4 \end{Bmatrix} \right.$$

$$\left. - \left( \frac{E^*}{G} + \bar{I}_{cc} \right) \begin{Bmatrix} \mu_3^2 \\ \mu_4^2 \end{Bmatrix} + \begin{Bmatrix} \bar{I}_{cc} - \bar{\lambda}^2 \\ \bar{I}_{cc} - \bar{\lambda}^2 \end{Bmatrix} \right]$$

Similarly $\Xi_s(\bar{z})$ can be obtained by substituting (IV.12), (IV.14) and (IV.16) into the first equation of (IV. 7).

$$\Xi_s(\bar{z}) = K_1 n_1 \sin \mu_1 \bar{z} + K_2 n_2 \sin \mu_2 \bar{z} + K_3 n_3 \sinh \mu_3 \bar{z} + K_4 n_4 \sinh \mu_4 \bar{z}$$

$$+ K_5 n_1 \cos \mu_1 \bar{z} + K_6 n_2 \cos \mu_2 \bar{z} + K_7 n_3 \cosh \mu_3 \bar{z} + K_8 n_4 \cosh \mu_4 \bar{z}$$

(IV.18)

where

$$\begin{Bmatrix} n_1 \\ n_2 \end{Bmatrix} = \frac{E^*}{G\bar{\lambda}^2} \begin{Bmatrix} \mu_1^4 \\ \mu_2^4 \end{Bmatrix} - \begin{Bmatrix} \mu_1^2 \\ \mu_2^2 \end{Bmatrix} - \begin{Bmatrix} 1 \\ 1 \end{Bmatrix} - \bar{a}_y \begin{Bmatrix} e_1 \\ e_2 \end{Bmatrix} - \bar{a}_y \begin{Bmatrix} m_1 \\ m_2 \end{Bmatrix}$$

$$\begin{Bmatrix} n_3 \\ n_4 \end{Bmatrix} = \frac{E^*}{G\bar{\lambda}^2} \begin{Bmatrix} \mu_3^4 \\ \mu_4^4 \end{Bmatrix} + \begin{Bmatrix} \mu_3^2 \\ \mu_4^2 \end{Bmatrix} - \begin{Bmatrix} 1 \\ 1 \end{Bmatrix} - \bar{a}_y \begin{Bmatrix} e_3 \\ e_4 \end{Bmatrix} - \bar{a}_y \begin{Bmatrix} m_3 \\ m_4 \end{Bmatrix} \qquad \text{(IV. 19)}$$

Thus, the solutions of the set of equations (IV. 7) are given by equations (IV.12), (IV.14), (IV.16) and (IV.18). The eight arbitrary constants $K_i$, $(i = 1, 2, \ldots, 8)$, are determined by imposing the proper boundary conditions at both ends of the beam as given in (IV. 5). Boundary conditions encountered in common practice are fixed ends, pinned ends and free ends. Mathematically, these conditions are expressed, using (IV. 6), as:

Fixed end: $\quad \Xi = 0, \ \frac{\partial \Xi_b}{\partial \bar{z}} = 0; \ \Theta = 0, \ \frac{\partial \Theta_b}{\partial \bar{z}} = 0$

Pinned end: $\quad \Xi = 0, \ \frac{\partial^2 \Xi_b}{\partial \bar{z}^2} = 0; \ \Theta = 0, \ \frac{\partial^2 \Theta_b}{\partial \bar{z}^2} = 0$

Free end: $\quad \frac{\partial^2 \Xi_b}{\partial \bar{z}^2} = 0, \ \bar{I}_{cc} \frac{\partial \Xi_s}{\partial \bar{z}} + \bar{I}_{hc} \frac{\partial \Theta_s}{\partial \bar{z}} = 0;$

$$\frac{\partial^2 \Theta_b}{\partial \bar{z}^2} = 0, \ \bar{I}_{hc} \frac{\partial \Xi_s}{\partial \bar{z}} + \bar{I}_{hh} \frac{\partial \Theta_s}{\partial \bar{z}} + \bar{I}_d \frac{\partial \Theta}{\partial \bar{z}} = 0 \qquad \text{(IV. 20)}$$

There are four conditions at each end and all together there are eight conditions to be satisfied. In general, it is not possible to

satisfy all eight conditions simultaneously unless the frequency $\bar{\lambda}$ of the oscillations is a natural frequency of the system. If the frequency is one of the natural frequencies, the ratios among the arbitrary constants $K_i$ can also be determined. To illustrate the procedure, a beam held fixed at both ends, (i.e., no displacement, no slope, no rotation and complete restraint of warping), is considered. The corresponding boundary conditions are given by the first of (IV.20). Using the expressions (IV.12), (IV.14), (IV.16) and (IV.18) and evaluating them at $\bar{z} = 0$ and $\bar{z} = \ell/r$ in turn, there is obtained

$$
\begin{bmatrix}
0 & 0 & 0 & 0 & 1+n_1 & 1+n_2 & 1+n_3 & 1+n_4 \\
\mu_1 & \mu_2 & \mu_3 & \mu_4 & 0 & 0 & 0 & 0 \\
0 & 0 & 0 & 0 & e_1+m_1 & e_2+m_2 & e_3+m_3 & e_4+m_4 \\
e_1\mu_1 & e_2\mu_2 & e_3\mu_3 & e_4\mu_4 & 0 & 0 & 0 & 0 \\
(1+n_1)S_1 & (1+n_2)S_2 & (1+n_3)Sh_3 & (1+n_4)Sh_4 & (1+n_1)C_1 & (1+n_2)C_2 & (1+n_3)Ch_3 & (1+n_4)Ch_4 \\
\mu_1C_1 & \mu_2C_2 & \mu_3Ch_3 & \mu_4Ch_4 & -\mu_1S_1 & -\mu_2S_2 & \mu_3Sh_3 & \mu_4Sh_4 \\
(e_1+m_1)S_1 & (e_2+m_2)S_2 & (e_3+m_3)Sh_3 & (e_4+m_4)Sh_4 & (e_1+m_1)C_1 & (e_2+m_2)C_2 & (e_3+m_3)Ch_3 & (e_4+m_4)Ch_4 \\
e_1\mu_1C_1 & e_2\mu_2C_2 & e_3\mu_3Ch_3 & e_4\mu_4Ch_4 & -e_1\mu_1S_1 & -e_2\mu_2S_2 & e_3\mu_3Sh_3 & e_4\mu_4Sh_4
\end{bmatrix}
\begin{Bmatrix} K_1 \\ K_2 \\ K_3 \\ K_4 \\ K_5 \\ K_6 \\ K_7 \\ K_8 \end{Bmatrix}
=
\begin{Bmatrix} 0 \\ 0 \\ 0 \\ 0 \\ 0 \\ 0 \\ 0 \\ 0 \end{Bmatrix}
\qquad \text{(IV. 21)}
$$

where

$$C_i = \cos \mu_i \frac{\ell}{r} \ , \quad S_i = \sin \mu_i \frac{\ell}{r} \qquad (i = 1, 2)$$

$$Ch_j = \cosh \mu_j \frac{\ell}{r} \ , \quad Sh_j = \sinh \mu_j \frac{\ell}{r} \quad (j = 3, 4)$$

In shorthand notation, (IV. 21) can be written as

$$\left[M\right] \left\{k\right\} = \left\{0\right\} \tag{IV. 21a}$$

For non-trivial values of $\left\{k\right\}$, $\left[M\right]$ has to be singular. Thus, the natural frequency of the system under these specific boundary conditions is determined by requiring the determinant of $\left[M\right]$ to be zero, i.e.,

$$|M| = 0 \tag{IV. 22}$$

If (IV. 22) is satisfied, then $\left\{k\right\}$ can be determined up to a constant factor. Substituting the values of $\left\{k\right\}$ back into equations (IV.12), (IV.14), (IV.16) and (IV.18), $\Xi_b$, $\Xi_s$, $\Theta_b$ and $\Theta_s$ are determined respectively. The mode shape corresponding to that particular natural frequency is given by the vector function $\begin{Bmatrix} \Xi_b(\bar{z}) \\ \Xi_s(\bar{z}) \\ \Theta_b(\bar{z}) \\ \Theta_s(\bar{z}) \end{Bmatrix}$.

The simplest way to obtain the natural frequencies of the system is to assume an initial value of frequency. From (IV.13), the values of $\mu_j$, $(j = 1, 2, 3, 4)$ are then determined. For a given $\ell/r$,

the matrix $\left[M\right]$ can be formed and the determinant of $\left[M\right]$ is evaluated. In general, $|M|$ will not be zero. Another value of frequency is then chosen and the whole procedure is repeated. Since $|M|$ is a continuous function of the frequency parameter $\bar{\lambda}$, a plot of $|M|$ against $\bar{\lambda}$ can be made and the values of $\bar{\lambda}$ at which $|M|$ is zero will give the natural frequencies of the system. By varying the values of $\ell/r$, a spectrum plot can be obtained. A Fortran programme was written to carry out the scheme on the IBM 7090 electronic digital computor for five boundary conditions; namely, for a fixed-fixed beam, for a fixed-pinned beam, for a fixed-free beam (cantilever), for a pinned-pinned beam (simply supported), and for a pinned-free beam. Each trial value of frequency takes approximately 1/3 of a second machine time. This includes the forming and solving of the characteristic polynomial (IV.13), the forming of the matrix $\left[M\right]$ and the evaluation of the determinant of $\left[M\right]$ for all five boundary conditions.

A similar programme was written for the Gere theory. In non-dimensional form, Gere's equations are given in (II. 4).

$$\rho\begin{bmatrix} 1 & \bar{a}_y \\ \bar{a}_y & \bar{I}_p \end{bmatrix}\begin{Bmatrix} \ddot{\bar{\xi}} \\ \ddot{\theta} \end{Bmatrix} + \begin{bmatrix} \frac{E^*}{r^2} D_4 & 0 \\ 0 & \frac{E^*}{r^2}\bar{I}_{\omega\omega} D_4 - \frac{G}{r^2}\bar{I}_d D_2 \end{bmatrix}\begin{Bmatrix} \bar{\xi} \\ \theta \end{Bmatrix} = \begin{Bmatrix} 0 \\ 0 \end{Bmatrix} \tag{IV. 23}$$

Let $\begin{Bmatrix} \bar{\xi} \\ \theta \end{Bmatrix} = \begin{Bmatrix} \Xi(\bar{z}) \\ \Theta(\bar{z}) \end{Bmatrix} \sin \lambda t$ , equation (IV. 23) becomes

$$\begin{bmatrix} \frac{E^*}{G} D_4 - \bar{\lambda}^2 & -\bar{a}_y \bar{\lambda}^2 \\ -\bar{a}_y \bar{\lambda}^2 & \frac{E^*}{G} \bar{I}_{\omega\omega} D_4 - \bar{I}_d D_2 - \bar{I}_p \bar{\lambda}^2 \end{bmatrix} \begin{Bmatrix} \Xi(\bar{z}) \\ \Theta(\bar{z}) \end{Bmatrix} = \begin{Bmatrix} 0 \\ 0 \end{Bmatrix} \quad \text{(IV. 24)}$$

The solutions for (IV. 24) are given by

$$\Xi(\bar{z}) = K_1 \sin \mu_1 \bar{z} + K_2 \sin \mu_2 \bar{z} + K_3 \sinh \mu_3 \bar{z} + K_4 \sinh \mu_4 \bar{z}$$
$$+ K_5 \cos \mu_1 \bar{z} + K_6 \cos \mu_2 \bar{z} + K_7 \cosh \mu_3 \bar{z} + K_8 \cosh \mu_4 \bar{z} \quad \text{(IV. 25)}$$

$$\Theta(\bar{z}) = K_1 e_1 \sin \mu_1 \bar{z} + K_2 e_2 \sin \mu_2 \bar{z} + K_3 e_3 \sinh \mu_3 \bar{z} + K_4 e_4 \sinh \mu_4 \bar{z}$$
$$+ K_5 e_1 \cos \mu_1 \bar{z} + K_6 e_2 \cos \mu_2 \bar{z} + K_7 e_3 \cosh \mu_3 \bar{z} + K_8 e_4 \cosh \mu_4 \bar{z}$$

where $\mu_i$ (i = 1, 2, 3, 4) are the roots of the characteristic polynomial

$$\left(\frac{E^*}{G}\right)^2 \bar{I}_{\omega\omega} \mu^8 - \frac{E^*}{G} \bar{I}_d \mu^6 - \frac{E^*}{G} \bar{\lambda}^2 (\bar{I}_p - \bar{I}_{\omega\omega}) \mu^4 + \bar{\lambda}^2 \bar{I}_d \mu^2 + \bar{\lambda}^4 (\bar{I}_p - \bar{a}_y^2) = 0 \quad \text{(IV. 26)}$$

and

$$\begin{Bmatrix} e_1 \\ e_2 \\ e_3 \\ e_4 \end{Bmatrix} = \frac{E^*}{\bar{a}_y G \bar{\lambda}^2} \begin{Bmatrix} \mu_1^4 \\ \mu_2^4 \\ \mu_3^4 \\ \mu_4^4 \end{Bmatrix} - \frac{1}{\bar{a}_y} \begin{Bmatrix} 1 \\ 1 \\ 1 \\ 1 \end{Bmatrix} \quad \text{(IV. 27)}$$

The expressions for the boundary conditions of fixed end, pinned end and free end are given in (II. 3).

The sectional shape chosen for comparison was that of a

circular split ring. Such a shape is specified by three parameters: the radius a, the thickness c, and the central angle subtended by the two radii joining the edges of the section to the center $2\Phi$, as shown in Figure 3. The expressions for the various derived geometric parameters such as $I_{xx}$, $I_p$ are given in Appendix I. Two sections corresponding to $\Phi = 90^\circ$ and $\Phi = 135^\circ$ were employed for the computation of the spectrum curves. The curves are plotted with $\lambda/\lambda_G$ against the wave number $r/\ell$ where $\lambda$ is the natural frequency predicted by the higher order theory and $\lambda_G$ is the frequency calculated from Gere's equations. Not only the fundamental but also a few higher modes are presented. The modes are numbered in an ascending order according to the magnitude of their corresponding natural frequencies. If the frequency corresponding to the fourth mode is denoted by $(\lambda)_4$ and that corresponding to the third mode by $(\lambda)_3$, then the numbering of the modes implies that $(\lambda)_4$ is greater than $(\lambda)_3$ for the same wave number. The spectrum curves are shown in Figures 4 to 8.

If the beam is pinned ended at both ends, the mode shapes are simple. Since both (IV. 4) and (IV. 23) consist of even spatial derivatives only, it can be shown that $\Xi(\bar{z}) = \sin(\pi r\bar{z})/\ell$ and $\Theta(\bar{z}) = \sin(\pi r\bar{z})/\ell$ satisfy both the equations and boundary conditions for both theories. Under such conditions, the natural frequencies are easy to determine. Spectrum curves for different sections with the half angle $\Phi$ ranging from $45^\circ$ to $180^\circ$ under the pinned-pinned end conditions are plotted. In the plot, only modes having a wave length of $\ell/(\pi r)$ are shown. The spectrum curves for higher modes can be

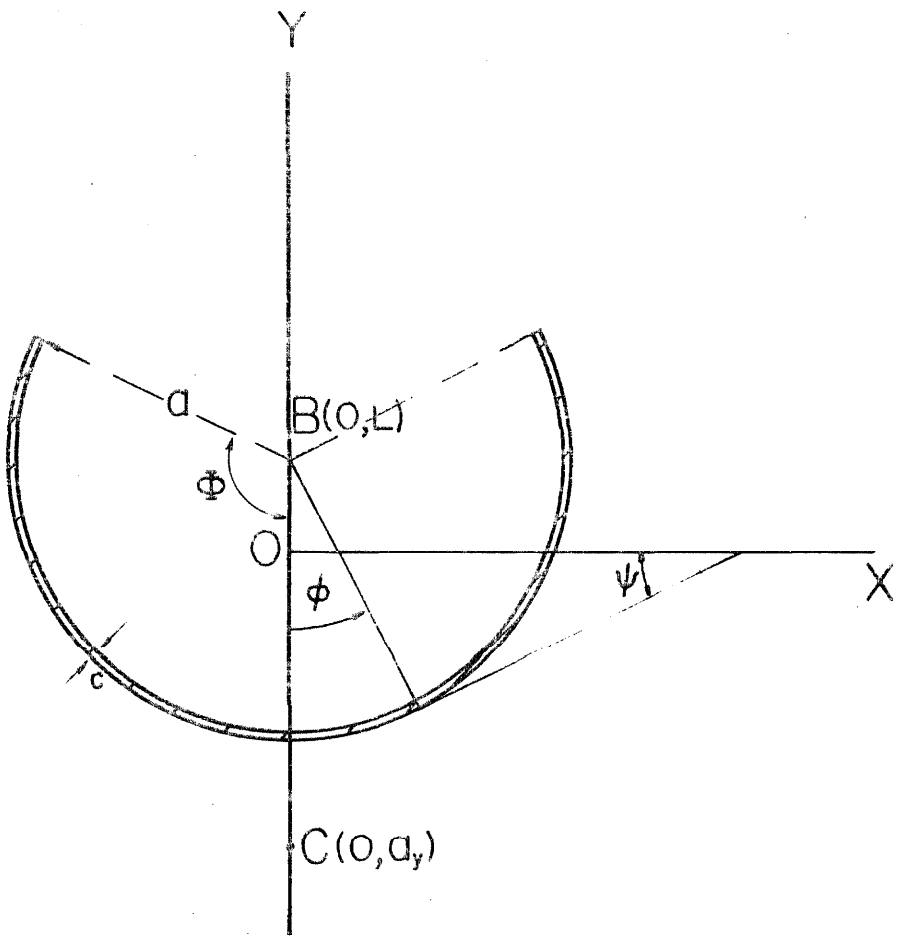


FIG. 3 SPLIT RING SECTION OF SEMI-CENTRAL ANGLE Φ

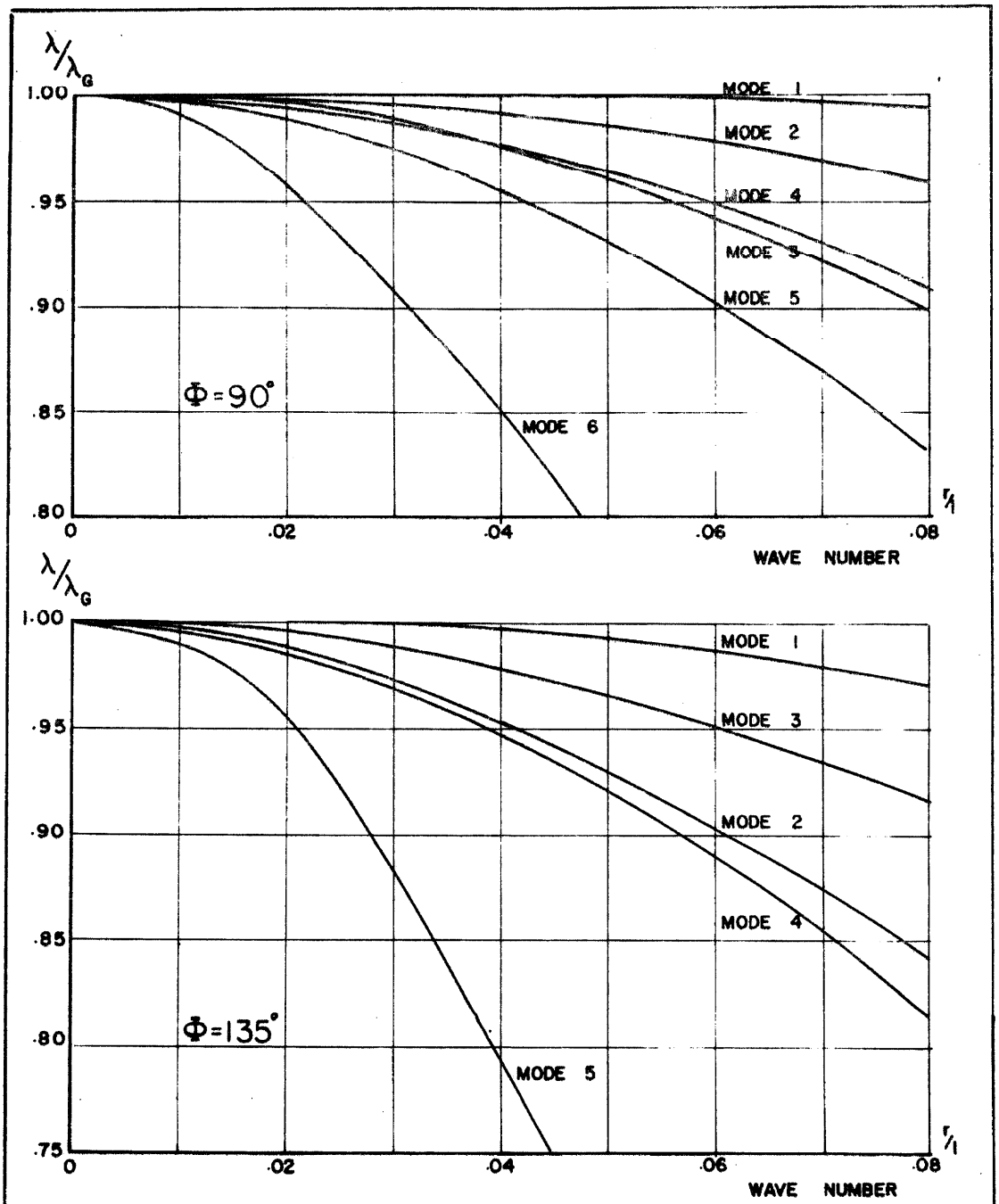


FIG. 4 FIXED - FREE Boundary Conditions

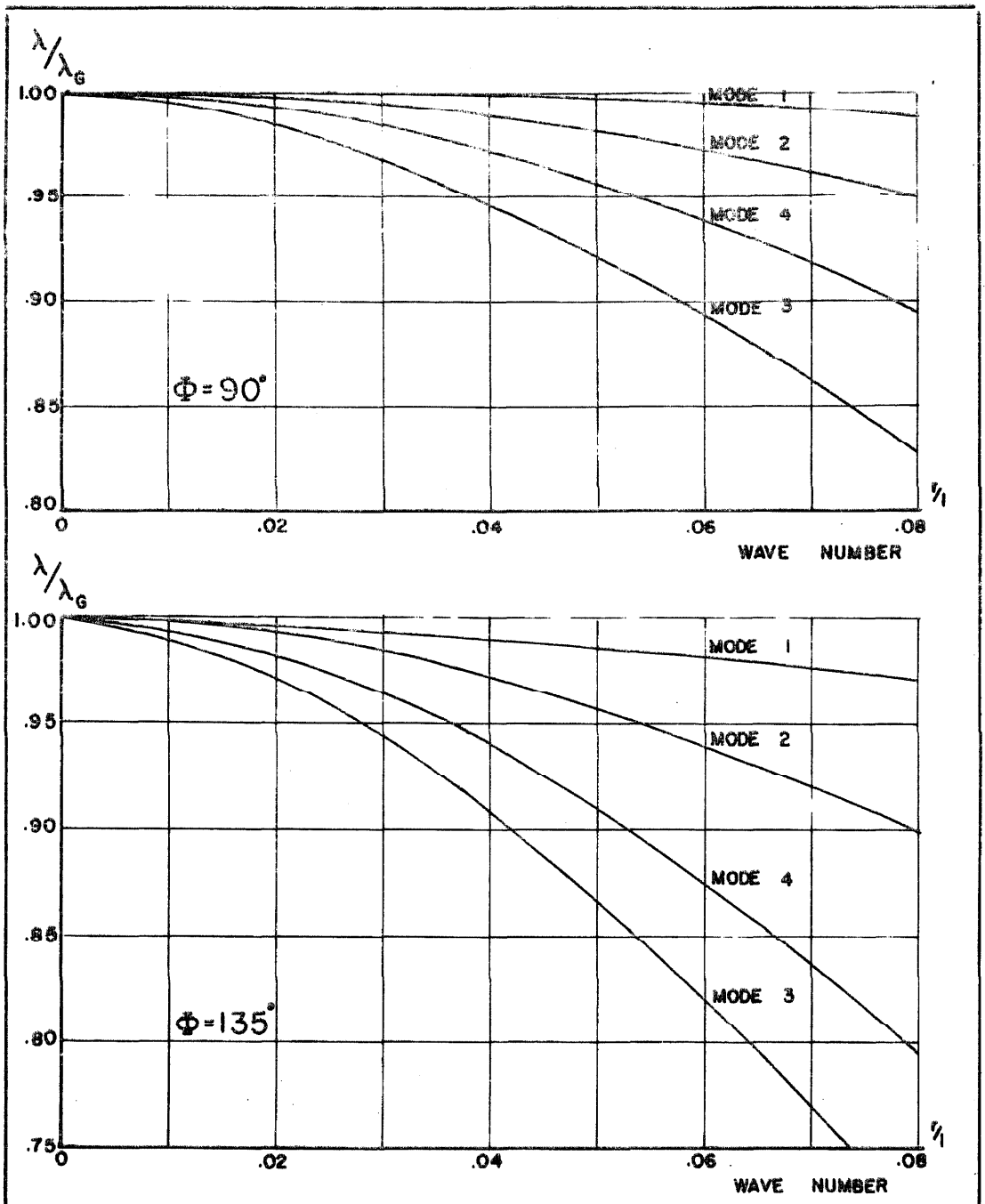


FIG. 5 PINNED PINNED Boundary Conditions

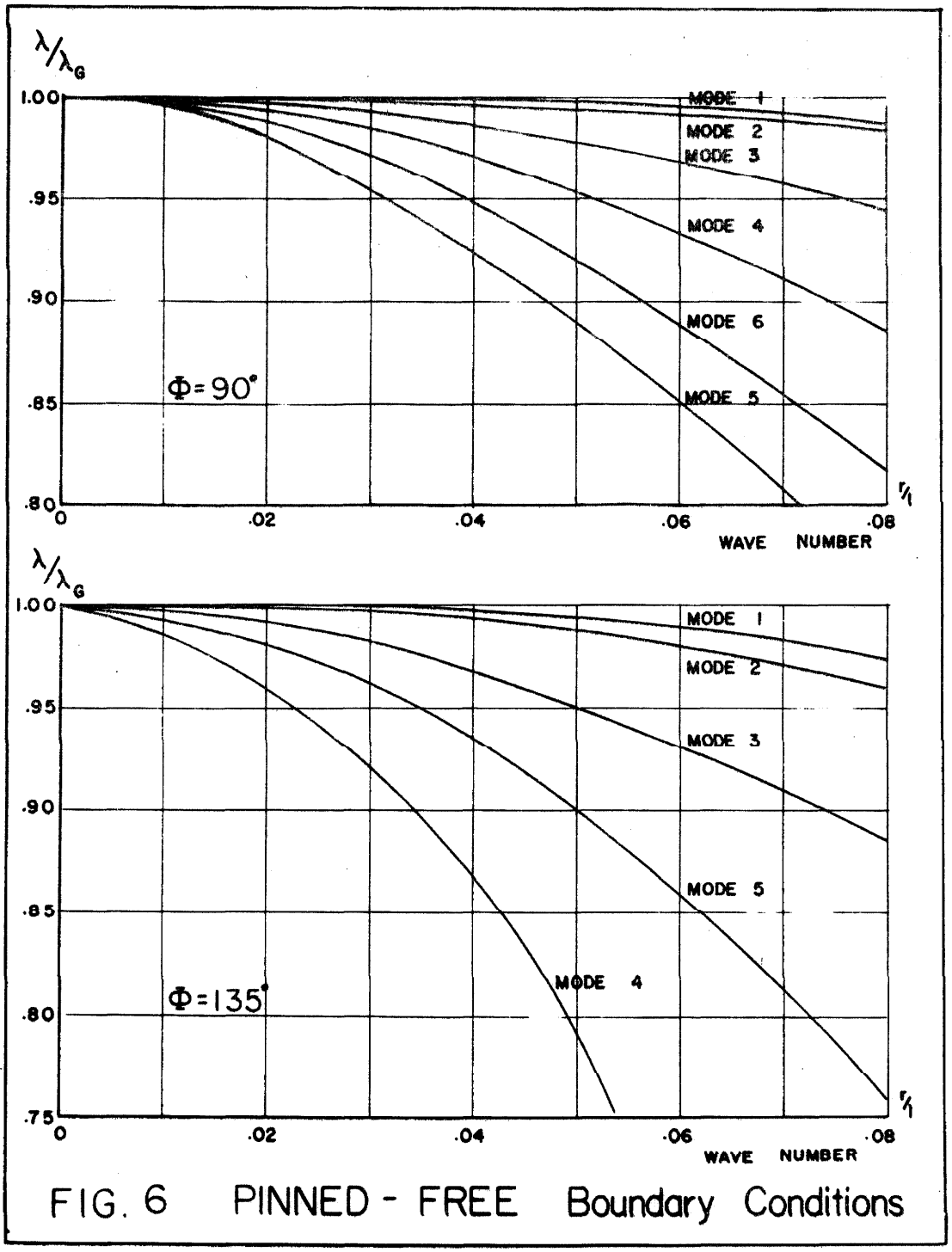


FIG. 6 PINNED - FREE Boundary Conditions

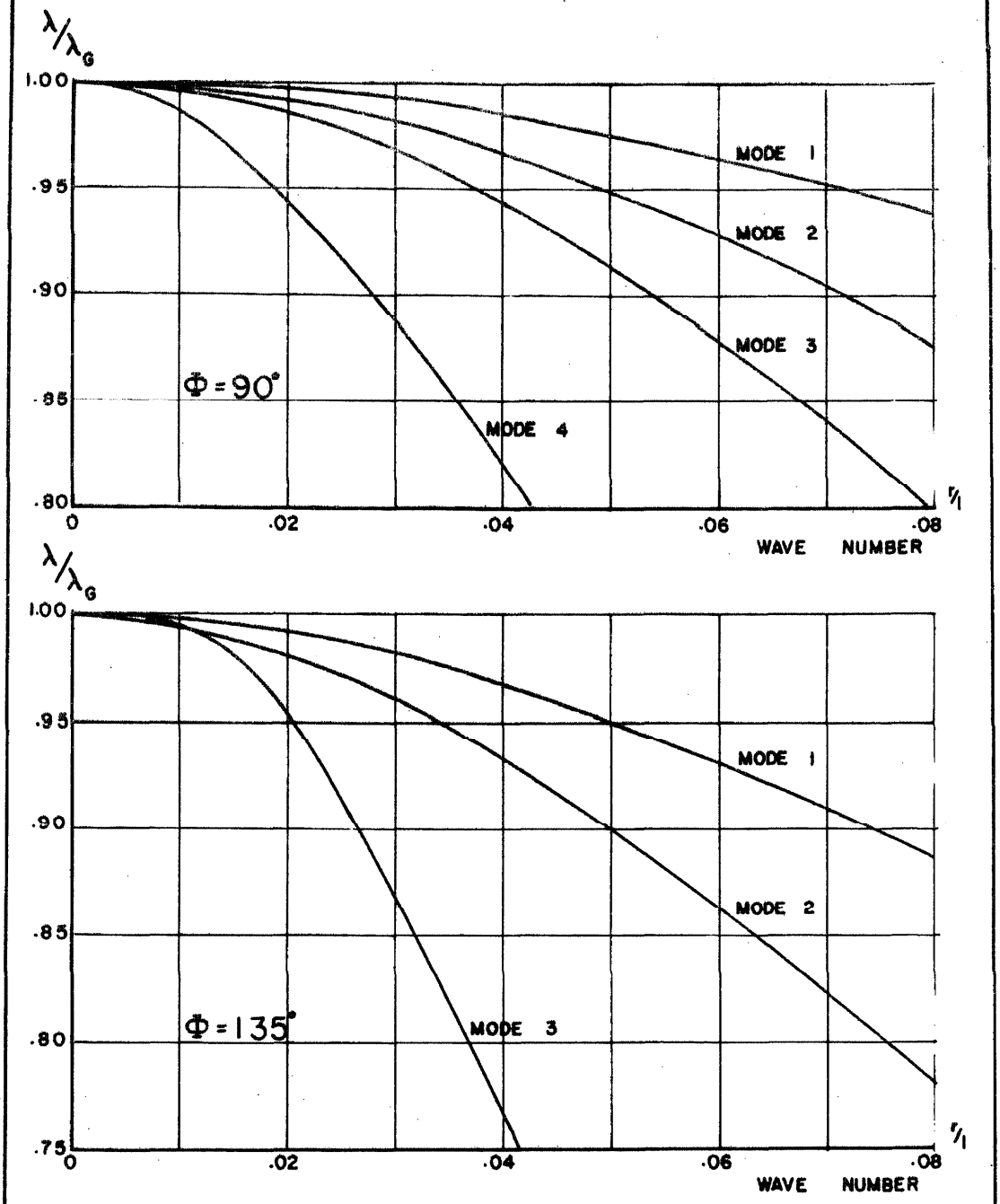


FIG. 7 FIXED - FIXED Boundary Conditions

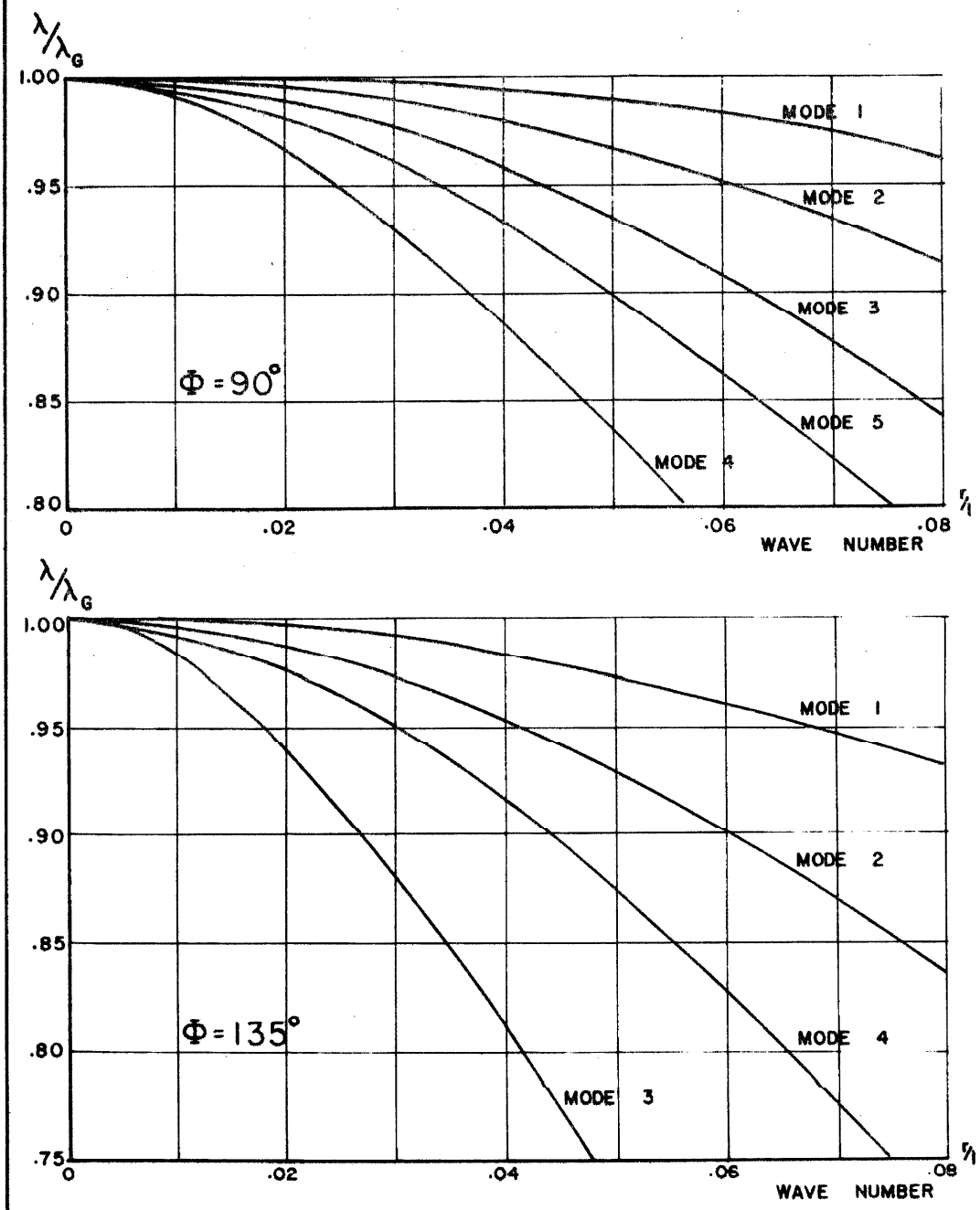


FIG. 8 FIXED-PINNED Boundary Conditions

constructed from the curves presented. The higher modes for the pinned-pinned end conditions are also sinusoidal in shape with a wave length of $\ell/(n\pi r)$ where n is an integer. Thus, the natural frequencies for the higher mode having a wave length of $\ell/(n\pi r)$ can be found by reading off the value of the frequency corresponding to a value of $(n\pi r)/\ell$ at the abscissa of the graphs.

For a given wave length, there exists two possible modes of vibration. It will be shown that in one of these modes, the motion of the beam consists mainly of rotation of the sections, while in the other mode, the motion is mainly translational. With the sections chosen, the bending rigidity is much larger than the torsional rigidity, except for a very long beam. Thus, the lower frequency mode is torsion predominant and the higher frequency mode is bending predominant. Both modes for various sections are shown in Figure 9.

3. Discussion on the Spectrum Curves

The following aspects of the spectrum curves are of interest:

1. Under all circumstances, the natural frequency predicted by the higher order theory is lower than that given by Gere's theory. Thus $(\lambda/\lambda_G)$ is always less than unity, and is equal to unity when the beam is infinitely long. Under this condition, both theories predict a natural frequency of zero. Since the higher order theory, through the introduction of three more deformational coordinates, essentially relaxes some constraints imposed by the elementary theory, it is not surprising that $(\lambda/\lambda_G) \leq 1$.

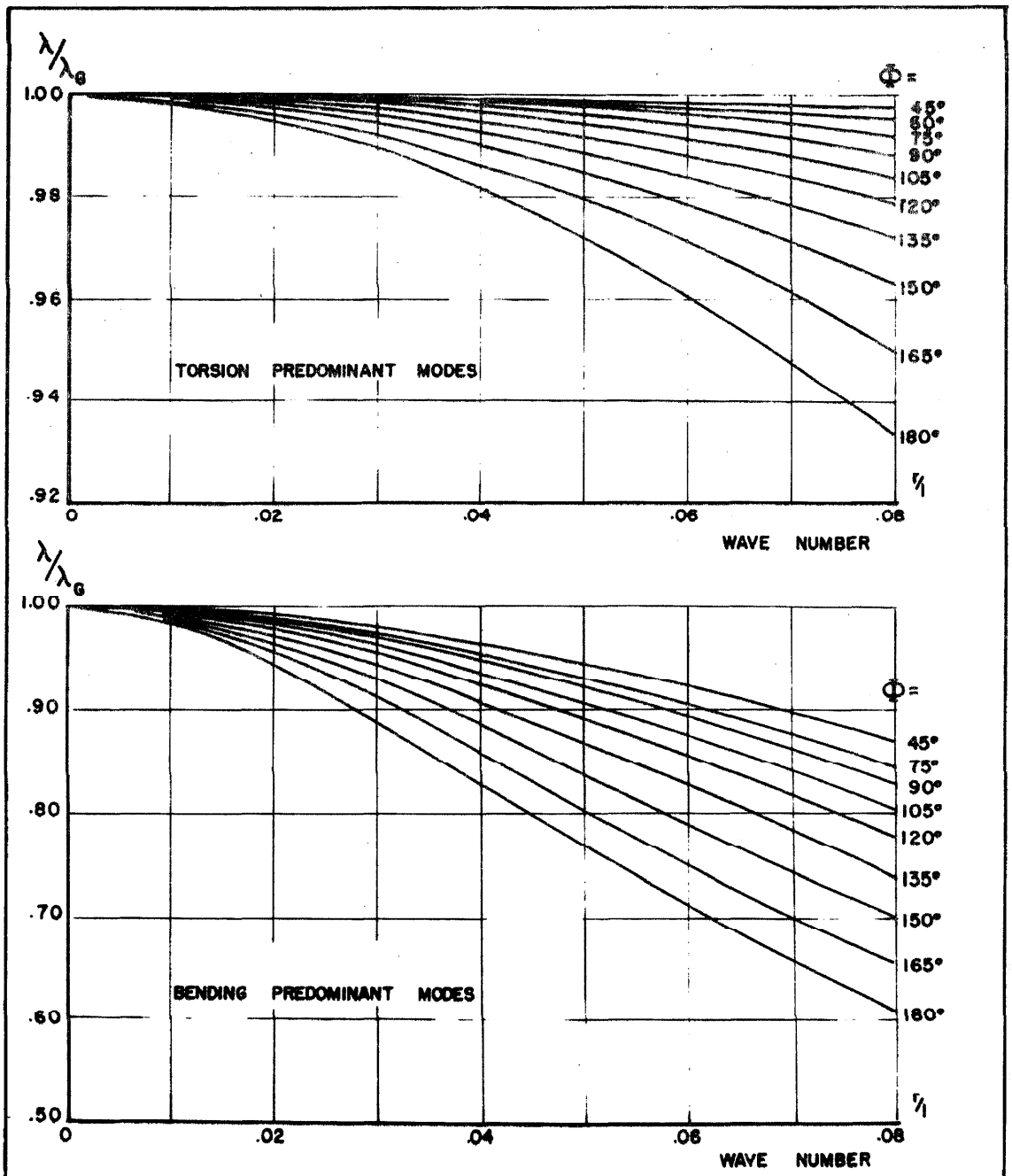


FIG. 9 PINNED - PINNED Boundary Conditions

2. For all curves, the difference between the two theories is negligible when $(r/\ell)$ is small, i.e., when the beam is long. This is also anticipated from past comparisons between the Euler-Bernoulli beam theory and the Timoshenko beam theory in bending. As the beam becomes shorter, the difference becomes progressively more prominent.

3. In general, for a given section, the difference is larger for higher modes than for lower modes. However, there are exceptions to this statement. For example, the fourth mode shows a larger difference than the fifth mode for the section $\Phi = 90^{\circ}$ with the boundary conditions fixed at one end and pinned at the other end. Similar exceptions occur for different boundary conditions and for the section $\Phi = 135^{\circ}$. Such exceptions can be explained by the fact that in the coupled vibrations, the motion of the beam consists essentially of torsional vibrations for certain modes and consists essentially of bending vibrations for some other modes. We shall denote these modes as torsion predominant modes and bending predominant modes respectively. For torsional vibration, the effect of shear strain correction is of third order, being generated by the second order effect of warping. However, the shear strain correction is a second order effect for bending vibrations. Thus, we can expect the difference between the two theories to be more significant for a bending predominant mode than a torsion predominant mode. A bending predominant mode may be associated with a lower natural frequency than that of some higher torsion predominant modes, yet the differ-

ence between the two theories will be larger for the bending predominant mode than some higher torsion predominant modes. The exceptions cited are examples of this.

4. It is interesting to note the effect of different sections for the same $(r/\ell)$ and the same boundary conditions. Consistently, the section $\Phi = 135^{\circ}$ shows a bigger difference between the two theories than the section $\Phi = 90^{\circ}$ for the same mode, same $(r/\ell)$ and same boundary conditions. This effect can be seen more clearly from plots of Figure 9 for the pinned ended conditions. It can be inferred that similar situations occur for other boundary conditions. The difference between the two theories increases as the semi-central angle $\Phi$ becomes larger. The increase is especially prominent as $\Phi$ passes over $90^{\circ}$. The intrinsic properties of the section that cause such behavior are the subject of investigation in the next chapter.

Chapter 5

# PARAMETRIC STUDY OF SECTIONAL PROPERTIES ON EFFECT OF COUPLING AND FREQUENCIES

## 1. Introduction

The Rayleigh-Ritz method for determining eigenvalues from known or assumed eigenvectors or eigenfunctions is well known[15]. In particular, it is applied to vibrational problems to determine the natural frequencies of a system, provided the mode shapes are given. If the mode shapes are known exactly, the method will give the natural frequencies of the system exactly. In this chapter, this method is employed to study the degree of coupling in the coupled torsional and bending vibrations. Also, this method provides a convenient way to assess the importance of various geometric parameters introduced by the higher order theory. With such an analysis, it is possible to estimate the necessity for using the higher order theory once the sectional properties of the specimen are given.

In section 2, the degree of coupling of torsional vibration and bending vibration under various conditions is examined according to Gere's theory. In section 3, the degree of coupling of the shear strain effect is examined for both the uncoupled bending vibration (Timoshenko beam theory) and uncoupled torsional vibration. In section 4, the effect of various geometric parameters on the natural frequencies of the higher order theory is studied.

## 2. Application of Rayleigh-Ritz Method to Thin-Walled Beams with Monosymmetric Section

The Rayleigh-Ritz method is applied to thin-walled beams of monosymmetric open section to study the degree of coupling of the torsional and bending vibrations. According to Gere's theory, the strain energy $V$ and the kinetic energy $T$ of the beam are given by the following expressions:

$$V = \frac{1}{2}\int_0^{\ell} \left[ E^* I_{xx} \xi''^2(z,t) + E^* I_{\omega\omega} \theta''^2(z,t) + GI_d \theta'^2(z,t) \right] dz \qquad (V.1)$$

$$T = \frac{1}{2}\int_0^{\ell} \rho \left[ A\dot{\xi}^2(z,t) + I_p \dot{\theta}^2(z,t) + 2Aa_y \dot{\xi}(z,t)\dot{\theta}(z,t) \right] dz \qquad (V.2)$$

For free vibrations, the solution $\xi$ and $\theta$ can be expressed in the form

$$\begin{aligned} \xi(z,t) &= \alpha r \Xi(z) \sin \lambda t \\ \theta(z,t) &= \gamma \Theta(z) \sin \lambda t \end{aligned} \qquad (V.3)$$

where $\alpha, \gamma$ represent the amplitudes and $\Xi(z)$ and $\Theta(z)$ are the normalized mode shapes. Substituting (V.3) into (V.1) and (V.2), there is obtained

$$V = \frac{1}{2}\left[ \int_0^{\ell} \alpha^2 r^2 E^* I_{xx} \Xi''^2(z) + \gamma^2 E^* I_{\omega\omega} \Theta''^2(z) + \gamma^2 GI_d \Theta'^2(z)\, dz \right] \sin^2 \lambda t \qquad (V.4)$$

$$T = \frac{1}{2}\left[\int_0^{\ell} \rho \left\{ a^2 r^2 A \Xi^2(z) + \gamma^2 I_p \Theta^2(z) + 2\alpha\gamma r A a_y \Xi(z)\Theta(z) \right\} dz \right] \lambda^2 \cos^2 \lambda t \qquad (V.5)$$

The Rayleigh-Ritz method is based on the principle of conservation of the total energy of the system. Equating the maximum kinetic energy of the system to its maximum strain energy, there is obtained

$$\lambda^2 = \frac{\int_0^{\ell} r^2 E^* \Xi''^2 dz + \bar{\gamma}^2 \left( \int_0^{\ell} r^2 E^* \bar{I}_{\omega\omega} \Theta''^2 + G\bar{I}_d \Theta'^2 dz \right)}{\int_0^{\ell} \rho \Xi^2 dz + \bar{\gamma}^2 \left( \int_0^{\ell} \rho \bar{I}_p \Theta^2 dz \right) + 2\bar{\gamma} \int_0^{\ell} \bar{a}_y \Xi\Theta dz} \qquad (V.6)$$

where $\bar{\gamma} = \gamma/a$ = ratio of the amplitudes of rotational motion and translational motion of the beam.

If the mode shapes $\Xi(z)$ and $\Theta(z)$ are known, all integrals in (V.6) can be evaluated. The remaining unknown in the equation is $\bar{\gamma}$. The value of $\bar{\gamma}$ is determined by the condition

$$\frac{\partial \lambda^2}{\partial \bar{\gamma}} = 0 \qquad (V.7)$$

Equation (V.7) results in a quadratic algebraic equation in $\bar{\gamma}$. Each root of (V.7) gives the degree of coupling of torsion and bending in the coupled vibrations. Substituting the value of $\bar{\gamma}$ into (V.6) yields the natural frequency for the particular mode.

In particular, the case of a beam simply supported at both ends will be considered. As noted in Chapter 4, the mode shapes in

this case are sinusoidal, i.e.,

$$\begin{Bmatrix} \Xi(z) \\ \Theta(z) \end{Bmatrix} = \begin{Bmatrix} \sin \frac{\pi z}{\ell} \\ \sin \frac{\pi z}{\ell} \end{Bmatrix} \tag{V.8}$$

Substituting (V.8) in (V.6) and writing the result in a non-dimensional form, there is obtained

$$\bar{\lambda}^2 = \frac{\frac{E^*}{G}\mu^4 + \bar{\gamma}^2\left[\frac{E^*}{G}\bar{I}_{\omega\omega}\mu^4 + \bar{I}_d\mu^2\right]}{1 + \bar{\gamma}^2\bar{I}_p + 2\bar{\gamma}\bar{a}_y} \tag{V.9}$$

where $\mu = (\pi r)/\ell$, and $\bar{\lambda}^2 = (\lambda^2\rho r^2)/G$. To find the value of $\bar{\gamma}$, condition (V.7) is used and the result becomes

$$\bar{\gamma}^2\bar{a}_y\left(\frac{E^*}{G}\bar{I}_{\omega\omega} + \frac{\bar{I}_d}{\mu^2}\right) + \bar{\gamma}\left[\frac{\bar{I}_d}{\mu^2} - \frac{E^*}{G}(\bar{I}_p - \bar{I}_{\omega\omega})\right] - \frac{E^*}{G}\bar{a}_y = 0 \tag{V.10}$$

Solving (V.10), there is obtained

$$\bar{\gamma}_{1\atop 2} = \frac{-\left[\frac{\bar{I}_d}{\mu^2} - \frac{E^*}{G}(\bar{I}_p - \bar{I}_{\omega\omega})\right] \pm \left\{\left[\frac{\bar{I}_d}{\mu^2} - \frac{E^*}{G}(\bar{I}_p - \bar{I}_{\omega\omega})\right]^2 + 4\frac{E^*}{G}\bar{a}_y^2\left(\frac{E^*}{G}\bar{I}_{\omega\omega} + \frac{\bar{I}_d}{\mu^2}\right)\right\}^{\frac{1}{2}}}{2\bar{a}_y\left(\frac{E^*}{G}\bar{I}_{\omega\omega} + \frac{\bar{I}_d}{\mu^2}\right)} \tag{V.11}$$

Since $4\frac{E^*}{G}\bar{a}_y^2\left(\frac{E^*}{G}\bar{I}_{\omega\omega} + \frac{\bar{I}_d}{\mu^2}\right) > 0$, the roots obtained are real and have opposite signs. A few special cases are considered to study the degree of coupling as the length of the beam varies.

Case (i): $\dfrac{\bar{I}_d}{\mu^2} - \dfrac{E^*}{G}(\bar{I}_p - \bar{I}_{\omega\omega}) = \dfrac{E^*}{G\epsilon}$ where $0 < \epsilon << 1$

This case corresponds to the length of the beam being very long. From (V.11), there is obtained

$$\bar{\gamma}_1 = \frac{-\dfrac{E^*}{G\epsilon} + \left[\left(\dfrac{E^*}{G\epsilon}\right)^2 + 4\bar{a}_y^2\left(\dfrac{E^*}{G}\right)^2\left(\bar{I}_p + \dfrac{1}{\epsilon}\right)\right]^{\frac{1}{2}}}{2\bar{a}_y \dfrac{E^*}{G}\left(\bar{I}_p + \dfrac{1}{\epsilon}\right)} \approx \bar{a}_y \epsilon + O(\epsilon^2) \qquad \text{(IV.12)}$$

For very long beams, $\epsilon$ is small and hence $\bar{\gamma}_1$ is small. This implies the ratio of the amplitude of torsional vibration to that of the bending vibration is small, corresponding to a bending predominant mode. For a split ring section, it is shown in Appendix I that $\bar{a}_y$ is negative. Therefore, $\bar{\gamma}_1$ is negative and this implies the torsional motion and the bending motion are out of phase with each other by $180^\circ$.

Substituting the approximate value of $\bar{\gamma}_1$ from (V.12) in (V.9), there is obtained

$$\lambda_1^2 = \frac{\dfrac{E^*}{G}\mu^4\left[1 + \left(\dfrac{1}{\epsilon} + \bar{I}_p\right)\bar{a}_y^2\epsilon^2\right]}{1 + \bar{a}_y^2(\bar{I}_p\epsilon^2 + 2\epsilon)}$$

$$= \frac{E^*}{G}\mu^4\left[1 - \bar{a}_y^2\epsilon + O(\epsilon^2)\right] \qquad \text{(V.13)}$$

For uncoupled bending vibrations, the Euler-Bernoulli theory predicts a frequency given by

$$\bar{\lambda}^2_{\text{bending}} = \frac{E^*}{G}\mu^4 \qquad \text{(V.14)}$$

Comparison between (V.13) and (V.14) shows the coupled vibrations give a lower frequency than the uncoupled case.

Using similar approximations, the other root of (V.11) and its corresponding frequency are determined.

$$\gamma_2 \approx \frac{-(1+\bar{a}_y^2\epsilon)}{\bar{a}_y(1+\bar{I}_p\epsilon)} \tag{V.15}$$

$$\bar{\lambda}_2^2 \approx \frac{\frac{E^*}{G}\mu^4(\bar{I}_p+\frac{1}{\epsilon}+3\bar{a}_y^2)}{\bar{I}_p-\bar{a}_y^2} \tag{V.16}$$

For uncoupled torsional vibrations, the frequency predicted by the theory, including the effect of warping[13], is given by

$$\bar{\lambda}^2_{\text{torsion}} = \frac{E^*}{G}\mu^4\left(1+\frac{1}{\bar{I}_p\epsilon}\right) \tag{V.17}$$

The value of $\bar{I}_p$ in (V.17) is the same as the non-dimensional polar moment of inertia about the centroid of the section, since the shear center coincides with the centroid for the uncoupled torsional vibrations. Also, it should be pointed out that $\bar{I}_p - \bar{a}_y^2$ as appearing in (V.16) is never zero because

$$\bar{I}_p - \bar{a}_y^2 = \frac{I_p}{Ar^2} - \frac{a_y^2}{r^2} = \frac{I_p - Aa_y^2}{Ar^2} = \frac{I_g}{Ar^2} = \bar{I}_g > 0$$

where $I_g$ is the polar moment of inertia of the section about the centroid O.

Equation (V.15) shows that the torsional motion and the bending motion are in phase and the coupling between the two is

approximately given by $1/\bar{a}_y$. The coupled vibrational frequency is higher than the uncoupled torsional vibrations as seen from (V.16) and (V.17). It is interesting to note that for long beams, the coupling between torsion and bending in a bending predominant mode can be made arbitrarily weak by making the length of the beam arbitrarily large. However, the coupling in the torsion predominant mode is determined by the value of $\bar{a}_y$ in the limit, and cannot be made arbitrarily small.

Case (ii): $\dfrac{\bar{I}_d}{\mu^2} - \dfrac{E^*}{G}(\bar{I}_p - \bar{I}_{\omega\omega}) = \dfrac{E^*\epsilon}{G} \qquad |\epsilon| \ll 1$

From (V.11), there is obtained

$$\bar{\gamma}_1 = \frac{-\epsilon + 2\bar{a}_y(\bar{I}_p + \epsilon)^{\frac{1}{2}}\left[1 + \dfrac{\epsilon^2}{4\bar{a}_y^2(\bar{I}_p + \epsilon)}\right]^{\frac{1}{2}}}{2\bar{a}_y(\bar{I}_p + \epsilon)} \tag{V.18}$$

If $\dfrac{\epsilon^2}{4\bar{a}_y^2(\bar{I}_p + \epsilon)} \ll 1$, equation (V.18) can be expanded and neglecting higher order terms in $\epsilon$, $\bar{\gamma}_1$ can be approximated to

$$\bar{\gamma}_1 \approx \frac{1}{(\bar{I}_p + \epsilon)^{\frac{1}{2}}}\left[1 - \frac{\epsilon}{2\bar{a}_y(\bar{I}_p + \epsilon)^{\frac{1}{2}}}\right] \tag{V.19}$$

Substituting (V.19) into (V. 9), the corresponding frequency is obtained.

$$\bar{\lambda}_1^2 \approx \frac{E^*\mu^4\bar{I}_p^{\frac{1}{2}}}{G(\bar{I}_p^{\frac{1}{2}} + \bar{a}_y)}\left[1 + \frac{\epsilon}{2\bar{I}_p} + O(\epsilon^2)\right] \tag{V.20}$$

Similarly, from (V.11) and (V. 9), there is obtained

$$\bar{\gamma}_2 \approx \frac{-1}{(\bar{I}_p + \epsilon)^{\frac{1}{2}}} \left[ 1 + \frac{\epsilon}{2\bar{a}_y(\bar{I}_p + \epsilon)^{\frac{1}{2}}} \right] \tag{V. 21}$$

$$\bar{\lambda}_2^2 \approx \frac{\frac{E^*}{G}\mu^4 \bar{I}_p^{\frac{1}{2}}}{\bar{I}_p^{\frac{1}{2}} - \bar{a}_y} \left[ 1 + \frac{\epsilon}{2\bar{I}_p} + O(\epsilon^2) \right] \tag{V. 22}$$

The frequency of the uncoupled torsional vibrations in this case is given by

$$\bar{\lambda}^2_{\text{torsion}} = \frac{E^*}{G}\mu^4\left(1 + \frac{\epsilon}{\bar{I}_p}\right) \tag{V. 23}$$

Taking $\bar{a}_y$ to be negative and $\epsilon$ positive, $|\bar{\gamma}|_2$ is less than $|\bar{\gamma}|_1$. Therefore, $\bar{\gamma}_2$ is associated with the bending predominant mode and $\bar{\gamma}_1$ with the torsion predominant mode. Comparing the coupled frequencies with the corresponding uncoupled frequencies as given in (V. 14) and (V. 23), it is seen that the coupled frequency for the bending predominant mode is lower and that for the torsion predominant mode is higher than the respective uncoupled frequencies.

In particular, when $\epsilon$ tends to zero, i.e., $\frac{\bar{I}_d}{\mu^2} = \frac{E^*}{G}(\bar{I}_p - \bar{I}_{\omega\omega})$, there is obtained,

$$\bar{\gamma}_1 = \frac{1}{\bar{I}_p^{\frac{1}{2}}} \tag{V. 24}$$

$$\bar{\lambda}_1^2 = \frac{E^*\mu^4 \bar{I}_p^{\frac{1}{2}}}{G(\bar{I}_p^{\frac{1}{2}} + \bar{a}_y)} \tag{V. 25}$$

$$\bar{\gamma}_2 = -\frac{1}{\bar{I}_p^{\frac{1}{2}}} \tag{V.26}$$

$$\bar{\lambda}_2^2 = \frac{E^* \mu^4 \bar{I}_p^{\frac{1}{2}}}{G(\bar{I}_p^{\frac{1}{2}} - \bar{a}_y)} \tag{V.27}$$

Under this condition, the uncoupled bending vibrations and torsional vibrations have the same frequency as given by (V.14), i.e., $\bar{\lambda}^2_{\text{uncoupled}} = \frac{E^*}{G}\mu^4$. The amplitude ratio for the two modes in the coupled vibrations is the same, but differs in phase. The frequency corresponding to the in-phase coupled mode has a higher frequency while the out of phase mode has a lower frequency than the uncoupled vibrations.

Case (iii) $\frac{\bar{I}_d}{\mu^2} - \frac{E^*}{G}(\bar{I}_p - \bar{I}_{\omega\omega}) = -\frac{E^*}{G}\chi$ where $\bar{I}_p - \bar{I}_{\omega\omega} \geq \chi > 0$

In this case, the value of $\chi$ is not restricted to be small, but the maximum value of $\chi$ is given by $\bar{I}_p - \bar{I}_{\omega\omega}$ since $\frac{\bar{I}_d}{\mu^2} \geq 0$. From equation (V.11), there is obtained

$$\bar{\gamma}_1 = \frac{\chi + \left[\chi^2 + 4\bar{a}_y^2(\bar{I}_p - \chi)\right]^{\frac{1}{2}}}{2\bar{a}_y(\bar{I}_p - \chi)} \tag{V.28}$$

If $\frac{\chi^2}{4\bar{a}_y^2(\bar{I}_p - \chi)} < 1$, the problem reduces to that of case (ii) with $-\chi$ replacing $\epsilon$. Equations (V.19) and (V.22) can then be taken as a first approximation for the frequencies and the degree of coupling.

If $\frac{\chi^2}{4\bar{a}_y^2(\bar{I}_p - \chi)} > 1$, equation (V.28) can be approximated to obtain

$$\bar{\gamma}_1 \approx \frac{\chi}{\bar{a}_y(\bar{I}_p - \chi)}\left[1 + \frac{\bar{a}_y^2(\bar{I}_p - \chi)}{\chi^2}\right] \tag{V.29}$$

The corresponding frequency is given by

$$\bar{\lambda}_1^2 \approx \frac{E^*}{G}\mu^4\left(1 - \frac{\chi}{\bar{I}_p}\right)\left[\frac{1}{1 + \left(\frac{\bar{a}_y^2(\bar{I}_p - \chi)}{\chi^2 + 3\bar{a}_y^2(\bar{I}_p - \chi)}\right)\left(\frac{\chi}{\bar{I}_p} + \frac{2\bar{a}_y^2(\bar{I}_p - \chi)}{\chi}\right)}\right] \tag{V.30}$$

Similarly, for the bending predominant mode, there is obtained

$$\bar{\gamma}_2 \approx -\frac{\bar{a}_y}{\chi}\left[1 - \frac{\bar{a}_y^2(\bar{I}_p - \chi)}{\chi^2}\right] \tag{V.31}$$

$$\bar{\lambda}_2^2 \approx \frac{E^*}{G}\mu^4\left[\frac{1}{1 - \frac{\bar{a}_y^2\chi}{\chi^2 + \bar{a}_y^2(\bar{I}_p - \chi)}}\right] \tag{V.32}$$

A summary of the various couplings and frequencies for different wave lengths is given in Table I. The frequencies are written in the form of the products of the corresponding uncoupled frequency and a correction factor. In this way, not only the corrections to uncoupled frequencies can easily be seen, but also the nature of the coupled mode, whether bending predominant or torsion predominant, can be identified by noting the factor representing the uncoupled frequency in front. The modifications for the frequencies of the coupled vibrations can be summarized in one statement: the coupling has the effect of splitting up the original uncoupled frequencies,

TABLE I

| CASE | CONDITIONS | $\bar{\gamma}_1$ | $\bar{\gamma}_2$ | $\bar{\lambda}_1^2/\left(\frac{E^*}{G}\mu^4\right)$ | $\bar{\lambda}_2^2/\left(\frac{E^*}{G}\mu^4\right)$ |
|---|---|---|---|---|---|
| A | $\frac{\bar{\Gamma}_d}{\mu^2} - \frac{E^*}{G}(\bar{\Gamma}_p - \bar{\Gamma}_{\omega\omega}) = \frac{E^*}{G}\frac{1}{\epsilon}$ <br> $0 < \epsilon \ll 1$ | $\bar{a}_y\epsilon$ | $\frac{-(1+\bar{a}_y\epsilon)}{\bar{a}_y(1+\bar{\Gamma}_p\epsilon)}$ | $1 - \bar{a}_y^2\epsilon$ | $\left(1+\frac{1}{\bar{\Gamma}_p\epsilon}\right)\frac{\left[1+3\bar{a}_y^2\epsilon\right]}{\left[1-(\bar{a}_y^2/\bar{\Gamma}_p)\right]}$ |
| B | $\frac{\bar{\Gamma}_d}{\mu^2} - \frac{E^*}{G}(\bar{\Gamma}_p - \bar{\Gamma}_{\omega\omega}) = \frac{E^*}{G}\epsilon$ <br> $0 < \epsilon \ll 1$ | $\frac{1}{(\bar{\Gamma}_p+\epsilon)^{\frac{1}{2}}}\left[1-\frac{\epsilon}{2\bar{a}_y\bar{\Gamma}_p^{\frac{1}{2}}}\right]$ | $\frac{-1}{(\bar{\Gamma}_p+\epsilon)^{\frac{1}{2}}}\left[1+\frac{\epsilon}{2\bar{a}_y\bar{\Gamma}_p^{\frac{1}{2}}}\right]$ | $\left(1+\frac{\epsilon}{\bar{\Gamma}_p}\right)\frac{\left[1-(\epsilon/2\bar{\Gamma}_p)\right]}{\left[1+(\bar{a}_y/\bar{\Gamma}_p^{\frac{1}{2}})\right]}$ | $\frac{1+(\epsilon/2\bar{\Gamma}_p)}{1-(\bar{a}_y/\bar{\Gamma}_p^{\frac{1}{2}})}$ |
| C | $\frac{\bar{\Gamma}_d}{\mu^2} - \frac{E^*}{G}(\bar{\Gamma}_p - \bar{\Gamma}_{\omega\omega}) = 0$ | $\frac{1}{\bar{\Gamma}_p^{\frac{1}{2}}}$ | $-\frac{1}{\bar{\Gamma}_p^{\frac{1}{2}}}$ | $\frac{1}{1+(\bar{a}_y/\bar{\Gamma}_p^{\frac{1}{2}})}$ | $\frac{1}{1-(\bar{a}_y/\bar{\Gamma}_p^{\frac{1}{2}})}$ |
| D | $\frac{\bar{\Gamma}_d}{\mu^2} - \frac{E^*}{G}(\bar{\Gamma}_p - \bar{\Gamma}_{\omega\omega}) = -\frac{E^*}{G}\epsilon$ <br> $0 < \epsilon \ll 1$ | $\frac{1}{(\bar{\Gamma}_p-\epsilon)^{\frac{1}{2}}}\left[1+\frac{\epsilon}{2\bar{a}_y\bar{\Gamma}_p^{\frac{1}{2}}}\right]$ | $\frac{-1}{(\bar{\Gamma}_p-\epsilon)^{\frac{1}{2}}}\left[1-\frac{\epsilon}{2\bar{a}_y\bar{\Gamma}_p^{\frac{1}{2}}}\right]$ | $\frac{1-(\epsilon/2\bar{\Gamma}_p)}{1+(\bar{a}_y/\bar{\Gamma}_p^{\frac{1}{2}})}$ | $\left(1-\frac{\epsilon}{\bar{\Gamma}_p}\right)\frac{\left[1+(\epsilon/2\bar{\Gamma}_p)\right]}{\left[1-(\bar{a}_y/\bar{\Gamma}_p^{\frac{1}{2}})\right]}$ |
| E | $\frac{\bar{\Gamma}_d}{\mu^2} - \frac{E^*}{G}(\bar{\Gamma}_p - \bar{\Gamma}_{\omega\omega}) = -\frac{E^*}{G}\chi$ <br> $\chi > 0$ <br> $\frac{\chi^2}{4\bar{a}_y^2(\bar{\Gamma}_p-\chi)} > 1$ | $\frac{\chi}{\bar{a}_y(\bar{\Gamma}_p-\chi)}\left[1+\frac{\bar{a}_y^2(\bar{\Gamma}_p-\chi)}{\chi^2}\right]$ | $\frac{-\bar{a}_y}{\chi^2}\left[1-\frac{\bar{a}_y^2(\bar{\Gamma}_p-\chi)}{\chi^2}\right]$ | $\left(1-\frac{\chi}{\bar{\Gamma}_p}\right)\left[1+\left(\frac{\bar{a}_y^2(\bar{\Gamma}_p-\chi)}{\chi^2+3\bar{a}_y(\bar{\Gamma}_p-\chi)}\right)\left(\frac{\chi^2+2\bar{a}_y\bar{\Gamma}_p(\bar{\Gamma}_p-\chi)}{\bar{\Gamma}_p\chi}\right)\right]^{-1}$ | $\left[1-\frac{\bar{a}_y^2\chi}{\chi^2+\bar{a}_y^2(\bar{\Gamma}_p-\chi)}\right]^{-1}$ |

making the higher frequency higher, and the lower frequency lower.

It is interesting to consider a practical example to clarify what is meant by long or short wave lengths in the various cases discussed. A split thin-walled tube having a cross section of a semi-circular ring is taken as an example. The diameter of the tube is 2" and the wall thickness is 1/16 inch. It will be informative to calculate the length of the beam that corresponds to the situation where the uncoupled bending and torsional vibration frequencies are equal. The values of the geometric properties of such a section can be taken from Table II.

$$r = 0.707"; \quad \bar{I}_p = 2.00; \quad \bar{I}_{\omega\omega} = 0.048; \quad \bar{I}_d = 0.0026$$

For the condition as stated in case C in Table I, i.e. $\frac{\bar{I}_d}{\mu^2} = \frac{E^*}{G}(\bar{I}_p - \bar{I}_{\omega\omega})$, there is obtained

$$\left(\frac{\ell}{r}\right)^2 = \frac{\pi^2 E^*(\bar{I}_p - \bar{I}_{\omega\omega})}{G\bar{I}_d} = (3.14)^2(48.3)^2$$

$$\ell \approx 107.5"$$

For a tube of two inches in diameter, a length of 107.5" is considered a long beam by common practice. For beams in common use, the length would, in general, fall in the case E category in Table I.

When the length of the beam is such that the uncoupled torsional and bending frequencies are the same, $|\bar{\gamma}_1|$ is equal to $|\bar{\gamma}_2|$; and it is not possible to denote which coupled mode is bending predominant and which is torsion predominant.

In addition to the length, the parameter $\bar{a}_y/\bar{I}_p^{\frac{1}{2}}$ is a good indicator of the frequency corrections in the coupled vibrations. Referring to Table I, it can be seen that in case A, the correction for the torsional mode is of the order $(\bar{a}_y/\bar{I}_p^{\frac{1}{2}})^2$. The corrections in cases B, C, and D are of the order $\bar{a}_y/\bar{I}_p^{\frac{1}{2}}$ in both modes. The correction in case E is of the order $\bar{a}_y^2/\chi$. In this case, the length of the beam is short and $\bar{I}_d/\mu^2$ can be considered small. Also, $\bar{I}_{\omega\omega} << \bar{I}_p$ for most thin-walled sections. In view of the condition stated in case E in Table I, $\chi \approx \bar{I}_p$, and the correction is then of the order $(\bar{a}_y/\bar{I}_p^{\frac{1}{2}})^2$. Since $\left| \frac{\bar{a}_y^2}{\bar{I}_p} \right| = \left| \frac{Aa_y^2}{Aa_y^2 + I_g} \right| < 1$, the corrections for frequencies are greatest in the range when the uncoupled bending and torsional frequencies are near each other. This fact has been shown graphically by Gere and Lin in their spectrum plots[2].

3. Effect of Shear Coupling in Uncoupled Bending and Torsional Vibrations

Before the effects of various parameters in the higher order theory for coupled torsional and bending vibrations are investigated, it is interesting to apply the same technique used in section 2 to show the modifications involved when the shear strain energy is also considered in the cases of uncoupled bending and torsional vibrations. The case of uncoupled bending vibrations taking into account the effect of shear and rotary inertia is generally known as the Timoshenko beam theory[16]. It has been studied extensively in many

technical papers; and is generally considered to be a better approximate theory than the Euler-Bernoulli beam theory when the wave length involved is short.

Considering the case of bending vibrations in the X direction, the strain energy and kinetic energy expressions can be written as

$$V = \frac{1}{2}\int_0^{\ell} \left[E^* I_{xx} \xi_b''^2(z,t) + GA\xi_s'(z,t)\right] dz \qquad (V.33)$$

$$T = \frac{1}{2}\int_0^{\ell} \rho\left[A\dot{\xi}^2(z,t) + I_{xx}\dot{\xi}_b'^2(z,t)\right] dz \qquad (V.34)$$

The first term in (V.33) represents the strain energy due to bending action, under the assumption that plane sections remain plane during deformation. The second term in (V.33) gives the contribution of shearing effect to the strain energy. The first term in (V.34) represents the lateral inertia and the second term represents the rotary inertia effect. Let

$$\xi = \xi_b + \xi_s, \quad \text{and} \quad \begin{Bmatrix} \xi_b(z,t) \\ \\ \xi_s(z,t) \end{Bmatrix} = \begin{Bmatrix} \Xi_b(z) \\ \\ \Xi_s(z) \end{Bmatrix} \sin \lambda t$$

From Rayleigh's principle, the frequency is given by

$$\lambda^2 = \frac{\int_0^{\ell} \left[E^* I_{xx} \Xi_b''^2 + AG\Xi_s'^2\right] dz}{\int_0^{\ell} \rho\left[A(\Xi_b + \Xi_s)^2 + I_{xx}\Xi_b'^2\right] dz} \qquad (V.35)$$

For a simply supported beam, ($\xi = \xi_b'' = 0$ at both ends), the mode shape is sinusoidal. Let

$$\begin{Bmatrix} \Xi_b \\ \Xi_s \end{Bmatrix} = \begin{Bmatrix} 1 \\ \bar{\beta} \end{Bmatrix} \sin \frac{\pi z}{\ell}$$

where $\bar{\beta}$ is the ratio of the amplitudes of $\Xi_s$ to $\Xi_b$. Substituting in (V.35), there is obtained

$$\bar{\lambda}^2 = \frac{\lambda^2 \rho r^2}{G} = \frac{\mu^2 (\frac{E^*}{G}\mu^2 + \bar{\beta}^2)}{(1+\bar{\beta})^2 + \mu^2} \qquad (V.36)$$

The value of $\bar{\beta}$ is found by setting $\partial\bar{\lambda}^2/\partial\bar{\beta} = 0$, giving

$$\bar{\beta}^2 + \bar{\beta}(1 + \mu^2 - \frac{E^*}{G}\mu^2) - \frac{E^*}{G}\mu^2 = 0 \qquad (V.37)$$

$$\bar{\beta} = -\frac{1}{2}(1 + \mu^2 - \frac{E^*}{G}\mu^2) \pm \frac{1}{2}\left[(1 + \mu^2 - \frac{E^*}{G}\mu^2)^2 + 4\frac{E^*}{G}\mu^2\right]^{\frac{1}{2}} \qquad (V.38)$$

Only the lower mode of the Timoshenko theory is of interest because in the lower mode, the bending action is the main feature and the shear effect is a modification. Seeking the root of $\bar{\beta}$ which gives a smaller absolute value, the positive sign in (V.38) is taken.

$$\bar{\beta} = -\frac{1}{2}(1 + \mu^2 - \frac{E^*}{G}\mu^2) + \frac{1}{2}\left[(1 + \mu^2 - \frac{E^*}{G}\mu^2)^2 + 4\frac{E^*}{G}\mu^2\right]^{\frac{1}{2}} \qquad (V.39)$$

For the range of wave numbers in which the approximate theory is valid, $\mu$ is small and the shear coupling parameter $\bar{\beta}$ can be approximated to

$$\bar{\beta} = \frac{1}{2}(1 + \mu^2 - \frac{E^*}{G}\mu^2)\left[-1+1+\frac{2E^*\mu^2}{G(1+\mu^2-\frac{E^*}{G}\mu^2)^2} + \ldots\right] \approx \frac{E^*}{G}\mu^2 + O(\mu^4) \qquad (V.40)$$

Substituting the approximate value of $\bar{\beta}$ in (V.36), there is obtained

$$\bar{\lambda}^2 = \frac{E^*}{G}\mu^4\left[1 - \mu^2\left(1 + \frac{E^*}{G}\right) + O(\mu^4)\right] \qquad (V.41)$$

The correction term for the frequency is given by the second term in (V.41) and is proportional to $\mu^2$. Therefore, the important geometric parameter for uncoupled bending vibrations is the ratio of the radius of gyration to that of the length of the beam. When $\mu^2$ becomes significant compared to unity, the shear contribution becomes important and the use of the Timoshenko beam theory is necessary.

For the case of uncoupled torsional vibrations for thin-walled sections, the effect of restraint of warping is important and should be considered in addition to St. Venant torsion. In general, each section of the beam tends to warp out of its own plane and if restraints are imposed so that the sections are not free to warp, longitudinal strains and stresses will develop. These longitudinal stresses contribute to the strain energy. The torsional problem including restraint of warping has been treated by Gere[13]. The resulting equation is similar to the Euler-Bernoulli beam equation with an axial load, being:

$$K_1\theta'''' - K_2\theta'' + K_3\ddot{\theta} = 0 \qquad (V.42)$$

where $K_1$, $K_2$ and $K_3$ are all positive constants. The first term represents the effect of longitudinal stresses set up due to restraint of warping. The second term is the restoring force from St. Venant

torsion. The third term is the inertia force term. It is seen that, depending on the magnitude of $K_1$, the effect of warping restraint on the natural frequencies of the system may be significant.

According to the compatibility equations in elasticity, certain shear strain is induced due to the restraint of warping of the sections. Such shear strain has not been considered in (V.42). The case of torsion including the shear strain effect has been studied by Barr[14] for non-circular bars. This problem with special reference to thin-walled open sections is considered in the following paragraphs. The strain energy and kinetic energy for this case can be written as

$$V = \frac{1}{2}\int_0^{\ell}\left[E^{*}I_{\omega\omega}\theta_b''^{2}(z,t) + GI_{hh}\theta_s'^{2}(z,t) + GI_d\theta'^{2}(z,t)\right]dz \quad (V.43)$$

$$T = \frac{1}{2}\int_0^{\ell}\rho\left[I_p\dot{\theta}^{2}(z,t) + I_{\omega\omega}\dot{\theta}_b'^{2}(z,t)\right]dz \quad (V.44)$$

The first term in (V.43) represents the contribution from axial strain; the second term corresponds to the shear strain set up due to the axial strain; and the third term corresponds to the St. Venant type torsional strain. The first term in (V.44) corresponds to the rotational inertia of the section and the second term represents the axial inertia from warping. The form of (V.43) and (V.44) resembles that of the Timoshenko beam equations, namely (V.33) and (V.34), except for the St. Venant torsion term in the strain energy expression.

Considering the case of a simply supported beam, corresponding to the conditions of no rotations at each end and the ends are

free to warp, the mode shapes are again sinusoidal. Let

$$\begin{Bmatrix} \theta_b \\ \theta_s \end{Bmatrix} = \begin{Bmatrix} \gamma \\ \delta \end{Bmatrix} \sin \frac{\pi z}{\ell} \sin \lambda t$$

Substituting in (V.43) and (V.44), the frequency expression can be obtained from Rayleigh's principle:

$$\bar{\lambda}^2 = \frac{\frac{E^*}{G}\bar{I}_{\omega\omega}\mu^4 + \bar{\delta}^2\bar{I}_{hh}\mu^2 + (1+\bar{\delta})^2\bar{I}_d\mu^2}{\bar{I}_p(1+\bar{\delta})^2 + \bar{I}_{\omega\omega}\mu^2} \qquad (V.45)$$

where $\bar{\delta} = \delta/\gamma$. Setting $\partial\bar{\lambda}^2/\partial\bar{\delta} = 0$, there is obtained

$$\bar{\delta}^2 + \bar{\delta}\left[1 + \mu^2\frac{\bar{I}_{\omega\omega}}{\bar{I}_p}\left(1 + \frac{\bar{I}_d - \frac{E^*}{G}\bar{I}_p}{\bar{I}_{hh}}\right)\right] - \frac{\mu^2\bar{I}_{\omega\omega}\left(\frac{E^*}{G}\bar{I}_p - \bar{I}_d\right)}{\bar{I}_p\bar{I}_{hh}} = 0 \qquad (V.46)$$

As in the case of the Timoshenko beam, only the smaller of the two roots is of interest. Hence, there is obtained:

$$\bar{\delta} \approx \frac{\mu^2\bar{I}_{\omega\omega}}{\bar{I}_{hh}\bar{I}_p}\left(\frac{E^*}{G}\bar{I}_p - \bar{I}_d\right) + O(\mu^4) \qquad (V.47)$$

Substituting the approximate value of $\bar{\delta}$ in (V.45), the corresponding frequency becomes

$$\bar{\lambda}^2 \approx \left(\frac{\frac{E^*}{G}\mu^4\bar{I}_{\omega\omega} + \bar{I}_d\mu^2}{\bar{I}_p}\right)\left[1 - \mu^2\frac{\bar{I}_{\omega\omega}}{\bar{I}_p} + O(\mu^4)\right] \qquad (V.48)$$

The first factor in (V.48) is the frequency predicted from Gere's equation for torsional vibration including the effect of warping. It can be seen then that the correction is proportional to $\mu^2$ and also to the ratio of $\bar{I}_{\omega\omega}$ to $\bar{I}_p$. For thin-walled open sections, $\bar{I}_{\omega\omega}$ is small compared to $\bar{I}_p$ in general. Consequently, the shear correction is not as important in torsional vibrations as it is in bending vibrations.

4. Effect of Geometric Parameters on Natural Frequencies

In this section, a study is made of the effect of the cross section of the beam on the difference between the natural frequencies of coupled torsional and bending vibrations predicted by the two theories. Any variation of the cross section is represented by variations of the different geometric parameters such as $I_{xx}$, $I_p$, etc. To study such effect, it is convenient to express explicitly the dependence of natural frequencies on the different geometric parameters.

Using the higher order theory, the strain energy and kinetic energy expressions for a monosymmetric open section can be deduced from (III.14) and (III.17). They can be written as

$$V = \frac{1}{2}\int_0^{\ell} \left[E^* I_{xx}\xi_b''^2 + E^* I_{\omega\omega}\theta_b''^2 + GI_{cc}\xi_s'^2 + GI_{hh}\theta_s'^2 + 2GI_{hc}\xi_s'\theta_s' + GI_d\theta'^2\right] dz \qquad (V.49)$$

$$T = \frac{1}{2}\int_0^{\ell} \rho\left[A\dot{\xi}^2 + I_p\dot{\theta}^2 + 2a_y A\dot{\theta}\dot{\xi} + I_{xx}\dot{\xi}_b'^2 + I_{\omega\omega}\dot{\theta}_b'^2\right] dz \qquad (V.50)$$

For simply supported end conditions, let

$$\begin{Bmatrix} \frac{\xi_b}{r}(z,t) \\ \frac{\xi_s}{r}(z,t) \\ \theta_b(z,t) \\ \theta_s(z,t) \end{Bmatrix} = \begin{Bmatrix} 1 \\ \beta \\ \gamma \\ \delta \end{Bmatrix} \sin\frac{\pi z}{\ell} \sin\lambda t \qquad (V.51)$$

Substituting (V.51) into (V.49) and (V.50), applying Rayleigh's principle, and grouping the terms in a convenient way, there is obtained

$$\bar{\lambda}^2 = \frac{\frac{E^*}{G}\mu^4(1+\beta)^2 + \gamma^2(1+\bar{\delta})^2\left(\frac{E^*}{G}\mu^4\bar{I}_{\omega\omega} + \mu^2\bar{I}_d\right)}{(1+\beta)^2 + \bar{I}_p\gamma^2(1+\bar{\delta})^2 + 2\bar{a}_y\gamma(1+\beta)(1+\bar{\delta}) + \mu^2 + \mu^2\bar{I}_{\omega\omega}\gamma^2}$$

$$+ \frac{\mu^2\left[\bar{I}_{cc}\beta^2 + \bar{I}_{hh}\gamma^2\bar{\delta}^2 + 2\bar{I}_{hc}\beta\gamma\bar{\delta}\right]}{(1+\beta)^2 + \bar{I}_p\gamma^2(1+\bar{\delta})^2 + 2\bar{a}_y\gamma(1+\beta)(1+\bar{\delta}) + \mu^2 + \mu^2\bar{I}_{\omega\omega}\gamma^2}$$

$$- \frac{\mu^4\frac{E^*}{G}\left[2\beta + \beta^2 + 2\bar{I}_{\omega\omega}\gamma^2\bar{\delta} + \bar{I}_{\omega\omega}\gamma^2\bar{\delta}^2\right]}{(1+\beta)^2 + \bar{I}_p\gamma^2(1+\bar{\delta})^2 + 2\bar{a}_y\gamma(1+\beta)(1+\bar{\delta}) + \mu^2 + \mu^2\bar{I}_{\omega\omega}\gamma^2} \qquad (V.52)$$

where $\bar{\delta} = \delta/\gamma$. The correct values of $\beta$, $\gamma$, $\bar{\delta}$ can be determined by the conditions $\partial\bar{\lambda}^2/\partial\beta = 0$, $\partial\bar{\lambda}^2/\partial\gamma = 0$, and $\partial\bar{\lambda}^2/\partial\bar{\delta} = 0$. This will result in a set of coupled inhomogeneous algebraic equations in $\beta$, $\gamma$, and $\bar{\delta}$. To solve such a set of equations explicitly is difficult, if not impossible. To solve the problem approximately, the following assumptions are made:

(i) The shear coupling $\beta$ between $\xi_b$ and $\xi_s$ in the coupled bending and torsional vibrations is approximately the same as given by the uncoupled bending vibrations, i.e., equation (V.40).

(ii) The shear coupling $\overline{\delta}$ between $\theta_b$ and $\theta_s$ in the coupled bending and torsional vibrations is approximately equal to that given by the uncoupled torsional vibrations, i.e., equation (V.47).

(iii) The torsion and bending coupling $(\frac{\gamma+\delta}{1+\beta})$ between $\xi$ and $\theta$ in the higher order theory is approximately equal to that $(\overline{\gamma})$ given by Gere's theory, i.e., equation (V.11).

From the assumptions (i), (ii), and (iii), there is obtained

$$\beta \approx \frac{E^*}{G}\mu^2$$

$$\overline{\delta} \approx \mu^2 \frac{\overline{I}_{\omega\omega}}{\overline{I}_p \overline{I}_{hh}} \left(\frac{E^*}{G}\overline{I}_p - \overline{I}_d\right) \approx \frac{E^*}{G}\mu^2 \frac{\overline{I}_{\omega\omega}}{\overline{I}_{hh}} \qquad \text{(V.53)}$$

$$\gamma \approx \frac{\overline{\gamma}(1+\beta)}{(1+\overline{\delta})}$$

Substituting the approximate values of $\beta$, $\gamma$, and $\overline{\delta}$ in (V.52), the frequency expression is given by

$$\bar{\lambda}^2 = \frac{\frac{E^*}{G}\mu^4 + \bar{\gamma}^2\left(\frac{E^*}{G}\bar{I}_{\omega\omega}\mu^4 + \bar{I}_d\mu^2\right) - \mu^6\left(\frac{E^*}{G}\right)^2\left(2 - \bar{I}_{cc} + \bar{\gamma}^2\frac{\bar{I}_{\omega\omega}^2}{\bar{I}_{hh}} - 2\bar{\gamma}\frac{\bar{I}_{hc}\bar{I}_{\omega\omega}}{\bar{I}_{hh}}\right) + O(\mu^8)}{1 + \bar{I}_p\bar{\gamma}^2 + 2\bar{a}_y\bar{\gamma} + \mu^2(1 + \bar{\gamma}^2\bar{I}_{\omega\omega}) + O(\mu^4)}$$

$$\approx \frac{\frac{E^*}{G}\mu^4 + \bar{\gamma}^2\left(\frac{E^*}{G}\bar{I}_{\omega\omega}\mu^4 + \bar{I}_d\mu^2\right)}{1 + \bar{I}_p\bar{\gamma}^2 + 2\bar{a}_y\bar{\gamma}}$$

$$- \frac{\mu^6\left[\left(\frac{E^*}{G}\right)^2\left(2 - \bar{I}_{cc} + \bar{\gamma}^2\frac{\bar{I}_{\omega\omega}^2}{\bar{I}_{hh}} - 2\bar{\gamma}\frac{\bar{I}_{hc}\bar{I}_{\omega\omega}}{\bar{I}_{hh}}\right) + \left(\frac{1 + \bar{\gamma}^2\bar{I}_{\omega\omega}}{1 + \bar{I}_p\bar{\gamma}^2 + 2\bar{a}_y\bar{\gamma}}\right)\left(\frac{E^*}{G} + \bar{\gamma}^2\frac{E^*}{G}\bar{I}_{\omega\omega} + \bar{\gamma}^2\frac{\bar{I}_d}{\mu^2}\right)\right]}{1 + \bar{I}_p\bar{\gamma}^2 + 2\bar{a}_y\bar{\gamma}} \qquad (V.54)$$

From (V.9), the frequency expression from Gere's theory is

$$\bar{\lambda}_G^2 = \frac{\frac{E^*}{G}\mu^4 + \bar{\gamma}^2\left(\frac{E^*}{G}\bar{I}_{\omega\omega}\mu^4 + \bar{I}_d\mu^2\right)}{1 + \bar{I}_p\bar{\gamma}^2 + 2\bar{a}_y\bar{\gamma}}$$

Therefore,

$$\frac{\bar{\lambda}^2 - \bar{\lambda}_G^2}{\bar{\lambda}_G^2} = -\mu^2\left\{\frac{\frac{E^*}{G}\left(2 - \bar{I}_{cc} - 2\bar{\gamma}\frac{\bar{I}_{hc}\bar{I}_{\omega\omega}}{\bar{I}_{hh}} + \bar{\gamma}^2\frac{\bar{I}_{\omega\omega}^2}{\bar{I}_{hh}}\right)}{1 + \bar{\gamma}^2\left(\bar{I}_{\omega\omega} + \frac{G}{E^*}\frac{\bar{I}_d}{\mu^2}\right)} + \frac{(1 + \bar{\gamma}^2\bar{I}_{\omega\omega})}{1 + \bar{I}_p\bar{\gamma}^2 + 2\bar{a}_y\bar{\gamma}}\right\} \qquad (V.55)$$

The relation of various geometric parameters to the difference of frequencies predicted from the two theories is shown in (V. 55). It can be seen that the difference of the square of the natural frequencies is proportional to $\mu^2$. Thus, the difference is small when the wave length is long; as shown in all the plotted spectrum curves. For a fixed wave length, $\mu^2$ is fixed and the difference in frequencies becomes large if $\bar{I}_{\omega\omega}$, $\bar{I}_{\omega\omega}/\bar{I}_{hh}$ are large, and $\bar{I}_{cc}$ is small. The values of the geometric parameters of various sections are given in Table II. From the table, it can be seen that as the semi-central angle $\Phi$ of the section increases from $15^\circ$ to $180^\circ$, $\bar{I}_{\omega\omega}$ and $\bar{I}_{\omega\omega}/\bar{I}_{hh}$ increase monotonicly, and $\bar{I}_{cc}$ decreases to a minimum at $\Phi = 135^\circ$. This explains the increase in the difference in frequencies predicted by the two theories for the different cross sections, as noted in section 3 of Chapter 4.

Table II

CALCULATION OF SECTIONAL PROPERTIES OF SPLIT CIRCULAR RING

radius = 1", thickness = 1/16"

| $\Phi$ deg. | L Distance of centroid to center in. | A $in.^2$ | r in. | $\bar{a}_y$ | $\bar{I}_p$ | $\bar{I}_{\omega\omega}$ | $\bar{I}_{cc}$ | $\bar{I}_{hc}$ | $\bar{I}_{hh}$ |
|---|---|---|---|---|---|---|---|---|---|
| 15 | 0.988 | 0.033 | 0.150 | -0.122 | 1.019 | 0 | 0.977 | 0.030 | 0.005 |
| 30 | 0.955 | 0.065 | 0.294 | -0.248 | 1.080 | 0.002 | 0.913 | 0.055 | 0.024 |
| 45 | 0.900 | 0.098 | 0.426 | -0.383 | 1.189 | 0.005 | 0.818 | 0.071 | 0.058 |
| 60 | 0.827 | 0.131 | 0.542 | -0.532 | 1.361 | 0.011 | 0.707 | 0.071 | 0.117 |
| 75 | 0.738 | 0.164 | 0.636 | -0.702 | 1.619 | 0.023 | 0.595 | 0.051 | 0.216 |
| 90 | 0.637 | 0.196 | 0.707 | -0.900 | 2.000 | 0.048 | 0.500 | 0 | 0.379 |
| 105 | 0.527 | 0.229 | 0.754 | -1.136 | 2.560 | 0.101 | 0.432 | -0.093 | 0.648 |
| 120 | 0.413 | 0.262 | 0.777 | -1.417 | 3.381 | 0.217 | 0.397 | -0.241 | 1.089 |
| 135 | 0.300 | 0.295 | 0.779 | -1.749 | 4.560 | 0.481 | 0.394 | -0.455 | 1.799 |
| 150 | 0.191 | 0.327 | 0.763 | -2.126 | 6.174 | 1.082 | 0.417 | -0.741 | 2.884 |
| 165 | 0.090 | 0.360 | 0.737 | -2.514 | 8.144 | 2.415 | 0.457 | -1.082 | 4.369 |
| 180 | 0 | 0.393 | 0.707 | -2.828 | 10.000 | 5.159 | 0.500 | -1.414 | 6.000 |

# Chapter 6

# EXPERIMENTAL VERIFICATION OF THE APPROXIMATE THEORIES

## 1. Introduction

In the previous chapters, Gere's theory is compared with a higher order theory which serves to check the range of validity of Gere's theory. It is shown from the spectrum curves that for small wave number, the two theories predict almost the same result, indicating that the elementary theory is good for long beams. However, the range of wave length over which the higher order theory is valid is still undetermined. In order to provide an indication of the validity of the higher order theory, either a yet higher order approximate theory may be constructed and checked against the developed higher order theory, or the approximate theories can be verified directly by experiment. In this chapter an account is presented of the experiments performed to verify the accuracy of the two approximate theories.

In section 2, the set up of the experiment is described. This includes the preparation of the test specimens and the instrumentation used. The actual experimental procedure is described in section 3. The experimental results are plotted against the calculated results given by the two approximate theories and a discussion of the results is given in section 4.

2. Experimental Set Up

In order to compare the theoretical and experimental results, the specimens used should necessarily have the same cross section as those used in the calculations of the spectrum curves in chapter 4. Such specimens were realised by splitting thin-walled circular aluminum tubes along their lengths with the proper central angle. The actual aluminum tubes used were ALCOA 6061T6WWT789 with an outer diameter of two inches and a thickness of 1/16 inch. Two specimens were prepared, one subtending a central angle of $180^{\circ}$ (half ring), and the other, an angle of $270^{\circ}$. The specimens were examined to ensure that any pretwist resulting from the release of the internal stresses during the cutting process was negligibly small. One end of the specimen was cast into a block of "Cerobase," a low melting high density alloy, to form a built-in end (i.e., the end conditions were such that there was no deflection, no rotation, no slope and complete restraint of warping). The other end was left free so that the system constituted a cantilever. The specimen was cast in such a way that the axis of symmetry of the section would be perpendicular to the direction of the excitation of the shaking table when the block was mounted on it. With the specimen mounted this way, there would be little or no excitation in the direction parallel to the axis of symmetry and hence the uncoupled bending vibration would not be excited. The block was mounted rigidly onto the shaking table by four steel bolts. Preferably, the size of the casting should be large enough to ensure that the fixed end conditions are satisfied and yet sufficiently

light to be within the capability of the shaking table. A compromise was necessary and the actual size used was 4" × 4" × 2-1/2". This cantilever open section beam constituted the mechanical system to be tested.

The experiment was carried out in the Vibrations Laboratory in Thomas Engineering Laboratory at California Institute of Technonogy. A Ling shaking table was used with a B & K oscillator control to give the forcing input to the cantilever beam. The B & K control panel had an automatic frequency sweep device which could vary the frequency of the shaking table either upward or downward at a specified rate. The frequency range of the shaker was from 5 - 5000 cycles per second with the resonant frequency of the table itself around 3800 cps.

The amplitude of the shaker was controlled by a feedback relay with an Endevco accelerometer (Accelerometer I) mounted on the table top to supply the feedback signal to the B & K control. The amplitude could be controlled by requiring the displacement of the table top to be constant. Alternately, the velocity or acceleration could be kept constant. A fourth alternative to control the amplitude was a setting called "Auto" on the panel. Under the "Auto" control, the displacement was kept constant at the lower frequency range and switched over to an acceleration constant control at a preset cross over frequency. When the range of the frequency was large, this method of controlling the amplitude was specially valuable since it could avoid excessive displacements at the lower frequency range and

yet gave sufficient excitation at the higher frequency range. The actual frequency of the shaking table was also displayed on an H. P. counter mounted on the control panel. The counter had a gate time of 1/10 second and 1 second. Using the 1 second gate time, the frequency of the shaker could be determined to within ± 1 cps.

The response of the beam could not be measured directly by mounting transducers on the beam because the mass of an ordinary transducer is comparable to that of the beam, and the additional mass on the beam would alter its natural frequency. An optical method was used to pick up the response of the system. The Optron, essentially a displacement measuring device, was used. The Optron is designed to measure the motion of its targets. A target is a small piece of cardboard, half of which is painted black and the other half has a shiny surface. When the Optron is in adjustment, a beam of light from the Optron is directed towards the boundary between the reflective and the dull parts of the target. Half of the amount of light sent out from the Optron is reflected back into the device from the reflective portion of the target. Any movement of the target causes variation in the amount of light reflected back to the Optron. The amount of light reflected back from the target serves as a feedback signal to a servo-mechanism in the Optron which in turn serves to keep the light beam centered on the target. A voltage proportional to the movement of the target is the output of the Optron. Various calibrated lenses are available to accommodate different ranges of displacement requirements. The particular lens used during the

experiment was Model 711, #12286 Canon, which gave a maximum displacement range of 0.1 inch peak to peak. When a target was mounted at some point on the beam, the response of the beam at that point could be ascertained.

The main interest in the experiment was the measurement of the resonant frequencies of the various modes of the beam. No attempt was made to measure the mode shapes. From the theory of self-adjoint operators[17], it can be shown that the eigenvalues are much more sensitive parameters than the eigenfunctions. It can then be argued that when the theoretical and experimental values of the resonant frequencies agree, the corresponding mode shapes will essentially be those predicted by the theory. Also, the actual shapes of the resonance curves (i.e., response of the system against external exciting frequency) are not of prime interest because no attempt is made to determine the material damping from the experiment. This justified the use of the output of the Optron as the response of the beam although the Optron was actually measuring the absolute displacement of the target while the response of the system should be reckoned relative to the base of the beam. The actual resonance curve could be derived from the response plot from the Optron when the displacement of the base was also measured.

Since the resonant frequency was the parameter of interest, it was not necessary to feed the output from the Optron into a recording oscillograph to obtain a time history of the response. Instead, the signal from the Optron was taken into the Moseley Logarithmic

Converter Model 60B. This device accepts an electrical signal at its input and produces at its output another signal which is the logarithm of the input. Also, this device accepts A. C. from 20 - 20,000 cps and converts it to D. C. with a value equal to the r. m. s. value of the input. The dynamic range of the instrument is 60 db which gives it a range of 1,000 : 1 ratio. The output of the Moseley Logarithmic Converter was fed into the Y axis of a Moseley Plotter. The X axis of the plotter was connected to the automatic frequency sweep of the B & K console. A plot of the response spectrum could then be obtained from the Moseley Plotter.

It was found necessary to pass the signal from the Optron through a band pass filter before feeding it into the Moseley Logarithmic Converter in order to cut out the 60 cycle noise that was inherent in the table. Measurements were made to determine the magnitude of the 60 cycle noise using the controlling accelerometer (Accelerometer I) on the shaker as the transducer. The noise was measured on the Ballentine r. m. s. Voltmeter Model 320 and found to be equivalent to a magnitude of $\frac{1}{2}$ g in acceleration. The existence of the 60 cycle noise at the shaker was a problem at high frequencies. The reason for this is as follows; let the 60 cycle noise be $n \sin 120\pi t$ and the signal for the accelerator on the table be $\sin 2\pi ft$. The total acceleration input is

$$\ddot{x} = \sin 2\pi ft + n \sin 120\pi t$$

and

$$x = -\frac{1}{(2\pi f)^2} \sin 2\pi ft - \frac{n}{(120\ \pi)^2} \sin 120\ \pi t$$

Thus, the noise to signal ratio is $n$ in acceleration and is $n(f/60)^2$ in displacement. If $(f/60)$ is larger than unity, the noise to signal ratio is magnified rapidly. Since the Optron was a displacement measuring device, the noise problem was significant. A free run (no load on the table) with and without the use of filter was made and the plots of the response are shown in Figures 10 and 11. The effect of the 60 cycle noise in the higher frequency range can be seen clearly. The response curves show the displacement of a steel bolt mounted on top of the table measured by the Optron. A Model 330-MR Krohn-Hite ultra low frequency band pass filter was then used. The attenuation of the filter is shown in Figure 12. It was found that a low filter setting at 150 cps would suppress the 60 cycle noise sufficiently and yet had very little attenuation for frequencies over 200 cps. Hence, it was decided to introduce the low band pass filter at a setting of 150 cps when the table frequency was at 200 cps in all subsequent testing. The high filter was set at 2500 cps. The arrangement of the test specimen on the shaker is shown in Figure 13.

Before the actual testing, a trial run was performed to check the amplitude control of the table top. It was done with and without the test specimen mounted on the table. The acceleration was measured by Accelerometer I. Plots of the response curves are shown in Figure 14. It can be seen that the unloaded table gave a cleaner trace. Certain irregularities in the traces were due to the interaction of the specimen and the table when the specimen was in resonance. A Stroboscope was used to check that there was no

# FIG. 10 DISPLACEMENT OF FREE TABLE
## Measured By Optron Without Filter

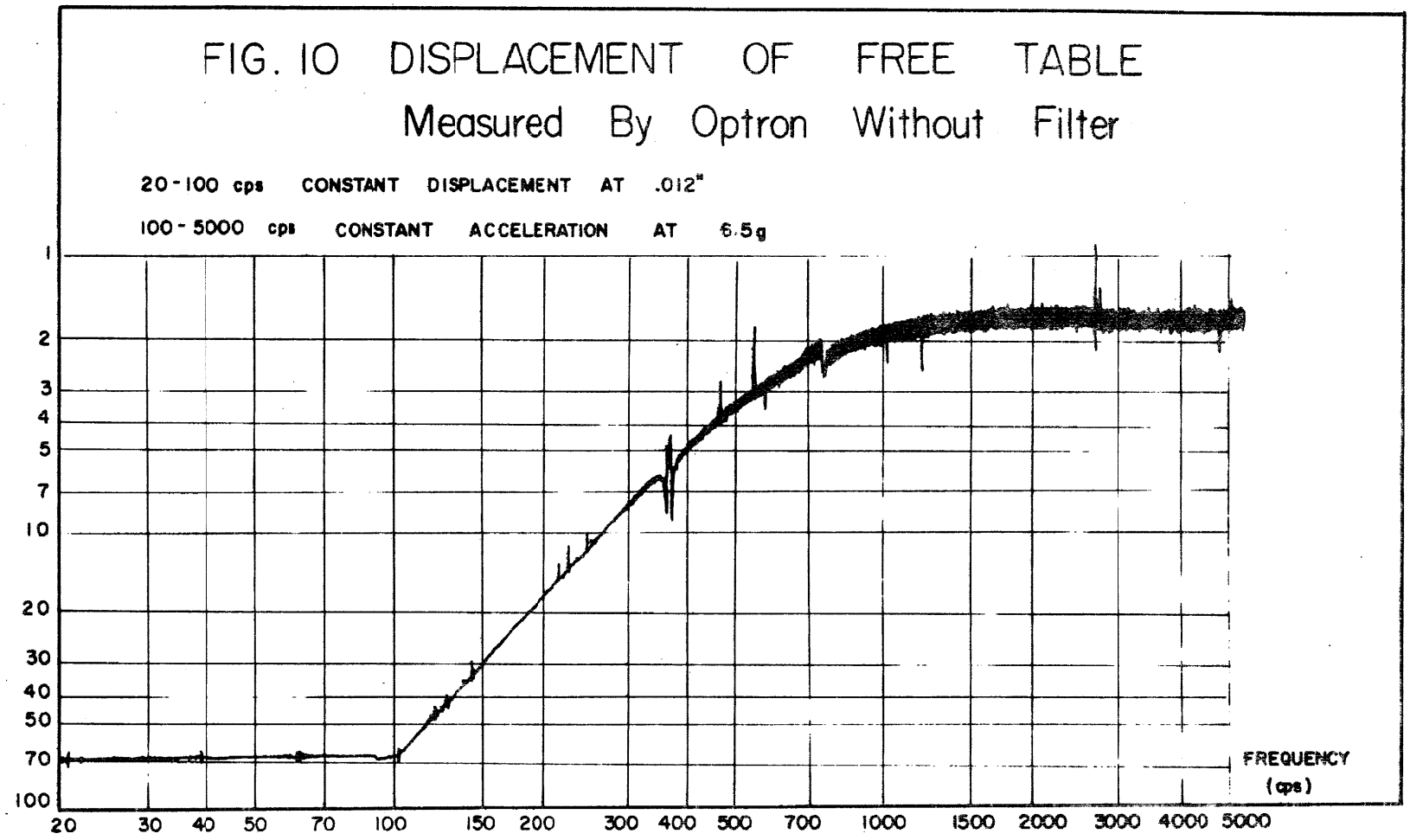

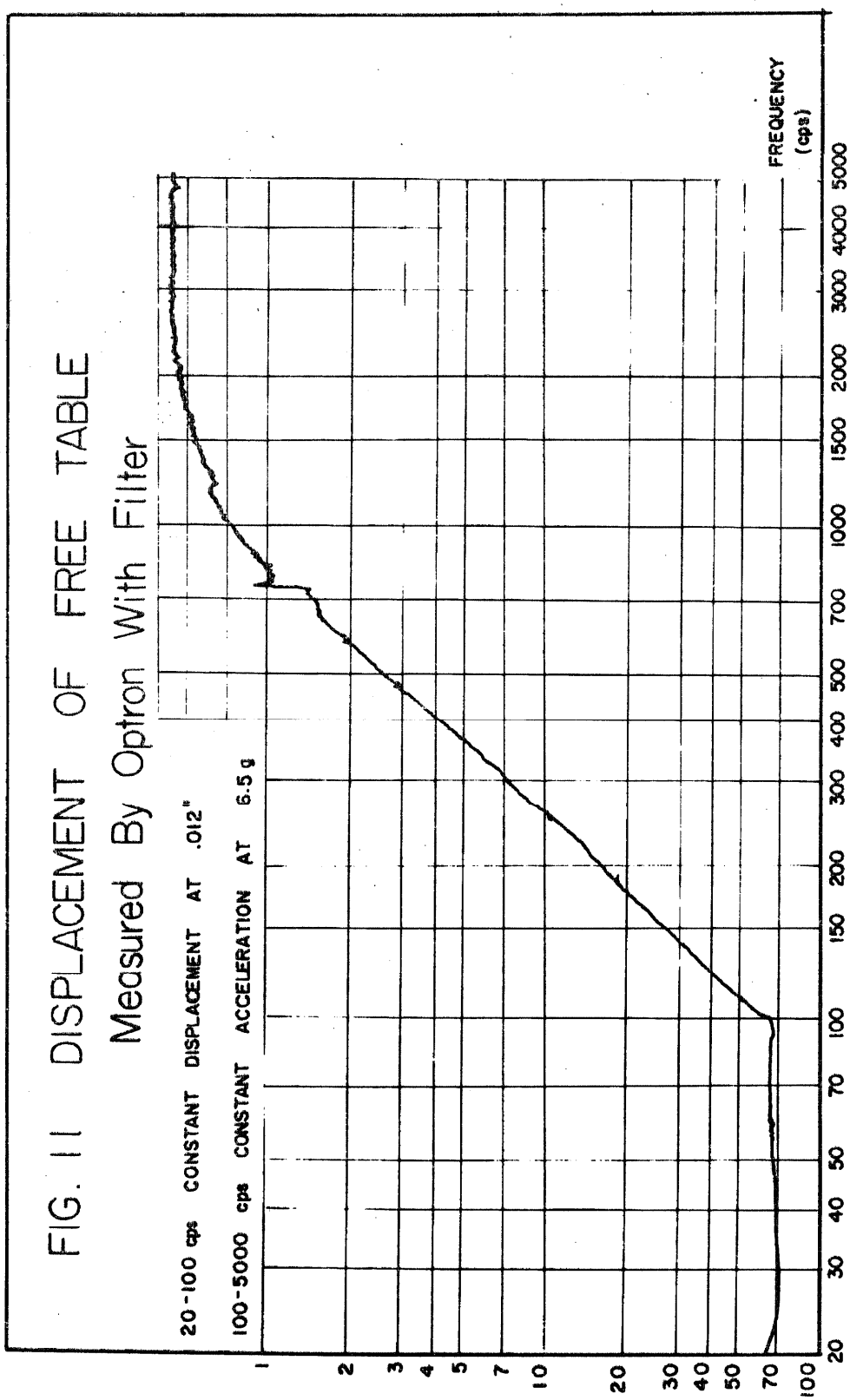
FIG. 11 DISPLACEMENT OF FREE TABLE
Measured By Optron With Filter
20-100 cps CONSTANT DISPLACEMENT AT .012"
100-5000 cps CONSTANT ACCELERATION AT 6.5 g
1
2
3
4
5
7
10
20
30
40
50
70
100
20
30
40
50
70
100
150
200
300
400
500
700
1000
1500
2000
3000
4000
5000
FREQUENCY (cps)

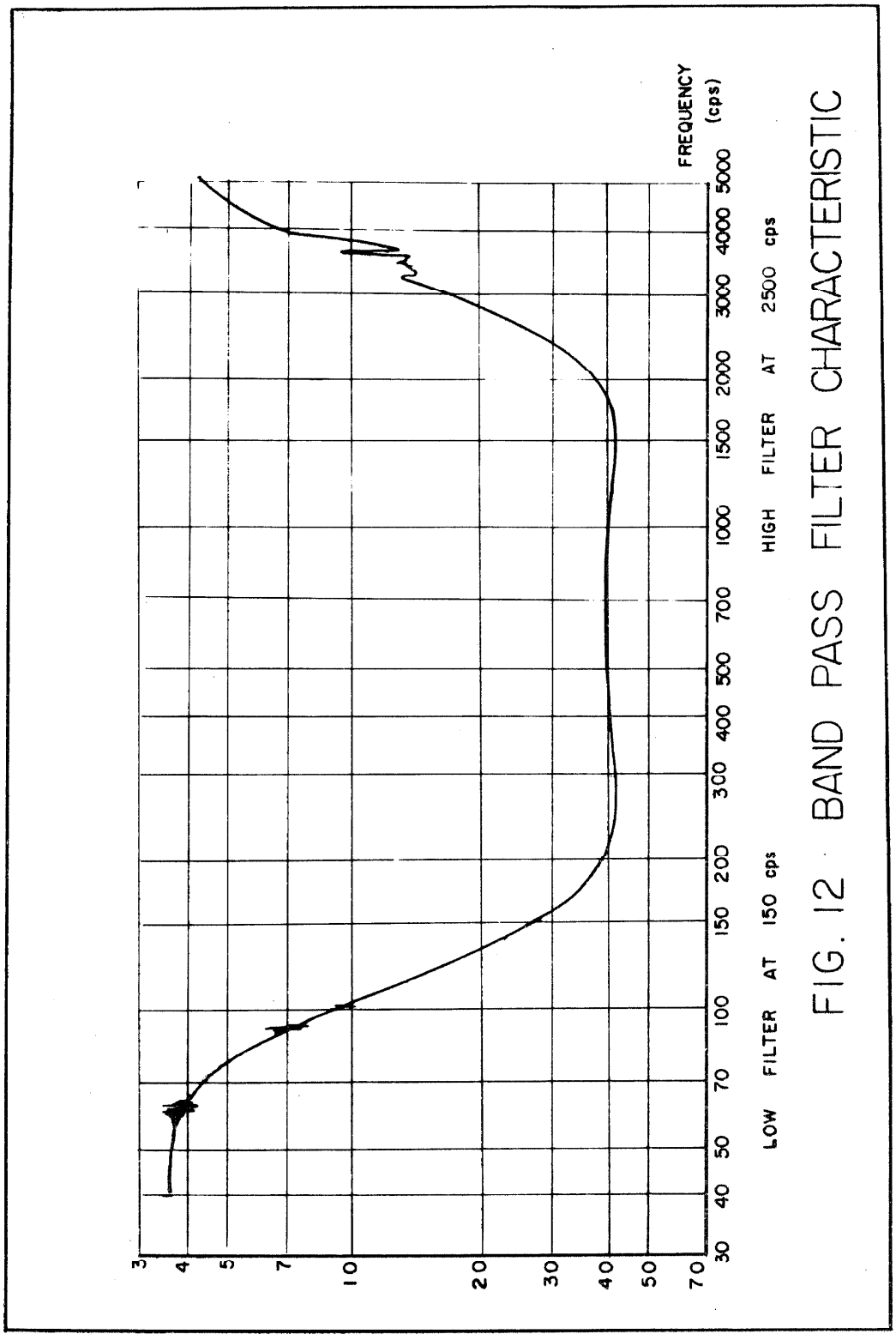


FIG. 12 BAND PASS FILTER CHARACTERISTIC

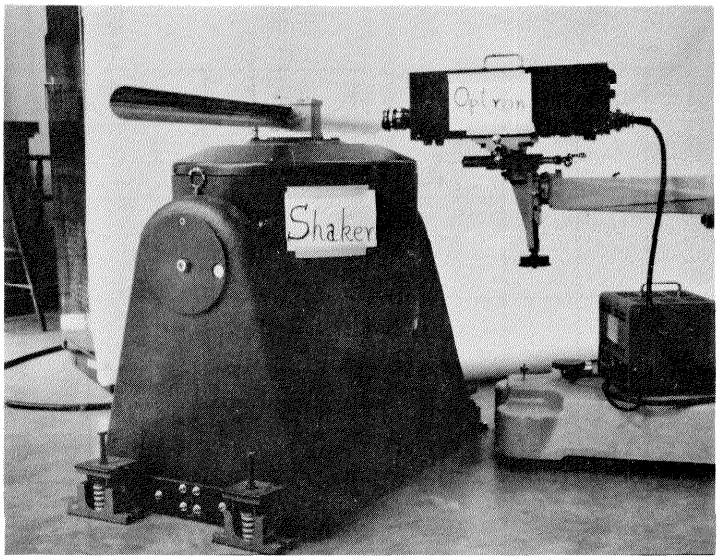


FIG. 13

MOUNTING OF TEST SPECIMEN (DOUBLE CANTILEVER) ON SHAKER

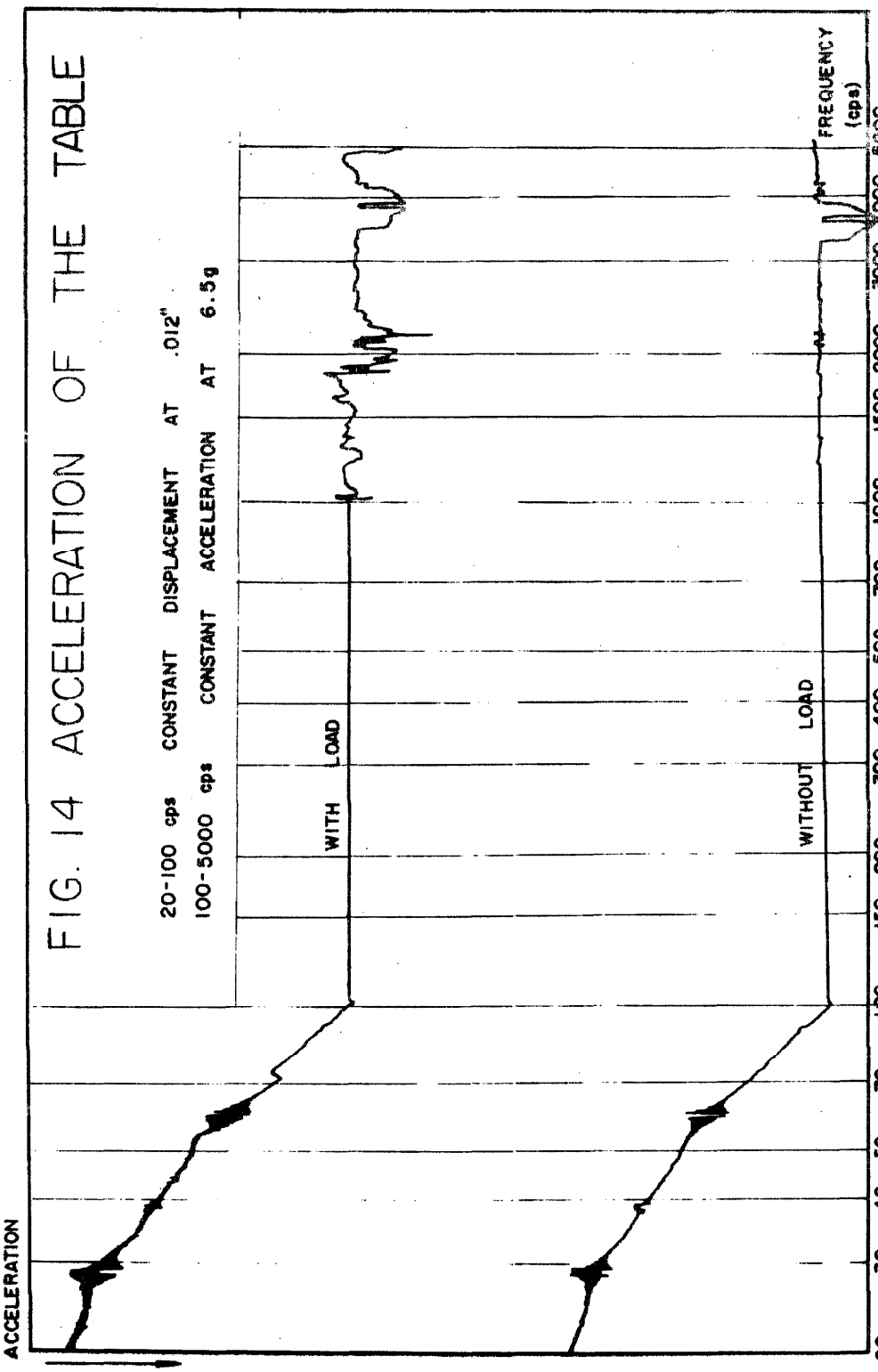
FIG. 14 ACCELERATION OF THE TABLE
20-100 cps CONSTANT DISPLACEMENT AT .012"
100-5000 cps CONSTANT ACCELERATION AT 6.5g
WITH LOAD
WITHOUT LOAD
ACCELERATION
FREQUENCY (cps)
20
30
40
50
70
100
150
200
300
400
500
700
1000
1500
2000
3000
5000

deformation of the cross section during the test by viewing the beam from the free end.

3. Experimental Procedure

Targets for the Optron were placed along the center line of the beam. After sufficient time was allowed for the instruments to warm up, the Optron was set to focus on one of the targets of the beam. The table was set to run at a constant displacement of 0.012" from 20 to 100 cps and then automatically switch over to constant acceleration control at 100 cps. The corresponding acceleration at 100 cps was approximately 6.5 g and was kept constant throughout the test from 100 to 1800 cps. The filter was used for frequencies over 200 cps. A spectrum plot was obtained from the Moseley Plotter as the frequency of the table swept from 20 cps up to 1800 cps. Then, the peaks in the spectrum plot were retraced by decreasing the table frequency from 1800 cps. Fine adjustments of the table frequency near the peak enabled the frequency that corresponded to the true maximum to be read within 1 cps on the H.P. counter. Thus, the spectrum plot gave only a guide to the distribution of the resonant frequencies while the actual resonant frequencies were not read from the plot but were read directly from the H.P. counter.

The whole process was repeated for another target on the beam. This served as a check for the resonant frequencies as measured in the previous target. When the beam was in resonance, the response at each point should be at a local maximum, except at

the nodes. Hence, the resonant frequencies determined from the various targets should be the same.

After the various natural frequencies were determined, a target was attached at the base of the beam and another spectrum curve was plotted for the displacement of the base. This essentially served as a base line for the spectrum plots of all the other targets. Finally, a calibration of the plotter was necessary. A grid was made to give a scale for the different plots. The various modes (whether bending predominant or torsion predominant) could be identified by sensing the number of nodes along the beam during resonance. For both specimens, the torsional rigidity was less than the bending rigidity and the lowest mode was torsion predominant. Also, the response for torsion predominant modes were more violent than that for the bending predominant modes.

After all the modes were identified and frequencies recorded, the specimen was shortened by a predetermined amount and the whole process was repeated. The beam was cut until it became so short that all except one or two of its natural frequencies were outside the test range. Two specimens were tested; one having a section of a half ring and the other subtending a central angle of $270^{o}$.

## 4. Experimental Results and Observations

Four of the actual spectrum plots on the Moseley Plotter are shown in Figures 15 to 18. They are plots for the semi-circular ring section ($\Phi = 90^{o}$) at a length of 19". They show the responses at the

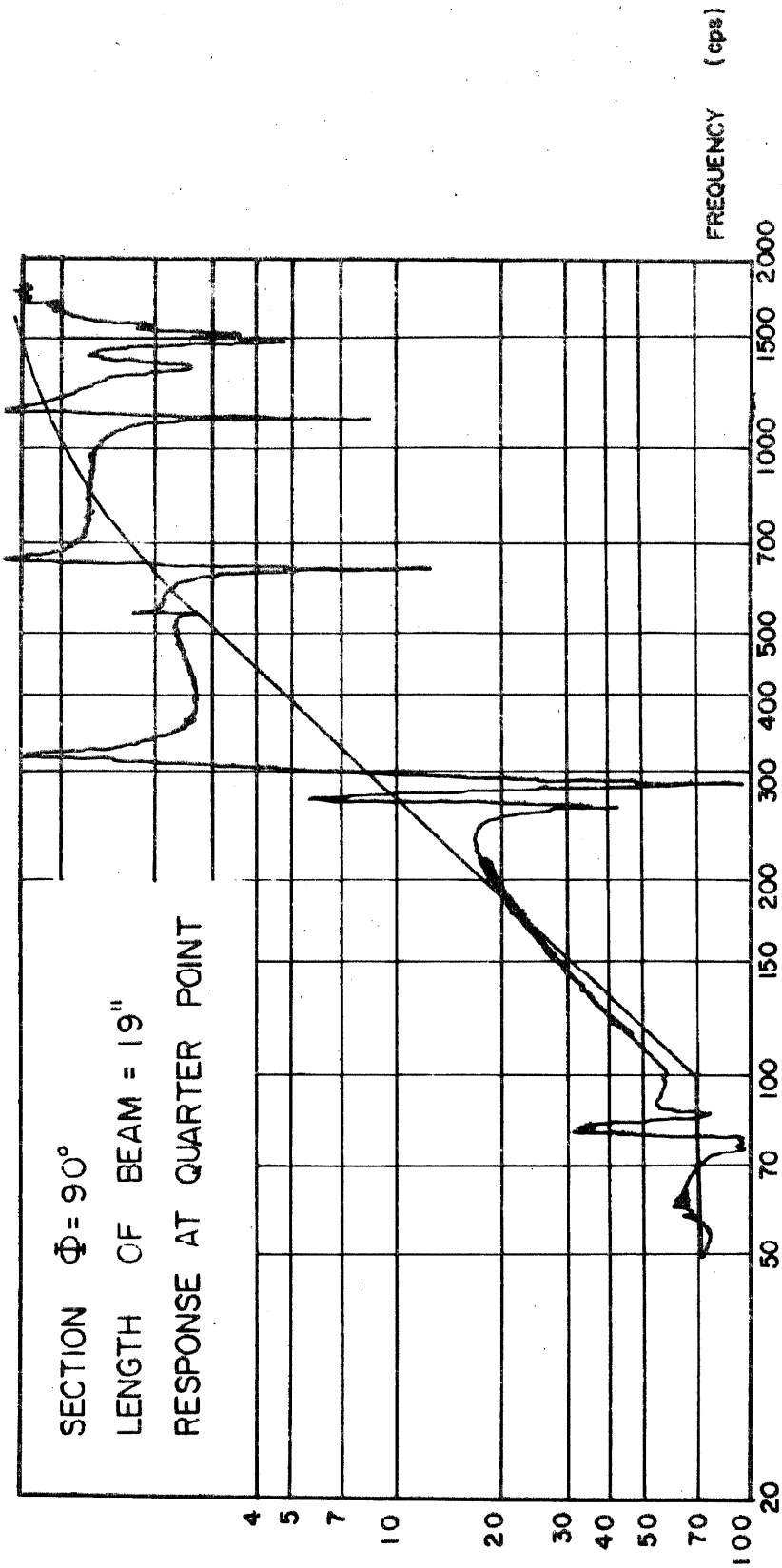


FIG. 15 SPECTRUM PLOT FROM MOSELEY PLOTTER

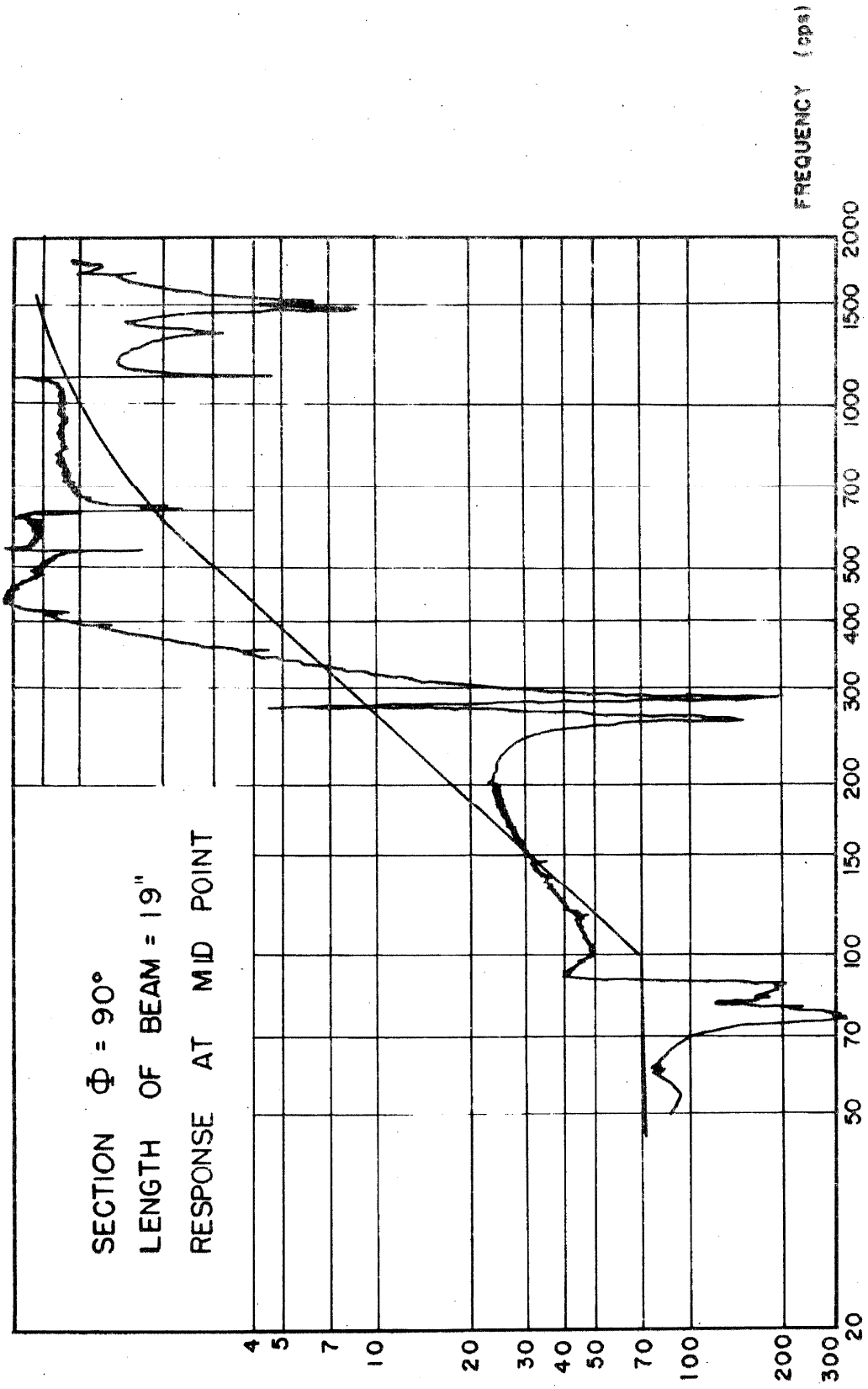


FIG. 16 SPECTRUM PLOT FROM MOSELEY PLOTTER

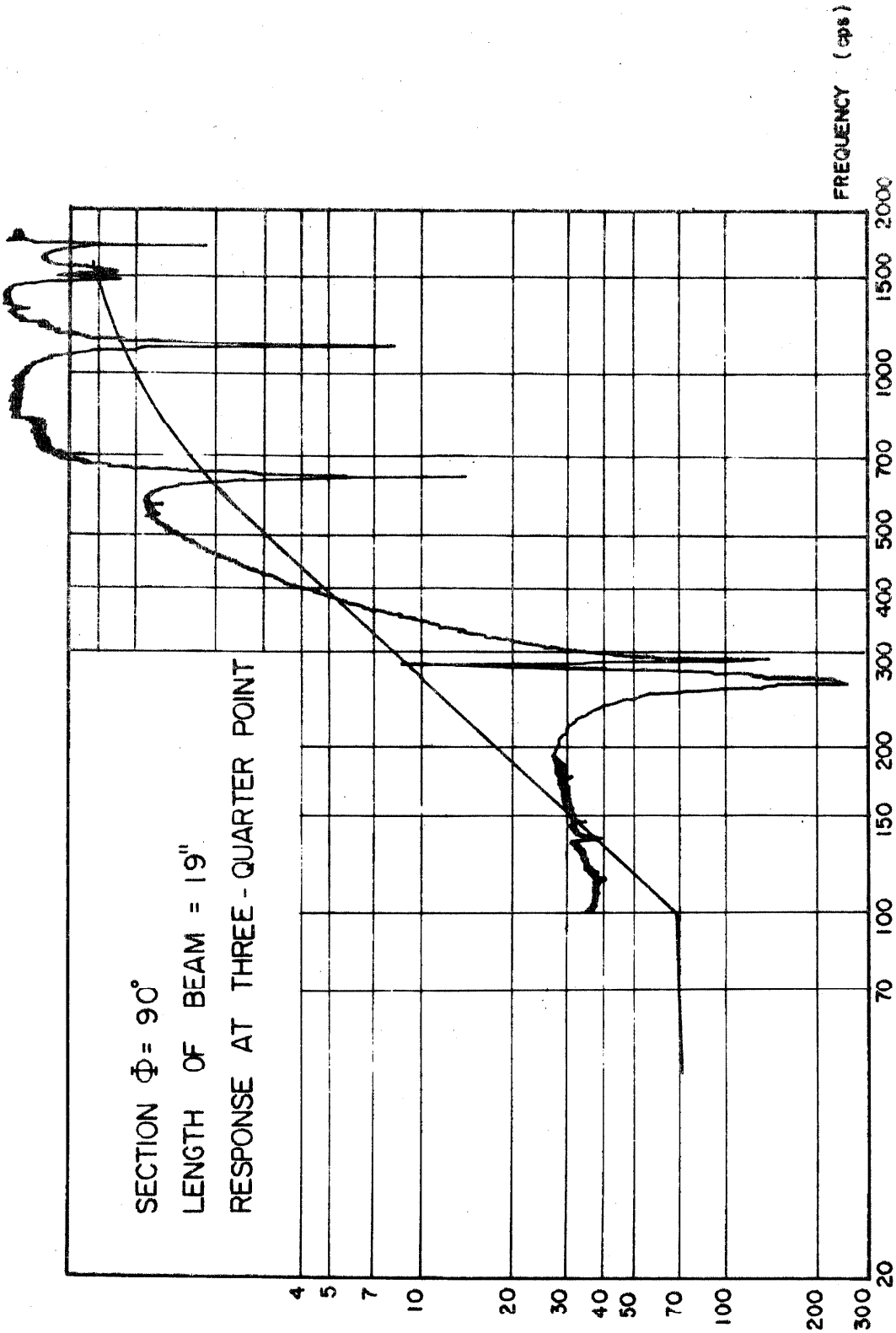


FIG. 17 SPECTRUM PLOT FROM MOSELEY PLOTTER

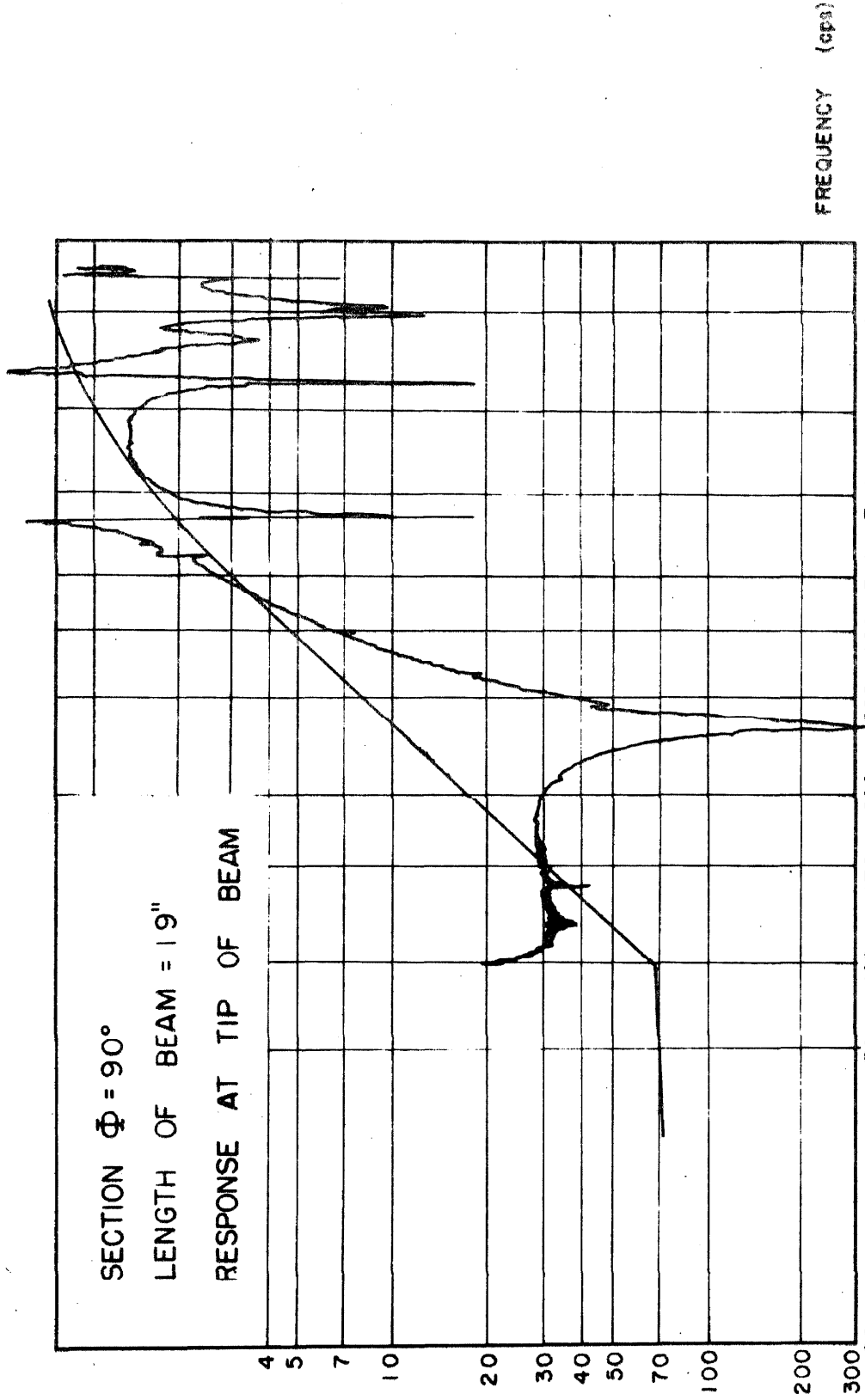


FIG. 18 SPECTRUM PLOT FROM MOSELEY PLOTTER

quarter point, the half point, the three-quarter point and at the tip of the beam. The peaks in the plots correspond to large displacements of the targets and indicate a state of resonance of the beam. The displacement of the base is also shown in the plots to give a baseline to the traces. Certain portions of the curves have a smaller value of displacement than the base. This can be explained by considering the phase relationship between the base and the point in question. The absolute movement of the point is the algebraic sum of the movement of the base and the movement of the point relative to the base. If the response of the point is out of phase by $180^{\circ}$ with the forcing function its movement will be in opposite direction to that of the base. Since the two movements are of opposite signs, the absolute displacement of the point can conceivably be smaller than that of the base.

The experimental results are tabulated in Tables III and IV. The resonant frequencies of six modes are presented. Of these, four are torsion predominant and two are bending predominant. Also the experimental results are compared with theoretical calculations and presented in graphical form. The value of $(1/2\pi)(G/\rho r^2)^{\frac{1}{2}}$ used to convert the non-dimensional frequencies in the spectrum curve calculations to cycles per second is determined by the best fit of the theoretical curve to the experimental values for the first mode of the specimen with semi-central angle $\Phi = 90^{\circ}$. In both specimens, the two approximate theories give essentially the same results for the first mode for the range of wave numbers considered. The fitting is

Table III. EXPERIMENTAL VALUES OF RESONANT FREQUENCIES

$\Phi = 90^{\circ}$

| Length in. | $r/\ell$ | 1st (cps) | 2nd (Bending) | 3rd (cps) | 4th (cps) | 5th (cps) | 6th (Bending) |
|---|---|---|---|---|---|---|---|
| 39.5 | 0.0179 | 29 | 72 | 108 | 202 | 333 | 376 |
| 35 | 0.0202 | 34-35 | 84 | 128 | 244 | 405 | 490 |
| 32 | 0.0221 | 38-39 | 109 | 147 | 280 | 470 | 576 |
| 29 | 0.0244 | 43 | 127 | 162 | 324 | 553 | 694 |
| 26 | 0.0272 | 50 | 154 | 188 | 388 | 669 | 853 |
| 23 | 0.0307 | 62-63 | 188 | 223 | 470 | 818 | 1050 |
| 21 | 0.0337 | 67 | 223 | 252 | 545 | 957 | 1224 |
| 19 | 0.0372 | 77-78 | 263 | 288 | 638 | 1121 | 1480 |
| 17 | 0.0416 | 89-90 | 329 | 345 | 774 | 1364 | 1768 |
| 15 | 0.0472 | 107 | 400 | 400 | 937 | 1650 | - |
| 13.5 | 0.0523 | 121 | 508 | 480 | 1141 | - | - |
| 12 | 0.0589 | 141 | 624 | 579 | 1419 | - | - |
| 10.38 | 0.0681 | 173 | 814 | 730 | 1749 | - | - |
| 8.88 | 0.0800 | 214 | 1066 | 935 | - | - | - |
| 8.0 | 0.0885 | 237 | 1393 | 1033 | - | - | - |

Table IV. EXPERIMENTAL VALUES OF RESONANT FREQUENCIES

$\Phi = 135^{o}$

| Length in. | r/ℓ | 1st (cps) | 2nd (Bending) | 3rd (cps) | 4th (cps) | 5th (cps) | 6th (Bending) |
|---|---|---|---|---|---|---|---|
| 44 | 0.0177 | 21.5 | 81 | 95 | 241 | 447 | 465 |
| 39 | 0.0200 | 26 | 91 | 124 | 302 | 560 | 572 |
| 36 | 0.0216 | 28.5 | 124 | 141 | 353 | 647 | 663 |
| 34 | 0.0229 | 31 | 136 | 156 | 393 | 716 | 736 |
| 31 | 0.0251 | 35 | 160 | 180 | 465 | 836 | 864 |
| 30 | 0.0260 | 37 | 170 | 191 | 491 | 873 | 907 |
| 28 | 0.0278 | 41 | 193 | 217 | 559 | 968 | 1024 |
| 26 | 0.0300 | 45 | 219 | 247 | 633 | 1071 | 1151 |
| 24 | 0.0324 | 62 | 252 | 284 | 723 | 1172 | 1291 |
| 22 | 0.0354 | 68 | 299 | 334 | 837 | 1270 | 1400 |
| 20 | 0.0389 | 76 | 353 | 396 | 965 | 1418 | - |
| 19 | 0.0409 | 81.5 | 385 | 434 | 1032 | - | - |
| 18 | 0.0432 | 89 | 423 | 477 | 1102 | - | - |
| 17 | 0.0457 | 103 | 468 | 529 | 1170 | - | - |
| 16 | 0.0487 | 109 | 505 | 577 | - | - | - |
| 15 | 0.0519 | 123 | 575 | 648 | - | - | - |
| 14 | 0.0556 | 136 | 646 | 729 | - | - | - |
| 13 | 0.0596 | 156 | 739 | 825 | - | - | - |
| 12 | 0.0649 | 180 | 846 | 934 | - | - | - |
| 11 | 0.0708 | 210 | 985 | 1058 | - | - | - |
| 10 | 0.0778 | 249 | 1125 | 1211 | - | - | - |

shown in Figure 19. The value of $K = (1/2\pi)(G/\rho r^2)^{\frac{1}{2}}$ is taken to be 27,000 and this value is used for computing the higher mode spectrum curves. The results are shown in Figure 20. The value of $(1/2\pi)(G/\rho r^2)^{\frac{1}{2}}$ for the section $\Phi = 135^{\circ}$ can be deduced since the two specimens are made of the same material and have the same shear modulus and density. The radius of gyration r for both specimens is given in Table II. The value calculated is approximately 22,000 and this value is used to compute all the spectrum curves for the section $\Phi = 135^{\circ}$. The results are shown in Figures 21 and 22. The resonant frequencies are plotted against wave number for different modes. The solid line represents the values predicted by the higher order theory and the dotted line is the values calculated from Gere's theory.

From the graphs presented, it can be seen that the experimental points agree with the theoretical calculations for small wave numbers. When the length of the beam becomes short, both approximate theories predict a higher value than the experimental result. The higher order theory gives a closer fit than Gere's theory. It is interesting to note that when the two approximate theories give essentially the same result, the experimental points fall right on the theoretical curve. It is only when the two theories begin to differ that the experimental points begin to drop below the theoretical values.

In the bending predominant modes, the curve from Gere's theory departs from the curve from the higher order theory at relatively small wave number. The experimental points fall on the

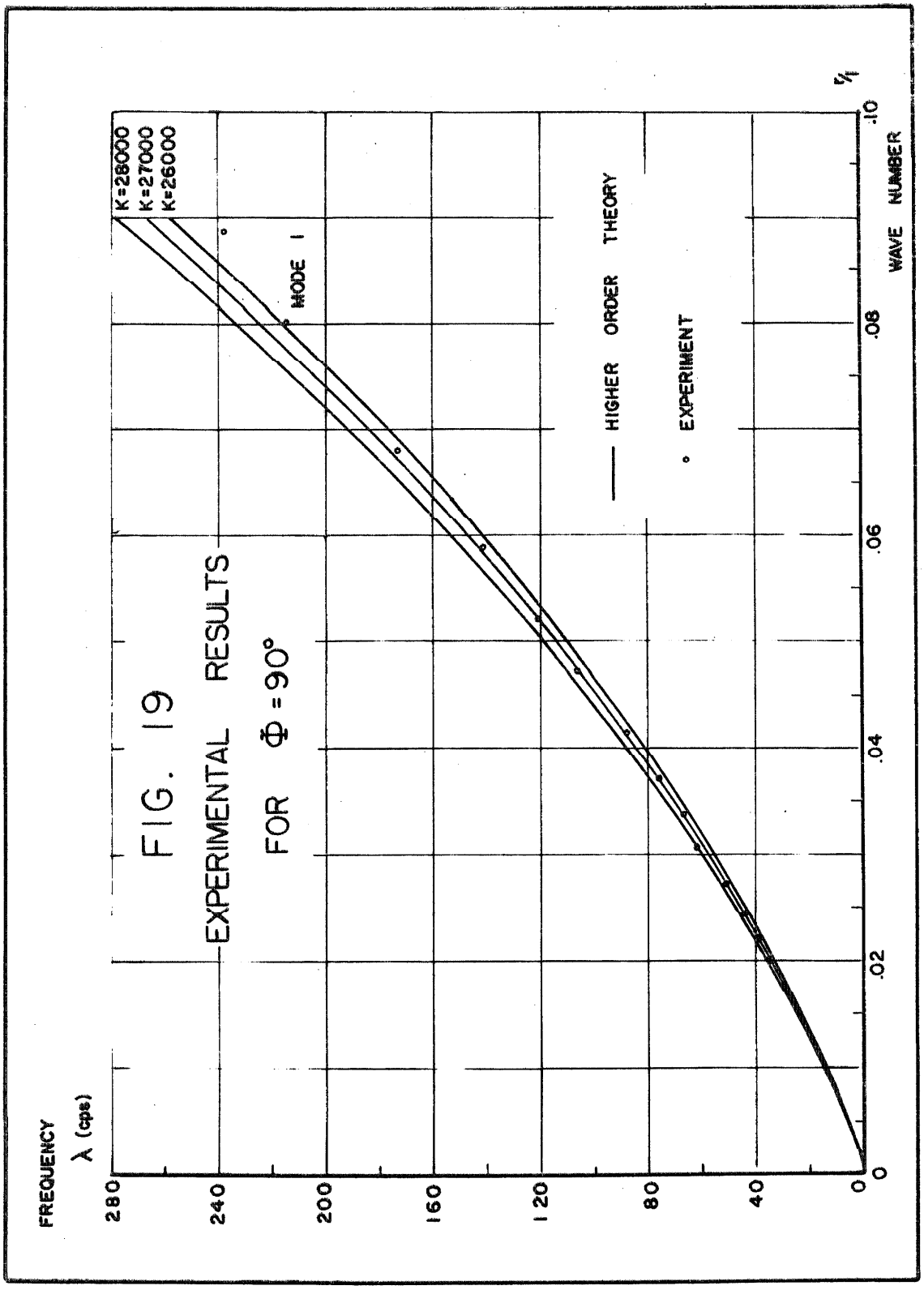


FIG. 19
EXPERIMENTAL RESULTS
FOR $\Phi = 90°$

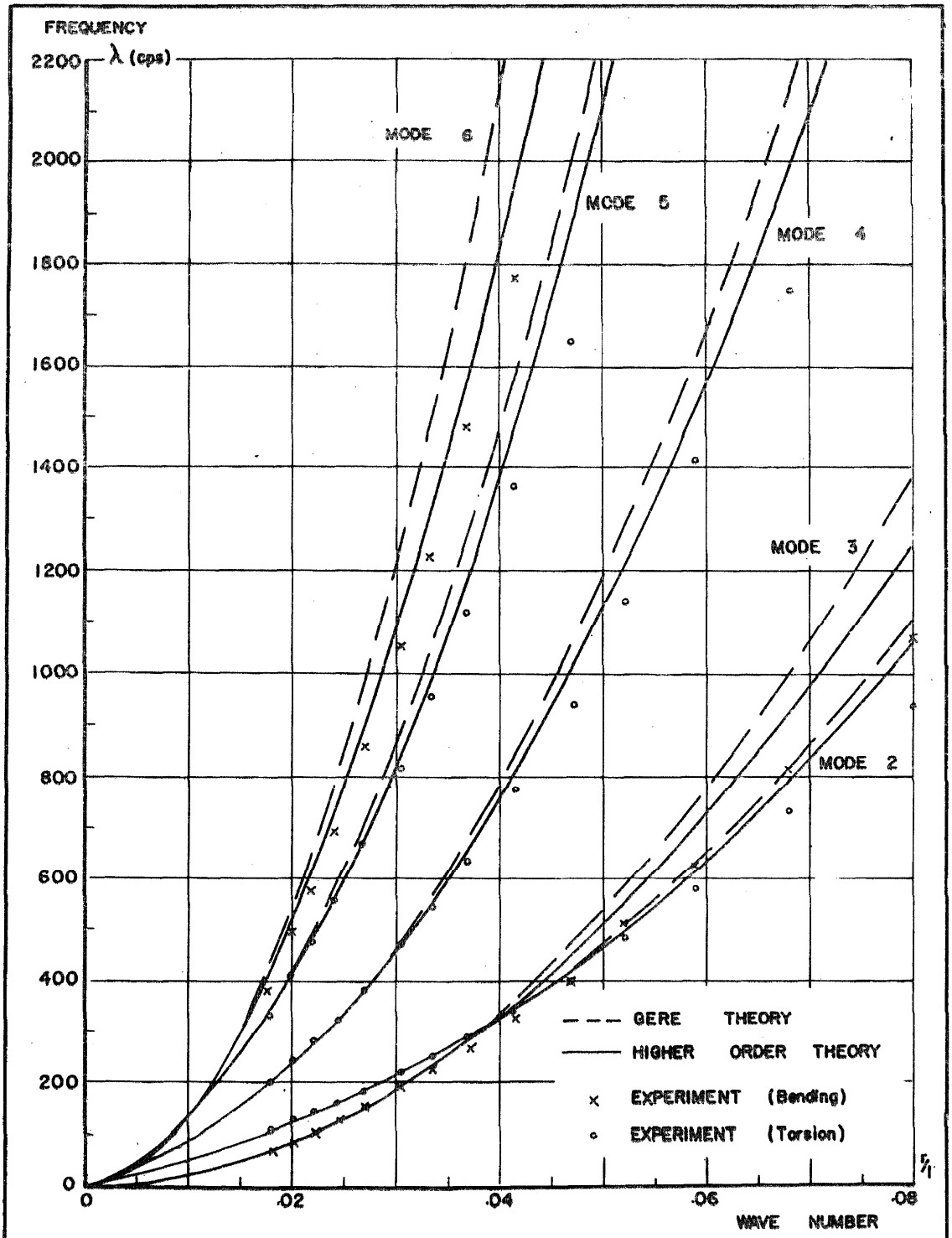


FIG. 20 EXPERIMENTAL RESULTS FOR $\Phi = 90°$

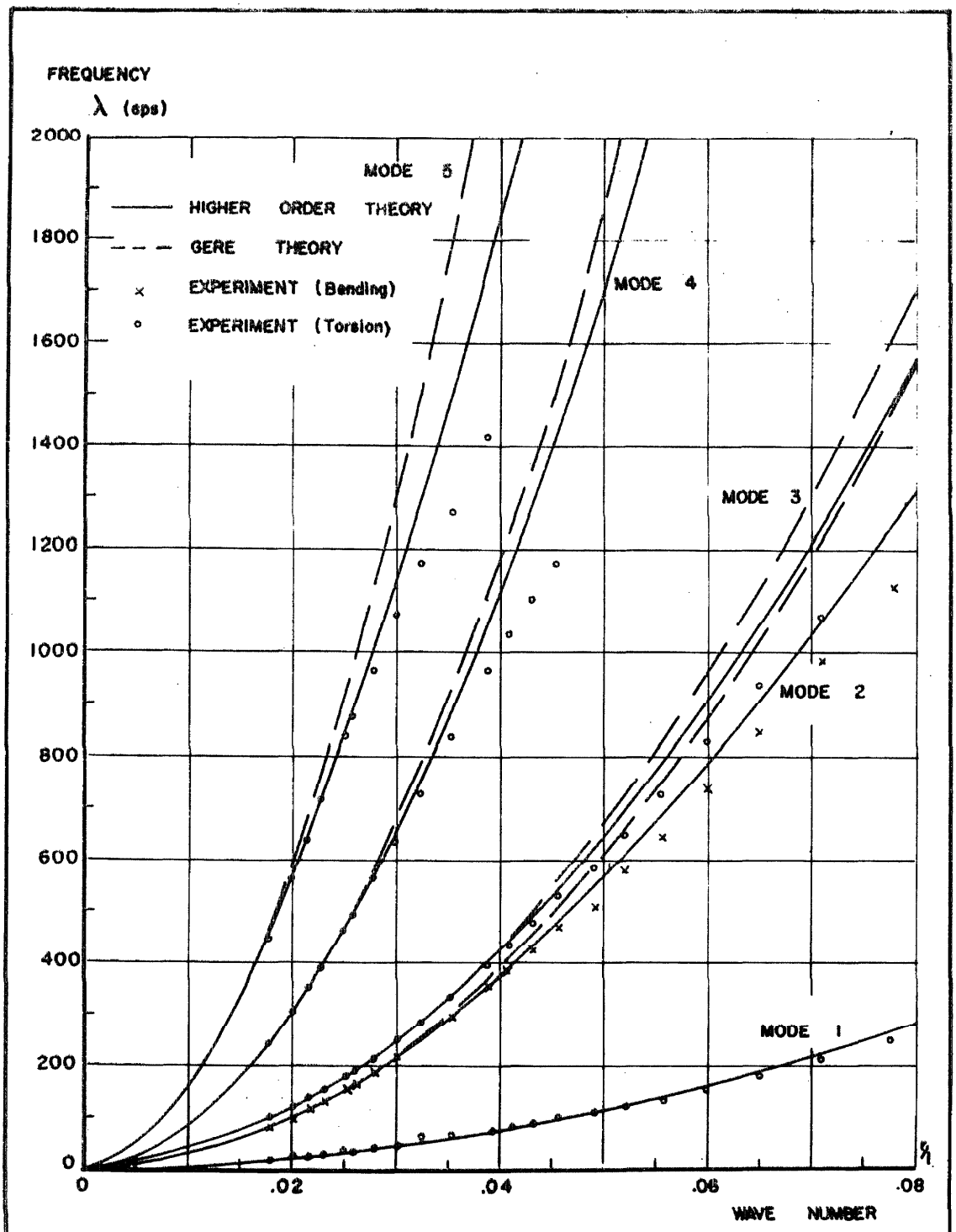


FIG. 21 EXPERIMENTAL RESULTS FOR $\Phi = 135°$

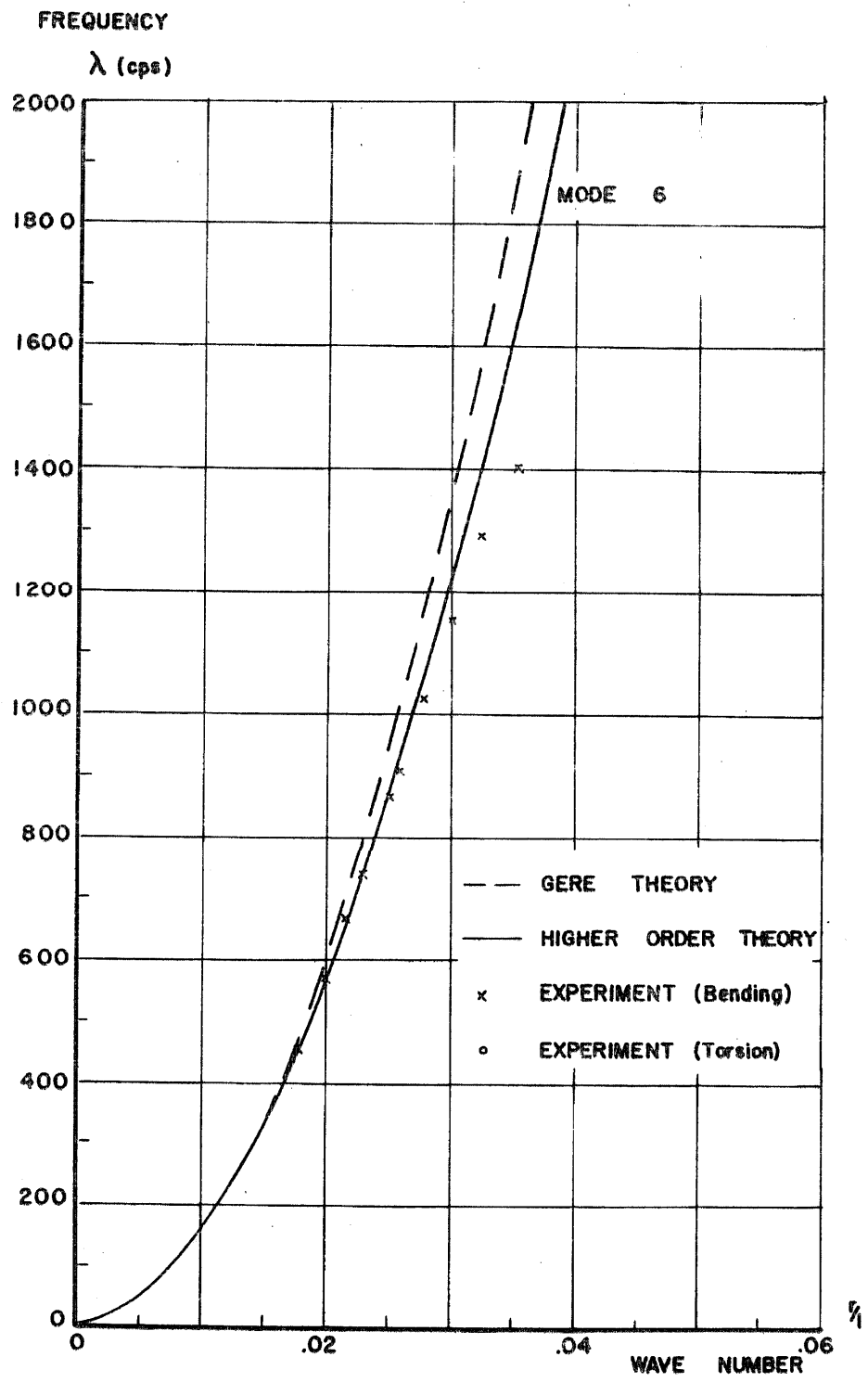


FIG. 22 EXPERIMENTAL RESULTS FOR $\Phi = 135°$

higher order theory curve for a larger range of wave number. This lesser accuracy of Gere's theory in predicting bending predominant mode frequencies could be expected in view of the lesser accuracy of the Euler-Bernoulli theory as compared with the Timoshenko theory in bending.

An examination of the results shown in Figures 19 to 22 suggests that it is useful to divide up the complete range of wave numbers into four categories; namely, "long beam," "medium beam," "short beam," and "very short beam." These categories are defined by comparing the spectrum curves of the elementary theory and the higher order theory. When the results predicted by both theories are essentially the same, the beam is considered long for that particular mode. A "medium beam" is one for which the results predicted by the elementary theory for bending predominant modes begin to differ from the values given by the higher order theory. However, the two theories give essentially the same result for the torsion predominant modes.

"Short beam" covers the range of beam length when the results of the higher modes as predicted by the two theories begin to differ and the two theories give similar results for the first mode only. "Very short beam" represents the range of beam length which the two theories predict different results even for the first mode vibration.

It is interesting to observe that for the section $\Phi = 90^{\circ}$, the spectrum curves cross at a wave number of about 0.04 as shown in Figure 20. For small wave numbers, the second mode corresponds

to a bending predominant mode with no node along the beam. The third mode corresponds to a torsion predominant mode with one node along the beam. However, for wave number larger than 0.04, the situation is reversed with the bending predominant mode having a higher resonant frequency than the torsion predominant mode. According to our convention of numbering the modes, the third mode then becomes bending predominant and the second mode torsion predominant. This exchange of ordering was also observed experimentally. The reason for such crossing lies in the fact that for bending deformations the resonant frequency varies inversely as the fourth power of the length of the beam; while for St. Venant torsion the frequency varies inversely as the second power of the length. The bending frequency increases more rapidly than the torsional frequency as the length of the beam is shortened. Thus, it is reasonable to expect the frequency of a bending predominant mode to be lower than that of a torsion predominant mode for long beams, but higher than the torsion predominant mode for sufficiently short beams. The cross over point results in a degenerate mode.

# Chapter 7

# NONLINEAR BEHAVIOR OF THIN-WALLED BEAM OF OPEN SECTION

## 1. Introduction

In the preceding chapters the dynamic behavior of the thin-walled elastic beam of open section is described and the experimental results are compared with results calculated from linearized theories. The linearization process is justified only if the behavior of the beam can be predicted satisfactorily by the linearized equations. During the course of the experiment, certain behavior was observed which could not be forseen from the linearized equations. The observed phenomenon can be described in two different ways. Taking the beam as a system, the shaking table excitation as the input to the system, and the response of the beam as the output of the system, the phenomenon can be described as being a high order subharmonic oscillation of the system under special conditions. When the shaking table frequency is at a multiple or near multiple of the fundamental frequency of the system and the system has one of its higher natural frequencies at the table frequency, both harmonic and subharmonic oscillations are exhibited by the response of the system, the subharmonic oscillations having a frequency close to the fundamental frequency of the system.

Alternatively, the phenomenon can be described in terms of the vibrational modes of the beam. When a higher mode resonant frequency of the beam is a multiple or near multiple of the lowest

mode, and when the beam is excited at this resonant frequency, there is a tendency for energy to transmit from the highest mode to the lowest mode, resulting very often in a high order subharmonic oscillation.

Most studies in nonlinear mechanics have been of single degree of freedom systems. For a single degree of freedom system subharmonics of high order are generally of very small amplitude and are seldom observed although subharmonics of order $\frac{1}{2}$ or $\frac{1}{3}$ are common. As far as the writer knows, the behavior as observed in his experiments has not been reported before.

In this chapter, a detailed account of this phenomenon as observed during the experiment is given in section 2. An analysis for such behavior is presented in the subsequent sections. Intuitively, such behavior can be explained in terms of the interaction of modes through nonlinear couplings.

When the rotation of the section is not infinitesimal, the linearization relationship of (III. 6) may not be valid. If such approximation is not made, the character of the governing equations will be changed. Firstly, the resulting equations become nonlinear in nature. This can be demonstrated from the following consideration. Let equations (I. 1), (I. 2) and (I. 3) be taken to be the equations for bending in the two principal directions and rotation along the axis of the beam. Using equation (III. 5) without assuming (III. 6), the inertial loads $p_x$, $p_y$, and $p_t$ become

$$p_x = -\rho A \frac{\partial^2}{\partial t^2}(\xi + a_y \sin\theta - a_x \cos\theta)$$

$$p_y = -\rho A \frac{\partial^2}{\partial t^2}(\eta - a_x \sin\theta - a_y \cos\theta) \qquad \text{(VII. 1)}$$

$$p_t = -\rho I_g \frac{\partial^2 \theta}{\partial t^2} - \rho A a_y \frac{\partial^2}{\partial t^2}(\xi + a_y \sin\theta - a_x \cos\theta)$$

$$+ \rho A a_x \frac{\partial^2}{\partial t^2}(\eta - a_x \sin\theta - a_y \cos\theta)$$

Substituting into (I. 1), (I. 2) and (I. 3), the governing equations become

$$EI_{xx}\xi'''' + \rho A\ddot{\xi} + a_y(\sin\theta)^{\cdot\cdot} - a_x(\cos\theta)^{\cdot\cdot} = 0$$

$$EI_{yy}\eta'''' + \rho A\ddot{\eta} - a_x(\sin\theta)^{\cdot\cdot} - a_y(\cos\theta)^{\cdot\cdot} = 0 \qquad \text{(VII. 2)}$$

$$EI_{\omega\omega}\theta'''' - GI_d\theta'' + \rho I_g\ddot{\theta} + \rho A a_y\ddot{\xi} - \rho A a_x\ddot{\eta}$$

$$+ \rho A(a_x^2 + a_y^2)(\sin\theta)^{\cdot\cdot} = 0$$

Comparing the set of equations (VII. 2) to equations (I. 4), (I. 5) and (I. 6), it can be seen that equations (VII. 2) are coupled nonlinear equations with nonlinear terms in the variable $\theta$. It is interesting to note that all three equations are coupled even for a monosymmetric section for which $a_x$ is zero. Only when the section has two axes of symmetry are the bending and torsional vibrations uncoupled.

Another effect of dropping the approximation (III. 6) is the coupling of the torsional motion and the longitudinal movement along the axis of the beam. Such coupling is not due to the asymmetry of

the section and can be termed the "shortening effect"[18]. The coupling between longitudinal motion and torsional motion of the beam can be made plausible as follows. Consider a rectangular strip whose ends are twisted with the end faces kept in the same transverse planes. Let the angle of rotation be $\theta$. An originally straight fibre of length $\ell$ at distance $y$ from the central axis of the strip is deformed into a helix. The length of such a helix described on a cylinder of radius $y$ and length $\ell$ is given by $(\ell^2 + y^2\theta^2)^{1/2}$. The increase in length is $(\ell^2 + y^2\theta^2)^{1/2} - \ell \approx y^2\theta^2/2\ell$. The axial strain is $(y\theta)^2/(2\ell^2)$ and the axial stress becomes $Ey^2\theta^2/2\ell^2$. Since the axial stress is an even function of $y$, summing up the stresses across the cross section gives a net resultant longitudinal force on the section. If this axial force is released, there will be a shortening of the beam so that the "average axial strain" across the section is zero. It is then seen that the torsional and longitudinal deformations are fundamentally coupled irrespective of the shape of the cross section. Such coupling is of higher order in the angle of rotation $\theta$. When nonlinear terms are neglected in the linearized theories, this coupling is omitted in the resulting equations and consequently the longitudinal deformation is uncoupled with the torsional deformation in linearized theories as noted in chapter 3.

A consistent set of nonlinear equations is derived in section 3 of this chapter and it will be seen that this set of equations exhibits all the coupling features that are discussed above.

When the modal analysis technique is applied to the governing

equations, it is found that each mode is coupled with the other modes due to the inherent nonlinearity of the equations. In addition, the equation for each mode contains nonlinear terms in the generalized coordinate associated with that particular mode. Thus, one can visualize each mode as a simple oscillator of one degree of freedom having a nonlinear spring and each oscillator being coupled to the other oscillators by nonlinear springs. It can be assumed that the input signal always contains a small amount of noise which causes each oscillator to vibrate with a small amplitude at its own natural frequency. When oscillator A is excited into resonance by the input signal, a certain oscillator B, having a natural frequency at or near a submultiple of the resonant frequency of oscillator A, may be excited through the nonlinear coupling between A and B. For example, consider the case when the nonlinear coupling spring between A and B exerts a force proportional to $\alpha(t)\beta^n(t)$ on oscillator B, where $\alpha(t)$ and $\beta(t)$ are the displacements of oscillators A and B respectively and n is a positive integer. If A and B are vibrating at their natural frequencies $\lambda_A$ and $\lambda_B$ respectively, the force from the coupling spring will have components with frequencies $\lambda_A \pm n\lambda_B$, $\lambda_A \pm (n-2)\lambda_B$, $\lambda_A \pm (n-4)\lambda_B$, etc. through the "detuning"[22] of the frequencies of the two oscillators. Since $\lambda_B$ is a submultiple of $\lambda_A$, it is possible for one component of the force from the coupling spring to have a frequency the same as $\lambda_B$. The amplitude of oscillator B can then grow under such forcing term, resulting in the excitation of two non-degenerate modes by a single-

frequency external excitation.

To supplement this intuitive description, a mathematical analysis is made of the system to show theoretically the possibility of such behavior. It is shown that such behavior is possible only when the amplitude of oscillator A exceeds certain critical value in addition to the special frequency relationship between the natural frequencies of oscillators A and B. In section 3, the full set of nonlinear equations are derived from equations of elasticity. Simplifications are made to reduce the set of equations to a pair of nonlinear partial differential equations. A modal approach is taken in section 4 to reduce further the equations to a pair of nonlinear ordinary differential equations. Further simplification reduces the problem to a single nonlinear ordinary differential equation with variable coefficients. This equation is partially solved in section 5 to show the possibility of subharmonic behavior as observed.

## 2. Nonlinear Behavior as Observed in the Experiment

The nonlinear behavior of the test specimen was first observed with the section $\Phi = 90^{\circ}$ at a beam length of 35". The response of the beam, as measured by the Optron and viewed through a cathode-ray oscilloscope appeared not to be purely sinusoidal for a small range of the exciting frequency as the shaking table frequency swept through the resonant frequency of the sixth mode (a bending predominant mode with one node). A careful examination of the response revealed that it was a superposition of two sinusoidal waves. The

frequencies of the two waves were identified by means of a wave analyser (the Radiometer Wave Analyser) in connection with a digital counter (the Beckman Berkeley Counter Model 7350). The signal from the Optron was fed into the wave analyser. The exact frequency at which the wave analyser was scanning was read from the Berkeley Counter. The amplitude of the wave was read from the meter on the wave analyser. In this case, one component of the signal had the shaking table frequency of 490 cps and the other component had a frequency of 35 cps. It was found that 35 cps was very close to the resonant frequency for the first mode of the system. Visual inspection of the mode shape of the beam indicated that the beam was essentially vibrating at the first mode. The frequency ratio indicated the system was executing a 14th subharmonic oscillation.

The range of table frequencies over which such subharmonic behavior was possible depended on the amplitude of excitation of the table. The larger the excitation, the wider was the critical range. In the case cited, the range was from 489-493 cps for an excitation of 2g acceleration amplitude of the shaking table. The corresponding ranges for 4g and 6g acceleration amplitude were 486-493 cps and 484-493 cps respectively.

The transition from harmonic to subharmonic oscillation also depended on the path of approach to the critical region. When the critical region was approached from above by decreasing the table frequencies slowly, the transition was relatively insensitive to external disturbance. When the critical region was approached from

below, the transition was sudden and highly sensitive to external disturbance. Over a narrow range of exciting frequencies, the system could be shock excited into subharmonic oscillations or could be returned to harmonic oscillations through external means. In other words, there existed two stable steady states within this narrow range of table frequency. The system displayed the "jump" phenomenon as commonly known in nonlinear mechanics. In the case cited, this multi-state range was 489-490 cps for the 2g constant acceleration excitation. The corresponding figures for the 4g and 6g constant acceleration were 486-488 cps and 484-486 cps respectively. Plots of the response against table frequency is shown in Figure 23 corresponding to excitations of 4g and 2g constant acceleration. The response plotted was the r.m.s. value of the displacement at the mid-point of the beam and normalized to the displacement at table frequency of 480 cps. It should be pointed out that the frequency plotted is the table frequency and not the frequency of the specimen. The specimen may execute harmonic or subharmonic oscillations. The plots show at least qualitatively the response of the beam as the critical region was approached from both directions. They also illustrate the existence of the "jump" region. At frequency 493 cps, it was at the borderline stage of entering the critical region and the amplitude of the response became very critical.

An effort was made to detect the existence of any other subharmonics, using the wave analyser to scan the whole frequency range. Also, the table frequency was changed to integral multiples

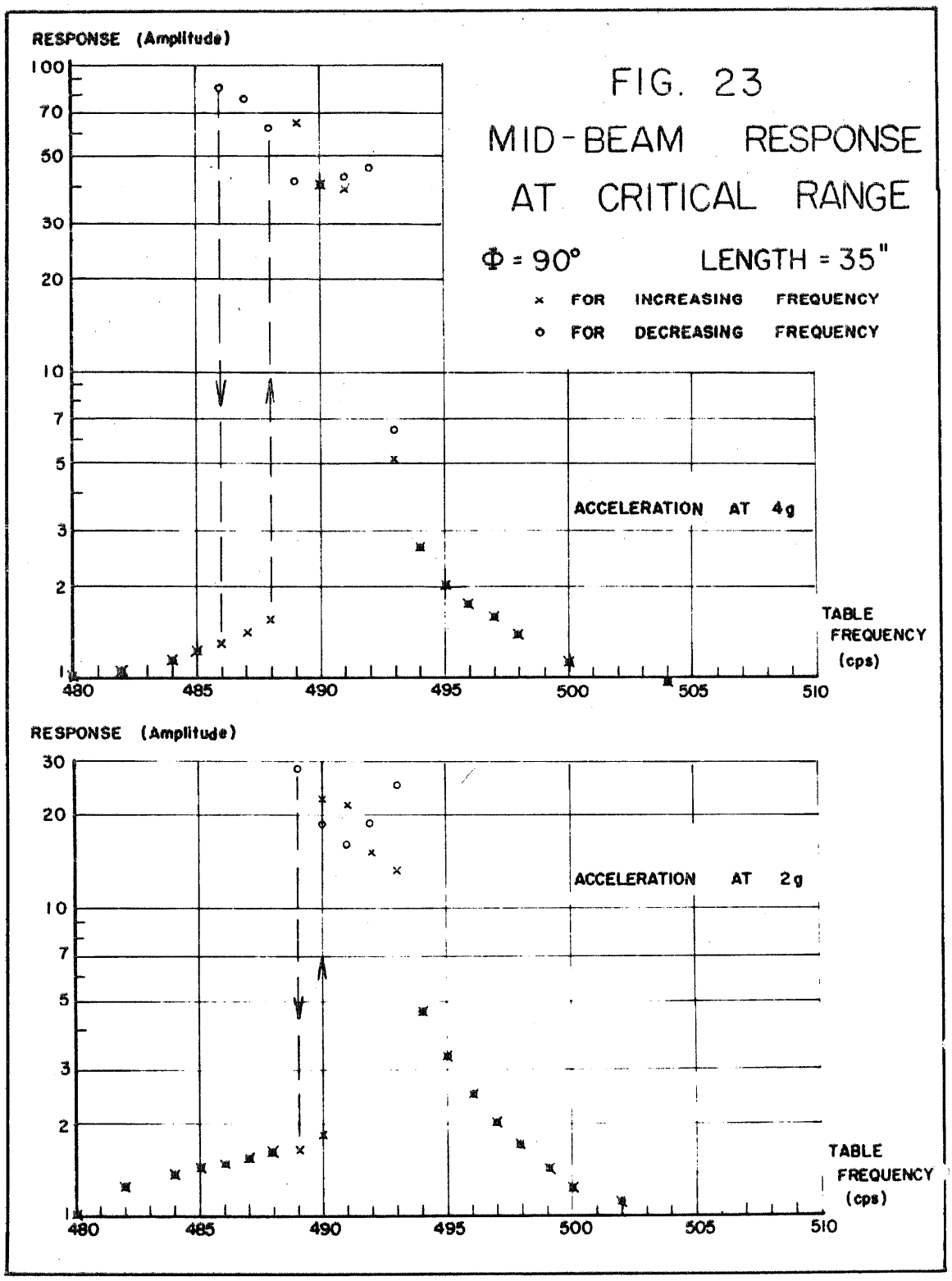
RESPONSE (Amplitude)
100
70
50
30
20
10
7
5
3
2
1
480
485
490
495
500
505
510
TABLE FREQUENCY (cps)
ACCELERATION AT 4g
FIG. 23
MID-BEAM RESPONSE AT CRITICAL RANGE
Φ = 90°
LENGTH = 35"
× FOR INCREASING FREQUENCY
o FOR DECREASING FREQUENCY
RESPONSE (Amplitude)
30
20
10
7
5
3
2
1
480
485
490
495
500
505
510
TABLE FREQUENCY (cps)
ACCELERATION AT 2g

of the resonant frequency of the first mode. Both efforts failed to detect anything other than harmonic response of the specimen.

As the beam was shortened, subharmonic oscillations were observed at beam lengths of 32", 29", 26", and 23". For the section $\Phi = 135^{o}$, this phenomenon was observed at beam lengths of 39" and 34". Ratios of the resonant frequencies for the different modes for the two specimens are given in Tables V and VI. For any given beam length, the resonant frequencies of the first six modes of a specimen are given in the table. Also the frequency ratios of these modes to the first three modes are presented. The modes that are bending predominant are labelled "bending" and the ratios corresponding to which nonlinear behaviors were observed are underlined. It can be seen that when subharmonic oscillation was observed, the higher mode resonant frequency was a multiple or near multiple of the first mode resonant frequency.

In order to eliminate the possibility that such behavior might be caused by the shaker due to unbalanced moments from the specimen, a double cantilever system was cast. The section used was $\Phi = 90^{o}$ and it was arranged in such a way that the system was symmetric in bending and antisymmetric in torsion relative to the base. Such a system could not exert moments on the shaker. For a beam length of 38-1/8" subharmonic oscillations were observed. The responses at the mid-point of the beam as seen on the oscilloscope are shown by a series of photographs as the table frequency varies. The table was set at a constant acceleration of 4g. In each picture in Figures 24

Table V. RATIOS OF RESONANT FREQUENCIES

$\Phi = 90^{o}$

| | 1st Mode | 2nd Mode (Bending) | 3rd Mode | 4th Mode | 5th Mode | 6th Mode (Bending) |
|---|---|---|---|---|---|---|
| Length = 39.5" | 29 cps | 72 cps | 108 cps | 202 cps | 333 cps | 376 cps |
| 1st Mode | 1 | 2.48 | 3.72 | 6.95 | 11.48 | 12.96 |
| 2nd Mode | | 1 | 1.50 | 2.80 | 4.64 | 5.20 |
| 3rd Mode | | | 1 | 1.87 | 3.08 | 3.48 |
| Length = 35" | 35 cps | 84 cps | 128 cps | 244 cps | 405 cps | 490 cps |
| 1st Mode | 1 | 2.40 | 3.66 | 6.94 | 11.57 | 14.00 |
| 2nd Mode | | 1 | 1.52 | 2.90 | 4.83 | 5.83 |
| 3rd Mode | | | 1 | 1.90 | 3.16 | 3.83 |
| Length = 32" | 38-39 cps | 109 cps | 147 cps | 280 cps | 470 cps | 576 cps |
| 1st Mode | 1 | 2.80 | 3.76 | 7.19 | 12.05 | 14.95 |
| 2nd Mode | | 1 | 1.35 | 2.57 | 4.31 | 5.28 |
| 3rd Mode | | | 1 | 1.91 | 3.20 | 3.94 |
| Length = 29" | 43 cps | 127 cps | 162 cps | 324 cps | 553 cps | 694 cps |
| 1st Mode | 1 | 2.98 | 3.76 | 7.54 | 12.86 | 16.14 |
| 2nd Mode | | 1 | 1.28 | 2.55 | 4.35 | 5.45 |
| 3rd Mode | | | 1 | 2.0 | 3.41 | 4.28 |
| Length = 26" | 50 cps | 154 cps | 188 cps | 388 cps | 669 cps | 853 cps |
| 1st Mode | 1 | 3.08 | 3.76 | 7.76 | 13.30 | 17.06 |
| 2nd Mode | | 1 | 1.22 | 2.52 | 4.35 | 5.53 |
| 3rd Mode | | | 1 | 2.06 | 3.56 | 4.54 |
| Length = 23" | 62 cps | 188 cps | 223 cps | 470 cps | 818 cps | 1050 cps |
| 1st Mode | 1 | 3.04 | 3.60 | 7.58 | 13.19 | 16.94 |
| 2nd Mode | | 1 | 1.18 | 2.50 | 4.35 | 5.57 |
| 3rd Mode | | | 1 | 2.11 | 3.95 | 4.7 |

Table VI. RATIOS OF RESONANT FREQUENCIES

$\Phi = 135^{o}$

| | 1st Mode | 2nd Mode (Bending) | 3rd Mode | 4th Mode | 5th Mode | 6th Mode (Bending) |
|---|---|---|---|---|---|---|
| Length = 44" | 21-22 cps | 81 cps | 95 cps | 241 cps | 447 cps | 465 cps |
| 1st Mode | 1 | 3.75 | 4.41 | 11.21 | 20.80 | 21.63 |
| 2nd Mode | | 1 | 1.18 | 2.97 | 5.55 | 5.74 |
| 3rd Mode | | | 1 | 2.54 | 4.70 | 4.90 |
| Length = 39" | 26 cps | 91 cps | 124 cps | 302 cps | 560 cps | 572 cps |
| 1st Mode | 1 | 3.50 | 4.76 | 11.62 | 21.54 | 22.00 |
| 2nd Mode | | 1 | 1.36 | 3.32 | 6.15 | 6.30 |
| 3rd Mode | | | 1 | 2.43 | 4.51 | 4.62 |
| Length = 36" | 28.5 cps | 124 cps | 141 cps | 353 cps | 647 cps | 663 cps |
| 1st Mode | 1 | 4.36 | 4.95 | 12.39 | 22.70 | 23.26 |
| 2nd Mode | | 1 | 1.14 | 2.85 | 5.21 | 5.35 |
| 3rd Mode | | | 1 | 2.50 | 4.59 | 4.70 |
| Length = 34" | 31 cps | 136 cps | 156 cps | 393 cps | 716 cps | 736 cps |
| 1st Mode | 1 | 4.39 | 5.04 | 12.68 | 23.10 | 23.74 |
| 2nd Mode | | 1 | 1.15 | 2.89 | 5.27 | 5.41 |
| 3rd Mode | | | 1 | 2.52 | 4.60 | 4.72 |
| Length = 31" | 35 cps | 160 cps | 181 cps | 465 cps | 836 cps | 864 cps |
| 1st Mode | 1 | 4.57 | 5.16 | 13.29 | 23.88 | 24.69 |
| 2nd Mode | | 1 | 1.13 | 2.90 | 5.23 | 5.40 |
| 3rd Mode | | | 1 | 2.57 | 4.62 | 4.77 |
| Length = 30" | 37 cps | 170 cps | 191 cps | 491 cps | 873 cps | 907 cps |
| 1st Mode | 1 | 4.60 | 5.16 | 13.27 | 23.60 | 24.51 |
| 2nd Mode | | 1 | 1.12 | 2.89 | 5.14 | 5.34 |
| 3rd Mode | | | 1 | 2.57 | 4.56 | 4.75 |

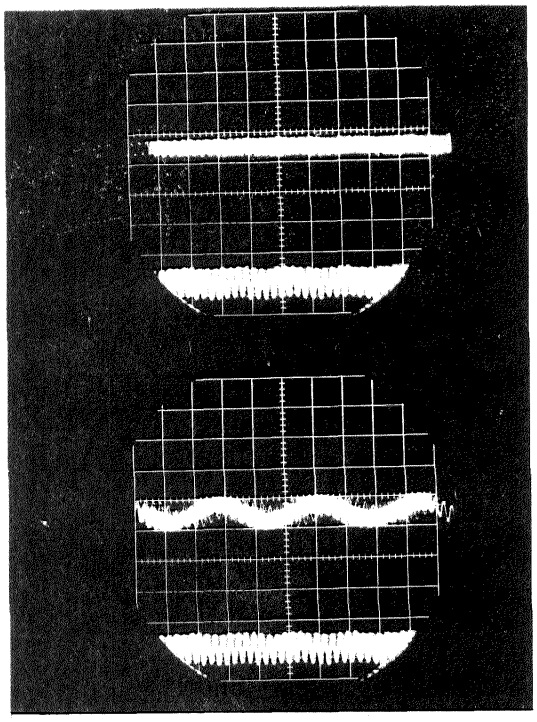

AT 405 cps

AT 406 cps

AT 407 cps

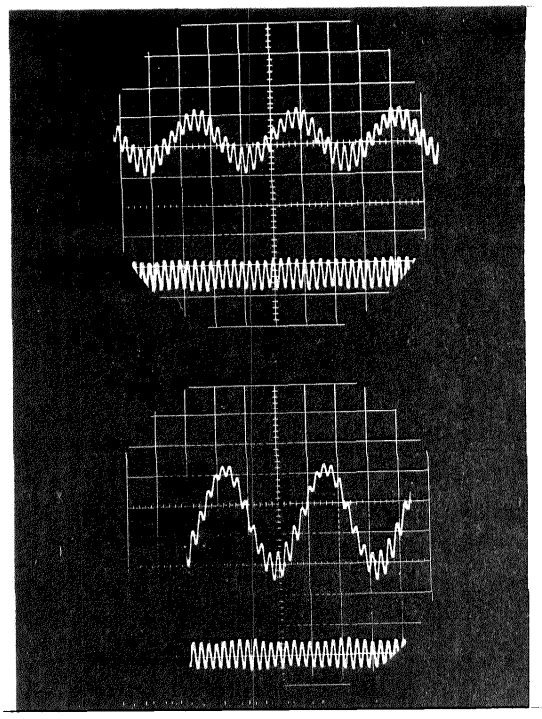

AT 409 cps

FIG. 24 SUBHARMONIC RESPONSES

DOUBLE CANTILEVER $\Phi = 90°$ LENGTH = 38.1"

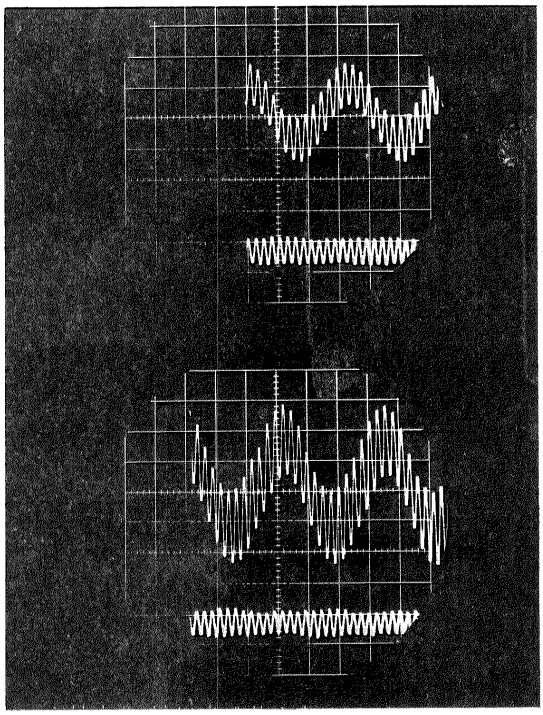

AT 410 cps

AT 412 cps

AT 413 cps

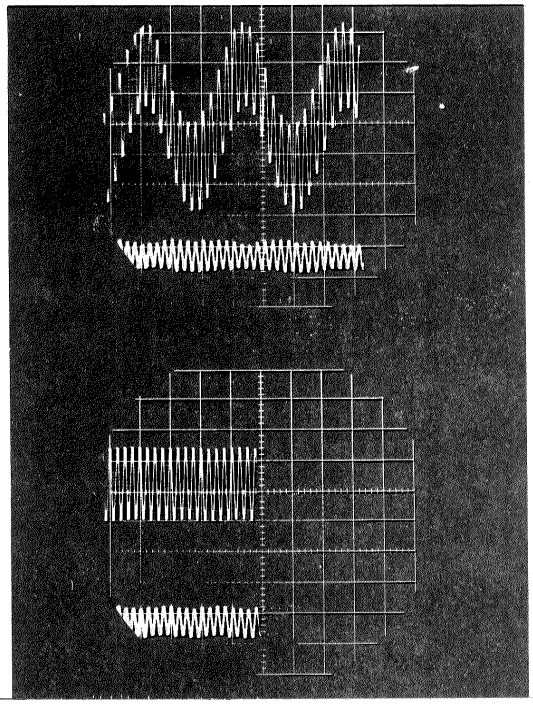

AT 414 cps

FIG. 25 SUBHARMONIC RESPONSES

DOUBLE CANTILEVER $\Phi = 90°$ LENGTH = 38.1"

and 25, the upper trace represents the response of the beam measured by the Optron. The lower trace is the acceleration measured by an auxiliary Endevco accelerometer mounted on the shaking table. The acceleration trace essentially gives a frequency scale to the response trace. At a table frequency of 405 cps, the response shows the beam is vibrating at the same frequency as the table and there are no subharmonic oscillations. At 406 cps, subharmonic oscillations begin. The responses at 407 cps and 409 cps show the subharmonic oscillations and the beam is vibrating mainly at the subharmonic frequency with harmonic oscillations superimposed on it. The rapid increase in amplitude due to the subharmonic oscillations should be noted. At 410 cps, it is seen that the amplitude of the harmonic oscillations begins to grow. Such growth is attributed to the resonance of the higher mode. It is interesting to note that the overall amplitude at 410 cps is less than the amplitude at 409 cps. The response at 412 cps table frequency shows the increase in amplitudes of both the harmonic and subharmonic oscillations. At 413 cps, the maximum response of the beam is shown. The last picture shows that the subharmonic oscillations have disappeared resulting in pure harmonic oscillations of large amplitude, corresponding to the resonant condition of the higher mode. The table frequency for this case is 414 cps. Further increase in the table frequency results in decrease of amplitude of the harmonic oscillations because the higher mode has passed over its resonant peak. The subharmonic frequency in this case is close to 32 cps which is the frequency of

the first mode. Again, visual inspection of the mode shape indicates that it is the first mode that is being excited. The frequencies 414 cps and 32 cps give a ratio of 12.94, or 13. Thus, the system is executing a 13th order subharmonic. This ratio can also be obtained by counting the number of cycles of high frequency oscillations during one cycle of the subharmonic oscillations.

It should be noted that the response shown on the photographs is the displacement of a point at the middle of the beam. If the displacement at the tip of the beam were taken for illustration, the difference in amplitudes due to the subharmonic oscillations would even be greater than shown in the photographs. In fact, the subharmonic behavior of the system is much more violent than the resonant motion of the higher mode. Such violent motion can lead to failure if it is not forseen and allowed for in design. Therefore, the subharmonic behavior is interesting both from the theoretical and practical point of view.

## 3. Derivation of the Complete Set of Equations

In order to have a better understanding of the subharmonic behavior, it is necessary to consider the complete set of nonlinear equations as derived from the equations of elasticity. This can be accomplished by following the steps given in chapter 3 without making use of the linearized approximations of (III. 6). From (III. 4) and (III. 5), there is obtained

$$v(s,z,t) = \xi \cos\psi + \eta \sin\psi + (\cos\theta - 1)n + h \sin\theta$$

$$w(s,z,t) = -\xi \sin\psi + \eta \cos\psi - (\cos\theta - 1)h + n \sin\theta \qquad \text{(VII. 3)}$$

From experimental observations, it was seen that when the subharmonic oscillations occurred, the length of the beam was sufficiently long so that the elementary linearized theory and the higher order linearized theory predict essentially the same result. In view of the experimental results from chapter 6, it is concluded that the effect of mid-plane shear strain may be neglected during the subharmonic oscillations. From $\gamma_{zs} = \frac{\partial u}{\partial s} + \frac{\partial v}{\partial z} = 0$, there is obtained

$$u(s,z,t) = \zeta - \xi' x - \eta' y + \theta' \Omega \sin\theta - \theta' \omega \cos\theta \qquad \text{(VII. 4)}$$

where

$$\Omega(s) = \int_0^s n(\bar{s})\, d\bar{s}$$

and $$\omega(s) = \int_0^s h(\bar{s})\, d\bar{s} \qquad \text{(VII. 5)}$$

Using the relations between displacements, strains and changes in curvature as given in (III. 3), there is obtained

$$\epsilon_z = \frac{\partial u}{\partial z} = \zeta' - \xi'' x - \eta'' y + (\theta'^2 \cos\theta + \theta'' \sin\theta)\Omega - (\theta'' \cos\theta - \theta'^2 \sin\theta)\omega$$

$$\epsilon_s = \frac{\partial v}{\partial s} - \frac{w}{R} = \cos\theta - 1 \qquad \text{(VII. 6)}$$

$$\gamma_{zs} = 0$$

$$\kappa_z = -\xi'' \sin\psi + \eta'' \cos\psi + (\theta'' \sin\theta + \theta'^2 \cos\theta)h$$
$$+ (\theta'' \cos\theta - \theta'^2 \sin\theta)n \qquad \text{(VII. 6)}$$
$$\kappa_s = 0$$
$$\tau = \theta' \cos\theta$$

As in chapter 3, the contribution of $\kappa_z$ to the strain energy density expression is small in comparison to $\epsilon_z$ and will be neglected. From (III. 2), thestrain energy density in this case becomes

$$U = \frac{E^* c}{2}(\epsilon_z^2 + \epsilon_s^2 + 2\nu\epsilon_z\epsilon_s) + \frac{E^* c^3}{12}(1-\nu)\tau^2 \qquad \text{(VII. 7)}$$

The strain energy V is given by

$$V = \int_0^{\ell}\int_s U\, ds\, dz \qquad \text{(VII. 8)}$$

The kinetic energy T can also be written in terms of the generalized coordinates using (III. 15) with u, v, and w given by (VII. 3) and (VII. 4). Applying Hamilton's Principle as given in (III. 1), the set of governing equations can be obtained. The equations obtained are as follows:

$$\rho[-A\ddot{\zeta} - I_\Omega \sin\theta(\ddot{\theta}' - \dot{\theta}^2\theta') - I_\Omega \cos\theta(2\dot{\theta}\dot{\theta}' + \ddot{\theta}\theta')]$$
$$+ E^*[A\zeta'' - A\nu\theta' \sin\theta + I_\Omega \sin\theta(\theta''' - \theta'^3) + 3I_\Omega \theta'\theta'' \cos\theta]$$
$$= 0 \qquad \text{(VII. 9)}$$

$$\rho[I_{xx}\ddot{\xi}'' - A\ddot{\xi} - Aa_x(\dot{\theta}\sin\theta)^{\cdot} - Aa_y(\dot{\theta}\cos\theta)^{\cdot}$$
$$- I_{\Omega x}\cos\theta(2\theta'\dot{\theta}' + \ddot{\theta}\theta'' + 2\dot{\theta}\dot{\theta}'' + 2\dot{\theta}'^2 - \theta'^2\dot{\theta}^2)$$
$$- I_{\Omega x}\sin\theta(\ddot{\theta}'' - \theta''\dot{\theta}^2 - 4\dot{\theta}\theta'\dot{\theta}' - \ddot{\theta}\theta'^2)]$$
$$+ E^*[-I_{xx}\xi'''' + I_{\Omega x}\cos\theta(4\theta'\theta''' + 3\theta''^2 - \theta'^4)$$
$$+ I_{\Omega x}\sin\theta(\theta'''' - 6\theta'^2\theta'')] = 0 \qquad \text{(VII.10)}$$

$$\rho[I_{yy}\ddot{\eta}'' - A\ddot{\eta} + Aa_x(\dot{\theta}\cos\theta)^{\cdot} - Aa_y(\dot{\theta}\sin\theta)^{\cdot}$$
$$- I_{\Omega y}\cos\theta(2\theta'\dot{\theta}' + \ddot{\theta}\theta'' + 2\dot{\theta}\dot{\theta}'' + 2\dot{\theta}'^2 - \dot{\theta}^2\theta'^2)$$
$$- I_{\Omega y}\sin\theta(\ddot{\theta}'' - \theta''\dot{\theta}^2 - 4\dot{\theta}\theta'\dot{\theta}' - \ddot{\theta}\theta'^2)]$$
$$+ E^*[-I_{yy}\eta'''' + I_{\Omega y}\cos\theta(4\theta'\theta''' + 3\theta''^2 - \theta'^4)$$
$$+ I_{\Omega y}\sin\theta(\theta'''' - 6\theta'^2\theta'')] = 0 \qquad \text{(VII.11)}$$

$$\rho[I_\Omega(\sin\theta)\ddot{\zeta}' - I_{\Omega x}(\sin\theta)\ddot{\xi}'' - I_{\Omega y}(\sin\theta)\ddot{\eta}''$$
$$+ I_{\Omega\Omega}\sin\theta(\theta'\sin\theta)^{\cdot\cdot\prime} + I_{\omega\omega}\cos\theta(\theta'\cos\theta)^{\cdot\cdot\prime}$$
$$- I_{\Omega\omega}\cos 2\theta(2\theta'\dot{\theta}' - \theta'^2\dot{\theta}^2 + 2\dot{\theta}'^2 + 2\dot{\theta}\dot{\theta}'' + \ddot{\theta}\theta'')$$
$$- I_{\Omega\omega}\sin 2\theta(\ddot{\theta}'' - \theta''\dot{\theta}^2 - 4\dot{\theta}\theta'\dot{\theta}' - \ddot{\theta}\theta'^2)$$
$$- I_p\ddot{\theta} - Aa_x(\sin\theta)\ddot{\xi} - (\cos\theta)\ddot{\eta}) - Aa_y(\sin\theta)\ddot{\eta} + (\cos\theta)\ddot{\xi})]$$
$$- E^*[I_{\omega\omega}\cos^2\theta(\theta'''' - 6\theta'^2\theta'') - I_{\omega\omega}\sin\theta\cos\theta(3\theta''^2 + 4\theta'\theta''' - \theta'^4)$$
$$- A\sin\theta(\cos\theta - 1 + \nu\zeta') + I_\Omega(\sin\theta)\zeta'''$$
$$- 2I_\Omega\nu\sin\theta(\sin\theta)\theta'' + (\cos\theta)\theta'^2) - I_{\Omega x}(\sin\theta)\xi''''$$
$$- I_{\Omega y}(\sin\theta)\eta'''' + I_{\Omega\Omega}\sin\theta\cos\theta(3\theta''^2 + 4\theta'\theta''' - \theta'^4)$$
$$+ I_{\Omega\Omega}\sin^2\theta(\theta'''' - 6\theta'^2\theta'') - I_{\Omega\omega}\cos 2\theta(3\theta''^2 + 4\theta'\theta''' - \theta'^4)$$
$$- I_{\Omega\omega}\sin 2\theta(\theta'''' - 6\theta'^2\theta'') - \frac{G}{E^*}I_d(\cos^2\theta\theta'' - \theta'^2\sin\theta\cos\theta)]$$
$$= 0 \qquad \text{(VII.12)}$$

where

$$I_{\Omega} = \int_s \Omega c \, ds \; ; \qquad I_{\Omega x} = \int_s \Omega x c \, ds \; ; \qquad I_{\Omega y} = \int_s \Omega y c \, ds \; ;$$

$$I_{\Omega\omega} = \int_s \Omega\omega c \, ds \; ; \qquad I_{\Omega\Omega} = \int_s \Omega^2 c \, ds$$

and the other quantities are defined in chapter 3.

Equations (VII. 9) to (VII. 12) are four coupled nonlinear partial differential equations for $\zeta$, $\xi$, $\eta$ and $\theta$. The coupling of the four equations is through the rotation coordinate $\theta$. The longitudinal displacement coordinate $\zeta$ is coupled to $\theta$ through the "shortening effect," and the bending displacement coordinates $\xi$ and $\eta$ are coupled to $\theta$ through the asymmetry of the section of the beam as stated in section 1 of this chapter. For a section with one axis of symmetry, the equation for the displacement parallel to the axis of symmetry is no longer uncoupled as in the linearized theories. Taking the axis of symmetry as the Y axis, it can be shown that the parameters $a_x$, $I_{\Omega x}$, and $I_{\Omega\omega}$ are zero. Rewriting equations (VII. 9) to (VII. 12) for a monosymmetric section in non-dimensional form, there is obtained

$$- \ddot{\bar{\zeta}} + \lambda_o^2 \frac{\partial^2 \bar{\zeta}}{\partial \bar{z}^2} - \lambda_o^2 \nu \sin\theta \frac{\partial \theta}{\partial \bar{z}}$$

$$+ \bar{I}_{\Omega} \Bigg[ \lambda_o^2 \sin\theta \left( \frac{\partial^3 \theta}{\partial \bar{z}^3} - \left( \frac{\partial \theta}{\partial \bar{z}} \right)^3 \right) + 3\lambda_o^2 \frac{\partial \theta}{\partial \bar{z}} \frac{\partial^2 \theta}{\partial \bar{z}^2} \cos\theta$$

$$- \sin\theta \left( \frac{\partial \ddot{\theta}}{\partial \bar{z}} - \dot{\theta}^2 \frac{\partial \theta}{\partial \bar{z}} \right) - \cos\theta \left( 2\dot{\theta} \frac{\partial \dot{\theta}}{\partial \bar{z}} + \ddot{\theta} \frac{\partial \theta}{\partial \bar{z}} \right) \Bigg] = 0$$

(VII. 13)

$$\frac{\partial^2 \ddot{\bar{\xi}}}{\partial \bar{z}^2} - \ddot{\bar{\xi}} - \bar{a}_y(\dot{\theta}\cos\theta)^{\cdot} - \lambda_o^2 \frac{\partial^4 \bar{\xi}}{\partial \bar{z}^4} = 0 \qquad \text{(VII.14)}$$

$$\bar{I}_{yy} \frac{\partial^2 \ddot{\bar{\eta}}}{\partial \bar{z}^2} - \ddot{\bar{\eta}} - \bar{a}_y(\dot{\theta}\sin\theta)^{\cdot} - \lambda_o^2 \bar{I}_{yy} \frac{\partial^4 \bar{\eta}}{\partial \bar{z}^4}$$

$$+ I_{\Omega y}\left[\lambda_o^2 \cos\theta\left(4\frac{\partial\theta}{\partial\bar{z}}\frac{\partial^3\theta}{\partial\bar{z}^3} + 3\left(\frac{\partial^2\theta}{\partial\bar{z}^2}\right)^2 - \left(\frac{\partial\theta}{\partial\bar{z}}\right)^4\right)\right.$$

$$+ \lambda_o^2 \sin\theta\left(\frac{\partial^4\theta}{\partial\bar{z}^4} - 6\frac{\partial^2\theta}{\partial\bar{z}^2}\left(\frac{\partial\theta}{\partial\bar{z}}\right)^2\right)$$

$$- \cos\theta\left(2\frac{\partial\theta}{\partial\bar{z}}\frac{\partial\ddot{\theta}}{\partial\bar{z}} + \ddot{\theta}\frac{\partial^2\theta}{\partial\bar{z}^2} + 2\dot{\theta}\frac{\partial^2\dot{\theta}}{\partial\bar{z}^2} - \dot{\theta}^2\left(\frac{\partial\theta}{\partial\bar{z}}\right)^2\right)$$

$$\left. - \sin\theta\left(\frac{\partial^2\ddot{\theta}}{\partial\bar{z}^2} - \dot{\theta}^2\frac{\partial^2\theta}{\partial\bar{z}^2} - 4\dot{\theta}\frac{\partial\theta}{\partial\bar{z}}\frac{\partial\dot{\theta}}{\partial\bar{z}} - \ddot{\theta}\left(\frac{\partial\theta}{\partial\bar{z}}\right)^2\right)\right] = 0$$

(VII.15)

$$
\begin{aligned}
&- \bar{I}_p \ddot{\theta} - \bar{a}_y \left(\sin\theta \ddot{\bar{\eta}} + \cos\theta \ddot{\bar{\xi}}\right) + \bar{I}_{\omega\omega} \cos\theta \frac{\partial}{\partial \bar{z}} \left(\cos\theta \frac{\partial \theta}{\partial \bar{z}}\right)^{\cdot\cdot} \\
&- \lambda_o^2 \bar{I}_{\omega\omega} \cos^2\theta \frac{\partial^4 \theta}{\partial \bar{z}^4} + \lambda_o^2 \frac{G}{E^*} \bar{I}_d \cos^2\theta \frac{\partial^2 \theta}{\partial \bar{z}^2} \\
&+ 6 \lambda_o^2 \bar{I}_{\omega\omega} \cos^2\theta \frac{\partial^2 \theta}{\partial \bar{z}^2} \left(\frac{\partial \theta}{\partial \bar{z}}\right)^2 \\
&+ \sin\theta \left[ \bar{I}_\Omega \frac{\partial \ddot{\bar{\zeta}}}{\partial \bar{z}} - \bar{I}_{\Omega y} \frac{\partial^2 \ddot{\bar{\eta}}}{\partial \bar{z}^2} + \bar{I}_{\Omega\Omega} \frac{\partial}{\partial \bar{z}} \left(\sin\theta \frac{\partial \theta}{\partial \bar{z}}\right)^{\cdot\cdot} \right. \\
&+ \lambda_o^2 \bar{I}_{\omega\omega} \cos\theta \left(4 \frac{\partial \theta}{\partial \bar{z}} \frac{\partial^3 \theta}{\partial \bar{z}^3} + 3 \left(\frac{\partial^2 \theta}{\partial \bar{z}^2}\right)^2 - \left(\frac{\partial \theta}{\partial \bar{z}}\right)^4\right) \\
&- \lambda_o^2 \left(1 - \cos\theta - \nu \frac{\partial \bar{\zeta}}{\partial \bar{z}} + \bar{I}_\Omega \frac{\partial^3 \bar{\zeta}}{\partial \bar{z}^3} - \bar{I}_{\Omega y} \frac{\partial^4 \bar{\eta}}{\partial \bar{z}^4}\right) \\
&+ 2 \lambda_o^2 \nu \bar{I}_\Omega \left(\sin\theta \frac{\partial^2 \theta}{\partial \bar{z}^2} + \cos\theta \left(\frac{\partial \theta}{\partial \bar{z}}\right)^2\right) \\
&- \lambda_o^2 \bar{I}_{\Omega\Omega} \cos\theta \left(4 \frac{\partial \theta}{\partial \bar{z}} \frac{\partial^3 \theta}{\partial \bar{z}^3} + 3 \left(\frac{\partial^2 \theta}{\partial \bar{z}^2}\right)^2 - \left(\frac{\partial \theta}{\partial \bar{z}}\right)^4\right) \\
&- \lambda_o^2 \bar{I}_{\Omega\Omega} \sin\theta \left(\frac{\partial^4 \theta}{\partial \bar{z}^4} - 6 \frac{\partial^2 \theta}{\partial \bar{z}^2} \left(\frac{\partial \theta}{\partial \bar{z}}\right)^2\right) \\
&\left. - \lambda_o^2 \frac{G}{E^*} \bar{I}_d \cos\theta \left(\frac{\partial \theta}{\partial \bar{z}}\right)^2 \right] = 0 \qquad \text{(VII. 16)}
\end{aligned}
$$

where

$$
\bar{I}_\Omega A r^2 = I_\Omega, \quad \bar{I}_{\Omega y} A r^3 = I_{\Omega y}, \quad \bar{I}_{\Omega\Omega} A r^4 = I_{\Omega\Omega},
$$

$$
\bar{I}_{yy} A r^2 = I_{yy}, \text{ and } \quad \lambda_o^2 = \frac{E^*}{\rho r^2}
$$

Equations (VII. 13) to (VII. 16) are too complicated to handle

directly. Simplifications are necessary to render the solution tractable. The nonlinear terms in the equations arise either from the variation of the kinetic energy expression or the variation of the strain energy expression. In analogy to the terminology used in linear vibrations for coupling, the nonlinear terms arise from the kinetic energy expression are termed dynamic nonlinearities and those from the strain energy expression are termed static nonlinearities. All dynamic nonlinearities involve time derivatives and the static nonlinearities are premultiplied by the quantity $\lambda_o^2$. When the system is executing harmonic oscillations, its frequency is the same as the shaking table frequency $\lambda$. When the system is vibrating in subharmonic motions, the frequency is less than the table frequency $\lambda$. Thus, for each time derivative, a factor of at most $\lambda$ is involved to multiply the dynamic nonlinearities. Since the shaking table frequency $\lambda$ was much smaller than $\lambda_o$ throughout the experiment, it is felt that the effects of the dynamic nonlinearities are negligible compared with those from the static nonlinearities.

It should be noted that all generalized coordinates refer to the undeformed state of the beam. When the base of the beam is shaken at a frequency $\lambda$ in the X direction, this has the effect of an inertial loading on the specimen. Mathematically this is represented by a forcing term in the $\bar{\xi}$ equation. Neglecting the dynamic nonlinearities, the axial inertia terms $\partial^2\ddot{\bar{\xi}}/\partial\bar{z}^2$, $\partial^2\ddot{\bar{\eta}}/\partial\bar{z}^2$ and $\partial^2\ddot{\theta}/\partial\bar{z}^2$, and including a forcing term in the $\bar{\xi}$ equation, equations (VII.13) to (VII.16) can be written as

$$-\frac{\ddot{\bar{\zeta}}}{\lambda_o^2}+\frac{\partial^2\bar{\zeta}}{\partial\bar{z}^2}-\nu\sin\theta\frac{\partial\theta}{\partial\bar{z}}$$

$$+\bar{I}_\Omega\left[\sin\theta\left\{\frac{\partial^3\theta}{\partial\bar{z}^3}-\left(\frac{\partial\theta}{\partial\bar{z}}\right)^3\right\}+3\cos\theta\frac{\partial\theta}{\partial\bar{z}}\frac{\partial^2\theta}{\partial\bar{z}^2}\right]=0 \quad \text{(VII.17)}$$

$$\frac{\ddot{\bar{\xi}}}{\lambda_o^2}+\frac{\bar{a}_y}{\lambda_o^2}\ddot{\theta}+\frac{\partial^4\bar{\xi}}{\partial\bar{z}^4}=\bar{P}\cos\lambda t \quad \text{(VII.18)}$$

$$\frac{\ddot{\bar{\eta}}}{\lambda_o^2}+\bar{I}_{yy}\frac{\partial^4\bar{\eta}}{\partial\bar{z}^4}-\bar{I}_{\Omega y}\left[\cos\theta\left\{4\frac{\partial\theta}{\partial\bar{z}}\frac{\partial^3\theta}{\partial\bar{z}^3}+3\left(\frac{\partial^2\theta}{\partial\bar{z}^2}\right)^2-\left(\frac{\partial\theta}{\partial\bar{z}}\right)^4\right\}\right.$$

$$\left.+\sin\theta\left\{\frac{\partial^4\theta}{\partial\bar{z}^4}-6\frac{\partial^2\theta}{\partial\bar{z}^2}\left(\frac{\partial\theta}{\partial\bar{z}}\right)^2\right\}\right]=0 \quad \text{(VII.19)}$$

$$-\frac{\bar{I}_p}{\lambda_o^2}\ddot{\theta}-\frac{\bar{a}_y}{\lambda_o^2}\ddot{\bar{\xi}}-\bar{I}_{\omega\omega}\frac{\partial^4\theta}{\partial\bar{z}^4}+\frac{G}{E^*}\bar{I}_d\frac{\partial^2\theta}{\partial\bar{z}^2}$$

$$+\nu\sin\theta\frac{\partial\bar{\zeta}}{\partial\bar{z}}-\bar{I}_\Omega\sin\theta\frac{\partial^3\bar{\zeta}}{\partial\bar{z}^3}+\bar{I}_{\Omega y}\sin\theta\frac{\partial^4\bar{\eta}}{\partial\bar{z}^4}$$

$$+2\nu\bar{I}_\Omega\sin\theta\left\{\sin\theta\frac{\partial^2\theta}{\partial\bar{z}^2}+\cos\theta\left(\frac{\partial\theta}{\partial\bar{z}}\right)^2\right\}$$

$$-\bar{I}_{\Omega\Omega}\sin\theta\left[\cos\theta\left\{4\frac{\partial\theta}{\partial\bar{z}}\frac{\partial^3\theta}{\partial\bar{z}^3}+3\left(\frac{\partial^2\theta}{\partial\bar{z}^2}\right)^2-\left(\frac{\partial\theta}{\partial\bar{z}}\right)^4\right\}\right.$$

$$\left.+\sin\theta\left\{\frac{\partial^4\theta}{\partial\bar{z}^4}-6\frac{\partial^2\theta}{\partial\bar{z}^2}\left(\frac{\partial\theta}{\partial\bar{z}}\right)^2\right\}\right]$$

$$+\bar{I}_{\omega\omega}\left[-6\cos^2\theta\frac{\partial^2\theta}{\partial\bar{z}^2}\left(\frac{\partial\theta}{\partial\bar{z}}\right)^2\right.$$

$$\left.-\frac{\sin 2\theta}{2}\left\{3\left(\frac{\partial^2\theta}{\partial\bar{z}^2}\right)^2+4\frac{\partial\theta}{\partial\bar{z}}\frac{\partial^3\theta}{\partial\bar{z}^3}-\left(\frac{\partial\theta}{\partial\bar{z}}\right)^4\right\}\right]=0$$

(VII. 20)

Neglecting $\ddot{\bar{\zeta}}$ and $\ddot{\bar{\eta}}$ in equations (VII.17) and (VII.19) respectively, $\partial\bar{\zeta}/\partial\bar{z}$, $\partial^3\bar{\zeta}/\partial\bar{z}^3$ and $\partial^4\bar{\eta}/\partial\bar{z}^4$ can be expressed in terms of $\theta$.

$$\frac{\partial\bar{\zeta}}{\partial\bar{z}} = -\nu\cos\theta - \bar{I}_\Omega\left[\sin\theta\,\frac{\partial^2\theta}{\partial\bar{z}^2} + \cos\theta\left(\frac{\partial\theta}{\partial\bar{z}}\right)^2\right]$$

$$\begin{aligned}\frac{\partial^3\bar{\zeta}}{\partial\bar{z}^3} &= \nu\sin\theta\,\frac{\partial^2\theta}{\partial\bar{z}^2} + \nu\cos\theta\left(\frac{\partial\theta}{\partial\bar{z}}\right)^2 \\ &\quad - \bar{I}_\Omega\left[\sin\theta\left\{\frac{\partial^4\theta}{\partial\bar{z}^4} - 6\,\frac{\partial^2\theta}{\partial\bar{z}^2}\left(\frac{\partial\theta}{\partial\bar{z}}\right)^2\right\}\right. \\ &\quad \left. + \cos\theta\left\{4\,\frac{\partial\theta}{\partial\bar{z}}\,\frac{\partial^3\theta}{\partial\bar{z}^3} + 3\left(\frac{\partial^2\theta}{\partial\bar{z}^2}\right)^2 - \left(\frac{\partial\theta}{\partial\bar{z}}\right)^4\right\}\right]\end{aligned} \qquad \text{(VII. 21)}$$

$$\begin{aligned}\frac{\partial^4\bar{\eta}}{\partial\bar{z}^4} &= \frac{\bar{I}_{\Omega y}}{\bar{I}_{yy}}\left[\cos\theta\left\{4\,\frac{\partial\theta}{\partial\bar{z}}\,\frac{\partial^3\theta}{\partial\bar{z}^3} + 3\left(\frac{\partial^2\theta}{\partial\bar{z}^2}\right)^2 - \left(\frac{\partial\theta}{\partial\bar{z}}\right)^4\right\}\right. \\ &\quad \left. + \sin\theta\left\{\frac{\partial^4\theta}{\partial\bar{z}^4} - 6\,\frac{\partial^2\theta}{\partial\bar{z}^2}\left(\frac{\partial\theta}{\partial\bar{z}}\right)^2\right\}\right]\end{aligned}$$

Substituting (VII. 21) into (VII. 20) and neglecting higher order terms such as $(\partial\theta/\partial\bar{z})^4$ in comparison with terms like $4(\partial\theta/\partial\bar{z})(\partial^3\theta/\partial\bar{z}^3)$, there is obtained

$$\frac{\bar{I}_p}{\lambda_o^2}\ddot{\theta} + \frac{\bar{a}_y}{\lambda_o^2}\ddot{\bar{\xi}} + \bar{I}_{\omega\omega}\frac{\partial^4\theta}{\partial\bar{z}^4} - \frac{G}{E^*}\bar{I}_d\frac{\partial^2\theta}{\partial\bar{z}^2} + N(\theta) = 0 \qquad \text{(VII. 22)}$$

where

$$\begin{aligned}N(\theta) &= \frac{\sin 2\theta}{2}\left\{\nu^2 + \bar{I}_n\left[4\,\frac{\partial\theta}{\partial\bar{z}}\,\frac{\partial^3\theta}{\partial\bar{z}^3} + 3\left(\frac{\partial^2\theta}{\partial\bar{z}^2}\right)^2\right]\right\} \\ &\quad + \frac{\bar{I}_n}{2}\,\frac{\partial^4\theta}{\partial\bar{z}^4}\,(1 - \cos 2\theta) - 3\bar{I}_n\,\frac{\partial^2\theta}{\partial\bar{z}^2}\left(\frac{\partial\theta}{\partial\bar{z}}\right)\end{aligned} \qquad \text{(VII. 23)}$$

and $\bar{I}_n$ is defined as $\bar{I}_n = \bar{I}_{\Omega\Omega} - \bar{I}_{\Omega}^2 - (\bar{I}_{\Omega y}^2 / \bar{I}_{yy})$. In obtaining (VII. 22), $\bar{I}_{\omega\omega}$ is neglected in comparison with $\bar{I}_n$. For the specimens tested, $\bar{I}_{\omega\omega}$ is small compared to $\bar{I}_n$ and leaving out $\bar{I}_{\omega\omega}$ is justifiable.

## 4. Modal Approach to the Governing Equations

In section 3, the governing equations were reduced to two coupled partial differential equations; namely,

$$\frac{1}{\lambda_o^2}\ddot{\bar{\xi}} + \frac{\bar{a}_y}{\lambda_o^2}\ddot{\theta} + \frac{\partial^4 \bar{\xi}}{\partial \bar{z}^4} = \bar{P}\cos \lambda t \qquad \text{(VII. 18)}$$

$$\frac{\bar{I}_p}{\lambda_o^2}\ddot{\theta} + \frac{\bar{a}_y}{\lambda_o^2}\ddot{\bar{\xi}} + \bar{I}_{\omega\omega}\frac{\partial^4 \theta}{\partial \bar{z}^4} - \frac{G}{E^*}\bar{I}_d \frac{\partial^2 \theta}{\partial \bar{z}^2} + N(\theta) = 0 \qquad \text{(VII. 22)}$$

and $N(\theta)$ is given by

$$N(\theta) = \frac{\sin 2\theta}{2}\left\{\nu^2 + \bar{I}_n\left[4\frac{\partial \theta}{\partial \bar{z}}\frac{\partial^3 \theta}{\partial \bar{z}^3} + 3\left(\frac{\partial^2 \theta}{\partial \bar{z}^2}\right)^2\right]\right\} + \frac{\bar{I}_n}{2}\frac{\partial^4 \theta}{\partial \bar{z}^4}(1 - \cos 2\theta) - 3\bar{I}_n \frac{\partial^2 \theta}{\partial \bar{z}^2}\left(\frac{\partial \theta}{\partial \bar{z}}\right)^2 \qquad \text{(VII. 23)}$$

It is interesting to note that equation (VII. 18) is a linear differential equation and is dynamically coupled to equation (VII. 22). Equation (VII. 22) is a nonlinear equation due to the term $N(\theta)$. There is no standard method of solution for a coupled pair of nonlinear partial differential equations. The method of analysis adopted is essentially guided by experimental observations and no attempt is made to solve the equations completely. The motivation for the

analysis is to show that the possibility of high order subharmonics is contained in the equations if nonlinear effects are taken into account. Therefore, simplifications consistent with the general theme are made whenever possible in order to simplify the algebra.

For the length of beam for which such nonlinear behavior was observed, the resonant frequencies predicted from the linearized theory agree well with the experimental values. This indicates that the linearized theory (Gere's theory) is adequate except for predicting the subharmonic behavior of the system. Thus, when the nonlinear terms are included, the same eigenvalue expansion technique is used to reduce the pair of partial differential equations to a pair of ordinary differential equations. In this approach, it is assumed that the mode shapes of the system are essentially the same for both the linearized theory and the nonlinear theory. Such an assumption seems reasonable on two counts. Firstly, for some nonlinear problems in continuum mechanics, such as the vibrations of a stretched string held fixed at both ends, the mode shape for both the linearized problem and the nonlinear problem is identical. By the linearized problem is meant the case where the tension in the string is assumed constant. When the variation of tension during vibration is taken into account, the problem is nonlinear in nature. Secondly, the mode shape observed in the experiment when the fundamental "mode" was parametrically excited did not differ markedly from that of the fundamental mode when it was externally excited.

In order to simplify the algebra, the case of a simply supported

beam is analyzed instead of a cantilever. For the simply supported beam, the eigenfunctions for both the displacement $\bar{\xi}$ and rotation $\theta$ are sine functions. Only two modes are of interest, namely, the mode which is excited into resonance by the external source, and the mode which is subharmonically excited. In the experiments it was always the first mode of the system that was subharmonically excited. Therefore, in the eigenvalue expansion process, only the lowest mode and another higher mode are considered. Let

$$\bar{\xi} = u_1(t) \sin \frac{\pi r \bar{z}}{\ell} + u_j(t) \sin \frac{j\pi r \bar{z}}{\ell}$$
$$\theta = v_1(t) \sin \frac{\pi r \bar{z}}{\ell} + v_j(t) \sin \frac{j\pi r \bar{z}}{\ell} \qquad \text{(VII. 24)}$$

where

$$j = 2, 3, 4, \ldots$$

Substituting (VII. 24) into (VII. 18), multiplying (VII. 18) by $\sin (\pi r \bar{z})/\ell$ and integrating through the length of the beam, there is obtained

$$\frac{\ddot{u}_1}{\lambda_o^2} + \frac{\bar{a}_y}{\lambda_o^2} \ddot{v}_1 + \mu_1^4 u_1 = q_1 \cos \lambda t \qquad \text{(VII. 25)}$$

where

$$q_1 = \frac{2r}{\ell} \int_0^{\ell/r} \bar{P} \sin \frac{\pi r \bar{z}}{\ell} \, d\bar{z} \qquad \text{(VII. 26)}$$

and

$$\mu_1 = \frac{\pi r}{\ell}$$

Similarly, multiplying (VII. 18) by $\sin (j\pi r \bar{z})/\ell$ and integrating, there is obtained

$$\frac{\ddot{u}_j}{\lambda_o^2} + \frac{\bar{a}_y}{\lambda_o^2}\ddot{v}_j + \mu_j^4 u_j = q_j \cos \lambda t \qquad \text{(VII. 27)}$$

where

$$q_j = \frac{2r}{\ell}\int_0^{\ell/r} \bar{P} \sin \frac{j\pi r\bar{z}}{\ell}\, d\bar{z} \quad \text{and} \quad \mu_j = \frac{j\pi r}{\ell} \qquad \text{(VII. 28)}$$

Similar operations apply to equation (VII. 22) and result in two equations

$$\frac{\bar{I}_p}{\lambda_o^2}\ddot{v}_1 + \frac{\bar{a}_y}{\lambda_o^2}\ddot{u}_1 + (\bar{I}_{\omega\omega}\mu_1^4 + \frac{G}{E^*}\bar{I}_d\mu_1^2)v_1 + F_1(v_1, v_j) = 0 \qquad \text{(VII. 29)}$$

$$\frac{\bar{I}_p}{\lambda_o^2}\ddot{v}_j + \frac{\bar{a}_y}{\lambda_o^2}\ddot{u}_j + (\bar{I}_{\omega\omega}\mu_j^4 + \frac{G}{E^*}\bar{I}_d\mu_j^2)v_j + F_j(v_1, v_j) = 0 \qquad \text{(VII. 30)}$$

where

$$F_j(v_1, v_j) = \frac{2r}{\ell}\int_0^{\ell/r} \sin \mu_j\bar{z}\, N(v_1 \sin \mu_1\bar{z}, v_j \sin \mu_j\bar{z})\, d\bar{z}$$

$$F_1(v_1, v_j) = \frac{2r}{\ell}\int_0^{\ell/r} \sin \mu_1\bar{z}\, N(v_1 \sin \mu_1\bar{z}, v_j \sin \mu_j\bar{z})\, d\bar{z} \qquad \text{(VII. 31)}$$

The equations (VII. 25), (VII. 27), (VII. 29) and (VII. 30) can be written in matrix form:

$$\frac{1}{\lambda_o^2}\begin{bmatrix} 1 & \bar{a}_y & 0 & 0 \\ \bar{a}_y & \bar{I}_p & 0 & 0 \\ 0 & 0 & 1 & \bar{a}_y \\ 0 & 0 & \bar{a}_y & \bar{I}_p \end{bmatrix}\begin{Bmatrix} \ddot{u}_1 \\ \ddot{v}_1 \\ \ddot{u}_j \\ \ddot{v}_j \end{Bmatrix} + \begin{bmatrix} \mu_1^4 & 0 & 0 & 0 \\ 0 & \mu_1^4 C_1 & 0 & 0 \\ 0 & 0 & \mu_j^4 & 0 \\ 0 & 0 & 0 & \mu_j^4 C_j \end{bmatrix}\begin{Bmatrix} u_1 \\ v_1 \\ u_j \\ v_j \end{Bmatrix}$$

$$\begin{Bmatrix} 0 \\ F_1(v_1, v_j) \\ 0 \\ F_j(v_1, v_j) \end{Bmatrix} = \begin{Bmatrix} q_1 \cos \lambda t \\ 0 \\ q_j \cos \lambda t \\ 0 \end{Bmatrix} \qquad \text{(VII. 32)}$$

where

$$C_j \equiv \bar{I}_{\omega\omega} + \frac{G}{E^*}\bar{I}_d \frac{1}{\mu_j^2} \qquad \text{(VII. 33)}$$

It can be seen that $u_1$ is coupled to $v_1$ only and $u_j$ is coupled to $v_j$. It is possible to make a linear transformation to uncouple the linear part of equation (VII. 32). Let

$$\begin{Bmatrix} u_1 \\ v_1 \\ u_j \\ v_j \end{Bmatrix} = \begin{bmatrix} a_{11} & a_{12} & 0 & 0 \\ 1 & 1 & 0 & 0 \\ 0 & 0 & a_{33} & a_{34} \\ 0 & 0 & 1 & 1 \end{bmatrix}\begin{Bmatrix} \alpha_1 \\ \beta_1 \\ \alpha_j \\ \beta_j \end{Bmatrix} \qquad \text{(VII. 34)}$$

where

$$\begin{Bmatrix} a_{11} \\ a_{12} \end{Bmatrix} = -\frac{1}{2}\left(\frac{\bar{I}_p - C_1}{\bar{a}_y}\right) \pm \left[\left(\frac{\bar{I}_p - C_1}{\bar{a}_y}\right)^2 + 4C_1\right]^{1/2}$$

$$\begin{Bmatrix} a_{33} \\ a_{34} \end{Bmatrix} = -\frac{1}{2}\left(\frac{\bar{I}_p - C_j}{\bar{a}_y}\right) \pm \left[\left(\frac{\bar{I}_p - C_j}{\bar{a}_y}\right)^2 + 4C_j\right]^{1/2} \qquad \text{(VII. 35)}$$

Substituting (VII. 34) into (VII. 32) and premultiplying (VII. 32) by

$$\begin{bmatrix} -\frac{C_1}{a_{12}} & 1 & 0 & 0 \\ -\frac{C_1}{a_{11}} & 1 & 0 & 0 \\ 0 & 0 & -\frac{C_j}{a_{34}} & 1 \\ 0 & 0 & -\frac{C_j}{a_{33}} & 1 \end{bmatrix}$$

there is obtained

$$\frac{1}{\lambda_o^2}\begin{bmatrix} m_{11} & 0 & 0 & 0 \\ 0 & m_{22} & 0 & 0 \\ 0 & 0 & m_{33} & 0 \\ 0 & 0 & 0 & m_{44} \end{bmatrix}\begin{Bmatrix} \ddot{\alpha}_1 \\ \ddot{\beta}_1 \\ \ddot{\alpha}_j \\ \ddot{\beta}_j \end{Bmatrix} + \begin{bmatrix} k_{11} & 0 & 0 & 0 \\ 0 & k_{22} & 0 & 0 \\ 0 & 0 & k_{33} & 0 \\ 0 & 0 & 0 & k_{44} \end{bmatrix}\begin{Bmatrix} \alpha_1 \\ \beta_1 \\ \alpha_j \\ \beta_j \end{Bmatrix}$$

$$+ \begin{Bmatrix} F_1 \\ F_1 \\ F_j \\ F_j \end{Bmatrix} = -\begin{Bmatrix} \frac{C_1}{a_{12}} q_1 \cos \lambda t \\ \frac{C_1}{a_{11}} q_1 \cos \lambda t \\ \frac{C_j}{a_{34}} q_j \cos \lambda t \\ \frac{C_j}{a_{33}} q_j \cos \lambda t \end{Bmatrix} \qquad \text{(VII. 36)}$$

where

$$
\begin{aligned}
m_{11} &= -\frac{C_1}{a_{12}}(a_{11} + \bar{a}_y) + (a_{11}\bar{a}_y + \bar{I}_p) \\
m_{22} &= -\frac{C_1}{a_{11}}(a_{12} + \bar{a}_y) + (a_{12}\bar{a}_y + \bar{I}_p) \\
m_{33} &= -\frac{C_j}{a_{34}}(a_{33} + \bar{a}_y) + (a_{33}\bar{a}_y + \bar{I}_p) \\
m_{44} &= -\frac{C_j}{a_{33}}(a_{34} + \bar{a}_y) + (a_{34}\bar{a}_y + \bar{I}_p) \\
k_{11} &= (1 - \frac{a_{11}}{a_{12}})\, C_1\mu_1^4 \\
k_{22} &= (1 - \frac{a_{12}}{a_{11}})\, C_1\mu_1^4 \\
k_{33} &= (1 - \frac{a_{33}}{a_{34}})C_j\mu_j^4 \\
k_{44} &= (1 - \frac{a_{34}}{a_{33}})C_j\mu_j^4
\end{aligned}
\qquad \text{(VII. 37)}
$$

In equation (VII. 36), $\alpha_1$, $\beta_1$, $\alpha_j$, $\beta_j$ each represent one mode of vibration. If the nonlinear terms in (VII. 22) are neglected, i.e., $N(\theta) = 0$, both $F_1$ and $F_j$ will be zero and the system is completely uncoupled. However, since $F_1$ and $F_j$ are not zero, each mode is coupled to another mode in a nonlinear fashion. From (VII. 34), we have

$$v_1 = \alpha_1 + \beta_1 , \quad v_j = \alpha_j + \beta_j$$

From experimental observations, only two modes were involved: the harmonic and the subharmonic mode. Let $\beta_j$ be the harmonic mode and $\alpha_1$ be the subharmonic mode. Then, modes $\beta_1$ and $\alpha_j$

are not excited under subharmonic oscillation conditions and can be neglected. Thus,

$$v_1 \approx \alpha_1 \; ; \qquad v_j \approx \beta_j \tag{VII. 38}$$

and also the second and third equations in (VII. 36) are left out in the analysis. Rewriting (VII. 36), there is obtained

$$\frac{1}{\lambda_o^2}\begin{bmatrix} m_{11} & 0 \\ 0 & m_{44} \end{bmatrix}\begin{Bmatrix} \ddot{\alpha}_1 \\ \ddot{\beta}_j \end{Bmatrix} + \begin{bmatrix} k_{11} & 0 \\ 0 & k_{44} \end{bmatrix}\begin{Bmatrix} \alpha_1 \\ \beta_j \end{Bmatrix} + \begin{Bmatrix} F_1(\alpha_1, \beta_j) \\ F_j(\alpha_1, \beta_j) \end{Bmatrix}$$

$$= -\begin{Bmatrix} \dfrac{C_1}{a_{12}} q_1 \cos \lambda t \\ \dfrac{C_j}{a_{33}} q_j \cos \lambda t \end{Bmatrix} \tag{VII. 39}$$

It remains to calculate $F_1(\alpha_1, \beta_j)$ and $F_j(\alpha_1, \beta_j)$ as defined in equation (VII. 31). $N(\theta)$ is given in (VII. 23) and $\theta$ is expressed in a form given in (VII. 24). In order to perform the integration in $\bar{z}$, it is necessary to express $\sin 2\theta$ and $\cos 2\theta$ in terms of elementary functions of $\bar{z}$.

$$\begin{aligned} \sin 2\theta &= \sin(2v_1 \sin \mu_1 \bar{z}) \cos(2v_j \sin \mu_j \bar{z}) \\ &\quad + \cos(2v_1 \sin \mu_1 \bar{z}) \sin(2v_j \sin \mu_j \bar{z}) \\ \cos 2\theta &= \cos(2v_1 \sin \mu_1 \bar{z}) \cos(2v_j \sin \mu_j \bar{z}) \\ &\quad - \sin(2v_1 \sin \mu_1 \bar{z}) \sin(2v_j \sin \mu_j \bar{z}) \end{aligned} \tag{VII. 40}$$

To express $\sin(2v_1 \sin \mu_1 \bar{z})$ etc. in terms of elementary functions of $\bar{z}$ and $v_1(t)$, the following identities are used.

$$\cos(z \sin x) \equiv J_o(z) + 2\sum_{i=1}^{\infty} J_{2i}(z) \cos 2ix$$

$$\sin(z \sin x) \equiv 2\sum_{i=1}^{\infty} J_{2i-1}(z) \sin(2i-1)x \qquad \text{(VII. 41)}$$

where $J_i(z)$ is the Bessel Function of the first kind of integral order i with argument z. Direct substitution of (VII. 41) into (VII. 40) results in very cumbersome expressions for sin 2θ and cos 2θ. Since $\sin(\mu_j \bar{z})$ is bounded by unity, approximations are made for small values of $v_j(t)$, i.e.,

$$\sin(2v_j \sin \mu_j \bar{z}) \approx 2v_j \sin \mu_j \bar{z}$$

$$\cos(2v_j \sin \mu_j \bar{z}) \approx 1 \qquad \text{(VII. 42)}$$

Using identities (VII. 41) and approximations (VII. 42), (VII. 40) can be written as

$$\sin 2\theta = 2v_j \sin(\mu_j \bar{z}) \left[ J_o(2v_1) + 2\sum_{i=1}^{\infty} J_{2i}(2v_1) \cos(2i\mu_1 \bar{z}) \right] + 2\sum_{i=1}^{\infty} J_{2i-1}(2v_1) \sin(2i-1)\mu_1 \bar{z}$$

$$\cos 2\theta = J_o(2v_1) + 2\sum_{i=1}^{\infty} J_{2i}(2v_1) \cos(2i\mu_1 \bar{z}) - 4v_j \sin(\mu_j \bar{z}) \sum_{i=1}^{\infty} J_{2i-1}(2v_1) \sin(2i-1)\mu_1 \bar{z} \qquad \text{(VII. 43)}$$

Substituting (VII. 43) into (VII. 23), the values of $F_1(v_1, v_j)$ and $F_j(v_1, v_j)$ can be calculated from (VII. 31) through simple integrations in $\bar{z}$.

A typical integration involved is

$$\int_0^{\ell/r} \sin(\mu_j \bar{z}) \sin(i\mu_1 \bar{z})\, d\bar{z} = \frac{\ell}{2r}\,\delta_{ij} \qquad i = 1, 2, 3, \ldots$$

where $\delta_{ij}$ is the Kronecker delta. The results obtained are:

$$\begin{aligned}
F_1(v_1 v_j) = \sum_{i=1}^{\infty} \Bigg[ & \nu^2 [v_j(\delta_{j,2i+1} - \delta_{j,2i-1}) J_{2i} + J_1] \\
& + \mu_1^4 \bar{I}_n \Bigg\{ v_1^2 v_j [-\tfrac{3}{2} j \delta_{j3} + \tfrac{5}{4}\delta_{j,2i+1} - \tfrac{5}{4}\delta_{j,2i-1} + \tfrac{7}{4}\delta_{j,2i-3} \\
& \quad - \tfrac{7}{4}\delta_{j,2i+3}] J_{2i} + v_1^2 v_j \delta_{j3} [-\tfrac{7}{8} J_o + \tfrac{3}{4} j^2] \\
& + v_1 v_j^2 [\tfrac{3}{2} j^2 + 3j^2 J_o - 3j^2 J_2 - 3j^2 J_{2j} \\
& \quad + (\tfrac{3}{2} j^2 - j^3 - j) J_{2j-2} + (\tfrac{3}{2} j^2 + j^3 + j) J_{2j+2}] \\
& + j^4 v_j^3 [\tfrac{5}{4}\delta_{j,2i+1} - \tfrac{5}{4}\delta_{j,2i-1} - \tfrac{7}{4}\delta_{3j,2i+1} + \tfrac{7}{4}\delta_{3j,2i-1}] J_{2i} \\
& + \frac{v_1}{2} [1 - J_o + J_2] + \tfrac{3}{4} v_1^3 \\
& + v_1^2 [\tfrac{5}{4} J_1 - \tfrac{7}{4} J_3] + v_1 v_j [(\tfrac{1}{2} - j - j^3 - \tfrac{3}{2} j^2)\delta_{j,2i-3} \\
& \quad + (\tfrac{1}{2} + j + j^3 - \tfrac{3}{2} j^2)\delta_{j,2i+1} + (3j^2 - 1)\delta_{j,2i-1}] J_{2i-1} \\
& + j^4 v_j^2 [\tfrac{1}{2} J_1 - \tfrac{9}{4} J_{2j+1} + \tfrac{9}{4} J_{2j-1}] - \tfrac{1}{2} j^4 v_j [\delta_{j,2i+1} - \delta_{j,2i-1}] J_{2i} \Bigg\} \Bigg]
\end{aligned}$$

(VII. 44)

$$F_j(v_1 v_j)=\sum_{i=1}^{\infty}\Bigg[\nu^2[v_j(J_o - J_{2j}) + \delta_{j,\,2i-1}J_{2i-1}]$$
$$+ \mu_1^4 \bar{I}_n \Bigg\{ v_1^2 v_j\left[\frac{3}{2}j^2 - \frac{1}{2}J_o - \frac{7}{2}J_2 + \frac{1}{2}J_{2j} + \frac{7}{4}J_{2j+2} + \frac{7}{4}J_{2j-2}\right]$$
$$+ v_1 v_j^2\left[-(j + j^3 + \frac{9}{2}j^2)\delta_{j,\,2i-1} + (\frac{9}{2}j^2 - j - j^3)\delta_{j,\,2i+1}\right.$$
$$\left. + (\frac{3}{2}j^2 + j + j^3)\delta_{3j,\,2i-1} + (j + j^3 + \frac{3}{2}j^2)\delta_{3j,\,2i+1}\right] J_{2i}$$
$$+ j^4 v_j^3\left[\frac{3}{4} + \frac{5}{4}J_o - 3J_{2j} + \frac{7}{4}J_{4j}\right]$$
$$+ j^4 v_j\left[\frac{1}{2} - \frac{J_o}{2} + \frac{J_{2j}}{2}\right] + \frac{3}{4}v_1^2\,\delta_{j,\,3}$$
$$+ v_1^2\left[-\frac{1}{2}\delta_{j,\,2i-1} - \frac{7}{4}\delta_{j,\,2i+1} - \frac{7}{4}\delta_{j,\,2i-3}\right] J_{2i-1}$$
$$+ v_i v_j\left[(1 + 3j^2)J_1 - (\frac{1}{2} + \frac{3}{2}j^2 + j + j^3)J_{2j+1} + (\frac{1}{2} + \frac{3}{2}j^2 - j - j^3)J_{2j-1}\right]$$
$$+ j^4 v_j^2\left[\frac{11}{4}\delta_{j,\,2i-1} - \frac{9}{4}\delta_{3j,\,2i-1}\right] J_{2i-1} - \frac{1}{2}v_1\left[\delta_{j,\,2i+1} - \delta_{j,\,2i-1}\right] J_{2i}\Bigg\}\Bigg] \qquad \text{(VII. 45)}$$

where all the arguments of the Bessel Functions are understood to be $2v_1(t)$.

From experimental observations, the transition generally occurred at the second bending predominant mode (a mode in which bending vibrations are predominant and has one node). Therefore, the case of $j = 2$ is considered here. For $j = 2$,

$$F_1(v_1, v_2) = \nu^2 J_1 + \bar{I}_n \mu_1^4 \left[ v_1^2 \left(\frac{5}{4} J_1 - \frac{7}{4} J_3\right) + v_1 v_2^2 (6 + 12J_o - 16J_2 - 12J_4 + 16J_6) \right.$$
$$\left. + 8v_2^2 \left(J_1 + \frac{9}{2} J_3 - \frac{9}{2} J_5\right) + \frac{v_1}{2} (1 - J_o + J_2) + \frac{3}{4} v_1^3 \right] \qquad \text{(VII. 46)}$$

$$F_2(v_1, v_2) = \nu^2 v_2 (J_o - J_4) + \bar{I}_n \mu_1^4 \left[ v_1^2 v_2 \left(6 - \frac{1}{2} J_o - \frac{7}{4} J_2 + \frac{1}{2} J_4 + \frac{7}{4} J_6\right) \right.$$
$$+ v_1 v_2 \left(13 J_1 - \frac{7}{2} J_3 - \frac{33}{2} J_5\right) + v_2^3 (12 + 20 J_o - 48 J_4 + 28 J_8)$$
$$\left. + v_2 (8 - 8J_o + 8J_4) \right] \qquad \text{(VII. 47)}$$

Using the relationship

$$J_n(2v_1) = \frac{(v_1)^n}{n!} \left[ 1 - \frac{(v_1)^2}{1(n+1)} + \frac{(v_1)^4}{1 \cdot 2(n+1)(n+2)} - \cdots \right] \qquad \text{(VII. 48)}$$

the Bessel Functions in (VII. 46) and (VII. 47) can be approximated in powers of their arguments for small values of $v_1$. When n is odd, $J_n$ is expandable into odd powers of its argument only. Similarly, when n is even, only even powers of the argument exist in the expansion.

The significant feature in (VII. 46) is the form the nonlinearity takes when expressed in terms of power of variables $v_1$ and $v_2$. $F_1(v_1, v_2)$ can be written in the form

$$F_1(v_1, v_2) = \sum_{i=1}^{\infty} a_i v_1^{2i+1} + v_2^2(t) \sum_{i=1}^{\infty} b_i v_1^{2i-1}(t)$$
$$\approx \sum_{i=1}^{\infty} a_i \alpha_1^{2i+1}(t) + \beta_2^2(t) \sum_{i=1}^{\infty} b_i \alpha_1^{2i-1}(t) \qquad \text{(VII. 49)}$$

where $a_i$ and $b_i$ are the coefficients of the nonlinear terms. Similarly, $F_2(v_1, v_2)$ can be written in the form

$$F_2(v_1, v_2) = v_2(t) \sum_{i=1}^{\infty} \bar{a}_i v_1^{2i}(t) + v_2^3(t) \sum_{i=0}^{\infty} \bar{b}_i v_1^{2i}(t) \qquad \text{(VII. 50)}$$

where $\bar{a}_i$ and $\bar{b}_i$ are again coefficients. The asymmetry $F_1(v_1, v_2)$ and $F_2(v_1, v_2)$ as shown in (VII. 49) and (VII. 50) is a consequence of the approximations of (VII. 42). In (VII. 42), the higher powers of $v_2(t)$ are neglected and hence no powers of $v_2(t)$ higher than the third power appears in (VII. 49) and (VII. 50). If the approximations (VII. 42) were not used, the forms of $F_1$ and $F_2$ would probably be as follows.

$$F_1 = \left(\sum_{i=1}^{\infty} a_i v_1^{2i-1}(t)\right)\left(\sum_{i=0}^{\infty} b_i v_2^{2i}(t)\right) - a_1 b_o v_1(t)$$

$$F_2 = \left(\sum_{i=1}^{\infty} \bar{a}_i v_2^{2i-1}(t)\right)\left(\sum_{i=0}^{\infty} \bar{b}_i v_1^{2i}(t)\right) - \bar{a}_1 \bar{b}_o v_2(t) \qquad \text{(VII. 51)}$$

Rewriting equation (VII. 39) there is obtained

$$\frac{m_{11}}{\lambda_o^2} \ddot{\alpha}_1 + k_{11}\alpha_1 = - F_1(\alpha_1, \beta_2) - \frac{C_1}{a_{12}} q_1 \cos \lambda t$$

$$\frac{m_{44}}{\lambda_o^2} \ddot{\beta}_2 + k_{44}\beta_2 = - F_2(\alpha_1, \beta_2) - \frac{C_2}{a_{33}} q_2 \cos \lambda t \qquad \text{(VII. 52)}$$

Guided by experimental observations, the possibility of a periodic solution for $\alpha_1(t)$ is sought under the condition when $\beta_2(t)$ is excited

in resonance. The exciting frequency $\lambda$ is assumed to be far away from the natural frequency of the $a_i$ mode and the response of $a_1$ mode to such external excitation is small. Therefore, the external forcing term in the first equation of (VII. 52) may be neglected.

By a trivial change of the time variable, the first equation of (VII. 52) can be written in the form

$$\ddot{a}_1 + a_1 = - F_1(a_1, \beta_2) \qquad \text{(VII. 53)}$$

In the next section, it is shown that a periodic solution for $a_1(t)$ of period $2\pi$ is possible under special circumstances.

## 5. Solution of a Parametrically Excited Nonlinear System

In section 4, the equation for the lower mode vibration is reduced to the form

$$\ddot{a}_1 + a_1 = - F_1(a_1, \beta_2) \qquad \text{(VII. 53)}$$

where $F_1$ is given by (VII. 51). For small $\beta_2$, $F_1$ can be approximated and is given by (VII. 46) or (VII. 49). Experimental observations showed that the higher mode was vibrating at table frequency before the subharmonic oscillations set in. Therefore, $\beta_2$ may be taken as

$$\beta_2 = R \cos \lambda t \qquad \text{(VII. 54)}$$

where $R$ is the amplitude of the higher mode and $\lambda$ is the table frequency.

In this section, a periodic solution of (VII. 53) is sought when $\lambda$ is at or near some integral value n. The algebra involved to find the solution of (VII. 53) including all the nonlinear terms of $F_1$ is formidable. Since only the mechanisms producing high order subharmonics are of interest, only terms in $F_1$ that are capable of producing high order subharmonics are retained. For any one particular order subharmonic, there are a number of terms in $F_1$ which are capable of producing it. Out of these, only the dominant term is taken in the analysis. For example, under suitable conditions, both terms $a_1^{n-1}\beta_2$ and $a_1^{2n-1}\beta_2^2$ are capable of producing a subharmonic of order n. Considering both $a_1$ and $\beta_2$ are smaller than unity, $a_1^{2n-1}\beta_2^2$ is a higher order term compared to $a_1^{n-1}\beta_2$. Thus, only the term $a_1^{n-1}\beta_2$ is retained in the analysis. It should be noted that a subharmonic of order n is the highest subharmonic possible produced by both terms.

Seeking a probable mechanism to produce a subharmonic of order n/2, it is proposed to retain only three terms in $F_1$. The three terms retained are $a_1^m$, $a_1^{n-1}$, and $a_1^{n-1}\beta_2^2$. Using (VII. 54), $a_1^{n-1}\beta_2^2$ can be written as $(R^2/2)(a_1^{n-1} + a_1^{n-1}\cos 2\lambda t)$; and the three terms retained become $a_1^m$, $a_1^{n-1}$ and $a_1^{n-1}\cos 2\lambda t$. For consistency, it is required that m be odd and n be even so that the terms retained are actually derivable from (VII. 49) or (VII. 51). Also, we consider the case where m is larger than n. Equation (VII. 53) then becomes

$$\ddot{a}_1 + a_1 = - b_1 a_1^m - b_2 a_1^{n-1} + b_3 R^2 a_1^{n-1} \cos 2\lambda t \qquad \text{(VII. 55)}$$

where $b_1$, $b_2$, and $b_3$ are positive constants and R is the amplitude of the higher mode. Equation (VII. 55) is a nonlinear ordinary differential equation parametrically excited through the coupling term with the higher mode. Nonlinear ordinary differential equations of second order have been extensively treated by many authors. Parametric excitations of linear systems have also been treated to a fair extent[19, 20, 21]. The stability of such a system can be obtained using Floquet theory and in particular, the theory of Mathieu's function[22, 23]. However, very little is known for parametrically excited nonlinear systems. In the following paragraphs, the behavior of such a system is studied. The technique used is a general perturbational method first introduced by Struble[24]. The method is essentially a combination of the technique of slowly varying parameters and that of perturbations. Assuming a solution of (VII. 55) to be of the form

$$a_1(t) = B(t) \cos (t - \phi(t)) \qquad \text{(VII. 56)}$$

and substituting (VII. 56) into (VII. 55), the left-hand side of (VII. 55) becomes

$$\text{L. H. S.} = [\ddot{B} + 2B\dot{\phi} - B\ddot{\phi}] \cos (t-\phi) + [B\ddot{\phi} + 2\dot{B}\dot{\phi} - 2\dot{B}] \sin (t-\phi) \qquad \text{(VII. 57)}$$

To evaluate the right-hand side of (VII. 55), it is convenient to express $\cos^{n-1}(t-\phi)$ and $\cos^{m}(t-\phi)$ in terms of multiple angles using the following identities:

$$2^{n-1}\cos^n(t-\phi) = \sum_{i=0}^{n/2} {}^nC_i \cos[(n-2i)(t-\phi)] - \frac{1}{2}\,{}^nC_{n/2} \quad \text{(for n even)}$$

$$2^{n-1}\cos^n(t-\phi) = \sum_{i=0}^{(n-1)/2} {}^nC_i \cos[(n-2i)(t-\phi)] \quad \text{(for n odd)} \qquad \text{(VII.58)}$$

where ${}^nC_i$ represents the possible combinations of choosing from n articles i articles at a time. In the multiple angles expansion, only the terms that are capable of producing secular terms are retained. For example, in the expansions for $b_1 a_1^m$ and $b_2 a_1^{n-1}$, only the $\cos(t-\phi)$ terms in the expansions are retained since they are actually the terms which give rise to secular terms. In the expansion of the term $b_3 R^2 a^{n-1} \cos 2\lambda t$, only the first term in the expansion is retained because only the highest possible subharmonic generated by such coupling term is considered here. The right-hand side of (VII.55) can then be written as

$$\text{R.H.S.} = -\frac{b_1 B^m}{2^{m-1}}\,{}^mC_{\frac{m-1}{2}} \cos(t-\phi) - \frac{b_2 B^{n-1}}{2^{n-2}}\,{}^{n-1}C_{\frac{n-2}{2}} \cos(t-\phi) + \frac{b_3 R^2 B^{n-1}}{2^{n-2}} \cos 2\lambda t \cos[(n-1)(t-\phi)] \qquad \text{(VII.59)}$$

The third term in (VII.59) can be expanded using the trigonometric identity

$$\cos 2\lambda t \cos[(n-1)(t-\phi)] = \frac{1}{2}\left\{\cos[(2\lambda+n-1)t-(n-1)\phi] + \cos[(2\lambda-n+1)t + (n-1)\phi]\right\} \qquad \text{(VII.60)}$$

It can be seen that when $\lambda = n/2$, the second term of (VII. 60) becomes a secular term while no positive values of $\lambda$ can make the first term a secular term. Since only terms which can lead to secular terms are retained, the first term in (VII. 60) is left out in further considerations. The second term in (VII. 60) can be written in the form $\frac{1}{2}[\cos(t-\phi)\cos\sigma - \sin(t-\phi)\sin\sigma]$. Then, (VII. 59) becomes

$$\text{R. H. S.} = -\frac{b_1 B^m}{2^{m-1}} {}^{m}C_{\frac{m-1}{2}} \cos(t-\phi) - \frac{b_2 B^{n-1}}{2^{n-2}} {}^{n-1}C_{\frac{n-2}{2}} \cos(t-\phi)$$

$$+ \frac{b_3 R^2 B^{n-1}}{2^{n-1}} \left[\cos(t-\phi)\cos\sigma - \sin(t-\phi)\sin\sigma\right] \qquad \text{(VII. 61)}$$

where

$$\sigma \equiv (2\lambda - n)t + n\phi \qquad \text{(VII. 62)}$$

Equating (VII. 57) and (VII. 61) with an examination of the terms suggests the following distribution:

$$\ddot{B} + 2B\dot{\phi} - B\dot{\phi}^2 = -\frac{b_1 B^m}{2^{m-1}} {}^{m}C_{\frac{m-1}{2}} - \frac{b_2 B^{n-1}}{2^{n-2}} {}^{n-1}C_{\frac{n-2}{2}}$$

$$+ \frac{b_3 R^2 B^{n-1}}{2^{n-1}} \cos\sigma \qquad \text{(VII. 63)}$$

$$B\ddot{\phi} + 2\dot{B}\dot{\phi} - 2\dot{B} = -\frac{b_3 R^2 B^{n-1}}{2^{n-1}} \sin\sigma \qquad \text{(VII. 64)}$$

If the variational parameters $B(t)$ and $\phi(t)$ are slowly varying, the time derivatives of the parameters are small and can be considered higher order terms compared with the parameters. Neglecting higher

order terms in the left-hand side of (VII. 63) and (VII. 64), there is obtained

$$B\dot{\phi}(t) = -\frac{b_1 B^m}{2^m}\, {}^mC_{\frac{m-1}{2}} - \frac{b_2 B^{n-1}}{2^{n-1}}\, {}^{n-1}C_{\frac{n-2}{2}} + \frac{b_3 R^2 B^{n-1}}{2^n}\cos\sigma \qquad \text{(VII. 65)}$$

$$\dot{B}(t) = \frac{b_3 R^2 B^{n-1}}{2^n}\sin\sigma \qquad \text{(VII. 66)}$$

Differentiating (VII. 62) with respect to $t$ and using (VII. 65), there is obtained

$$\dot{\sigma}(t) = (2\lambda - n) + \frac{n}{B}\left[-\frac{b_1 B^m}{2^m}\, {}^mC_{\frac{m-1}{2}} - \frac{b_2 B^{n-1}}{2^{n-1}}\, {}^{n-1}C_{\frac{n-2}{2}} + \frac{b_3 R^2 B^{n-1}}{2^n}\cos\sigma\right] \qquad \text{(VII. 67)}$$

Equations (VII. 65), (VII. 66) and (VII. 67) are three equations for the three unknowns $B$, $\phi$, and $\sigma$. It is difficult to write out explicitly the dependence of $B$, $\phi$ and $\sigma$ on time $t$. However, sufficient information can be obtained using the phase plane technique. From (VII. 66) and (VII. 67) there is obtained

$$\frac{dB}{d\sigma} = \frac{\frac{b_3 R^2 B^n}{2^n}\sin\sigma}{(2\lambda - n)B + n\left(\frac{-b_1 B^m}{2^m}\, {}^mC_{\frac{m-1}{2}} - \frac{b_2 B^{n-1}}{2^{n-1}}\, {}^{n-1}C_{\frac{n-2}{2}} + \frac{b_3 R^2 B^{n-1}}{2^n}\cos\sigma\right)} \qquad \text{(VII. 68)}$$

Equation (VII. 68) is an exact differential and its first integral is

$$\frac{(2\lambda-n)B^2}{2} - \frac{n}{(m+1)} \frac{b_1 B^{m+1}}{2^m} {}^{m}C_{\frac{m-1}{2}} - \frac{b_2 B^n}{2^{n-1}} {}^{n-1}C_{\frac{n-2}{2}}$$

$$+ \frac{b_3 R^2 B^n}{2^n} \cos\sigma = K \qquad \text{(VII. 69)}$$

where K is a constant of integration. For given values of m and n and for each value of K, a trajectory can be constructed from (VII. 69) in the B-$\sigma$ phase plane, using B as the polar distance from the origin and $\sigma$ as the polar angle.

However, it is more instructive to study the singularities in the B-$\sigma$ phase plane. The singularities are found by equating both the numerator and denominator of (VII. 68) to zero. The possible singularities are:

(i). B = 0, i.e., the origin is a singularity.

For $B \neq 0$, then

(ii). $\sin\sigma = 0$ (VII. 70)

and

$$\frac{b_1}{2^m} {}^{m}C_{\frac{m-1}{2}} B^{m-1} + (2b_2 {}^{n-1}C_{\frac{n-2}{2}} - b_3 R^2 \cos\sigma) \frac{B^{n-2}}{2^n}$$

$$- \frac{(2\lambda-n)}{n} = 0 \qquad \text{(VII. 71)}$$

To satisfy equation (VII. 70), $\sigma$ can be zero or $\pi$. For given values of m and n, equation (VII. 71) can be solved for B and the roots of

the equation give the locations of the singularities. Only positive roots of (VII. 71) are of interest because B, being the polar distance in the B-$\sigma$ phase plane, is never negative. The distribution of roots in equation (VII. 71) can be deduced from Descartes' rule for real roots of algebraic equations. It states that the number of positive roots is equal to the number of sign changes in the coefficients of the equation, or less than that by an even number. Zero coefficients are ignored in such counts. The number of positive roots of (VII. 71), and hence the number of singularities of (VII. 68), excluding the origin, is summarized in Table VII.

Table VII

DISTRIBUTION OF POSITIVE ROOTS OF (VII. 71) UNDER DIFFERENT CONDITIONS

| Conditions on Parametric Excitation Frequency | Amplitude | "phase" $\sigma$ | Number of Positive Roots |
|---|---|---|---|
| $2\lambda - n > 0$ | $b_3R^2 > 2b_2{}^{n-1}C_{\frac{n-2}{2}}$ | 0 | 1 |
| $2\lambda - n > 0$ | $b_3R^2 < 2b_2{}^{n-1}C_{\frac{n-2}{2}}$ | 0 | 1 |
| $2\lambda - n > 0$ | - | $\pi$ | 1 |
| $2\lambda - n < 0$ | $b_3R^2 > 2b_2{}^{n-1}C_{\frac{n-2}{2}}$ | 0 | 2 or zero |
| $2\lambda - n < 0$ | $b_3R^2 < 2b_2{}^{n-1}C_{\frac{n-2}{2}}$ | 0 | 0 |
| $2\lambda - n < 0$ | - | $\pi$ | 0 |

It is interesting to note that the number of singularities depends both on the frequency and the amplitude of the parametric excitation.

In order to investigate the nature of the singularities, it is necessary to have explicit expressions for the locations of the singularities. However, there is no formula in general to give the roots of (VII. 71) explicitly. To overcome this difficulty, a special case is considered and the nature of the singularities in this case is studied. The results from this special case are taken as a guide to the nature of the singularities in the general case.

The special case considered is for the values $m = 5$, and $n = 4$. In this case, ${}^{m}C_{\frac{m-1}{2}} = 10$, ${}^{n-1}C_{\frac{n-2}{2}} = 3$. Equation (VII. 68) becomes

$$\frac{dB}{d\sigma} = \frac{b_3 R^2 B^3 \sin\sigma}{16(2\lambda-4) - 20b_1 B^4 - 4B^2(6b_2 - b_3 R^2 \cos\sigma)} \qquad \text{(VII. 72)}$$

Equation (VII. 71) becomes

$$5b_1 B^4 + (6b_2 - b_3 R^2 \cos\sigma)B^2 - 4(2\lambda - 4) = 0 \qquad \text{(VII. 73)}$$

Solving, there is obtained,

$$B^2 = \frac{1}{10\, b_1}\left\{-(6b_2 - b_3 R^2 \cos\sigma) \pm \left[(6b_2 - b_3 R^2 \cos\sigma)^2 + 80\, b_1 (2\lambda - 4)\right]^{\frac{1}{2}}\right\} \qquad \text{(VII. 74)}$$

Only the positive roots of (VII. 74) are of interest. Considering for example, the case when $2\lambda - 4 > 0$, $\sigma = 0$ and $b_3 R^2 > 6b_2$, it is obtained

$$B^2 = \frac{(b_3R^2 - 6b_2)}{10\, b_1}\left[1 + \left(1 + \frac{80b_1(2\lambda - 4)}{(b_3R^2 - 6b_2)^2}\right)^{\frac{1}{2}}\right] \qquad \text{(VII. 75)}$$

Different approximations can be made to (VII. 75) under different conditions. For example, when $(2\lambda - 4)$ is small and $(b_3R^2 - 6b_2)^2$ is large, corresponding to the case when the exciting frequency is at or near multiples of the fundamental and the amplitude of the parametric excitation is large, the expression under the square root sign can be expanded into powers of $\left(\frac{80\, b_1(2\lambda - 4)}{(b_3R^2 - 6b_2)^2}\right)$ and only the first power term is retained. Alternately, the exciting frequency may not be near a multiple of the fundamental while the amplitude of the excitation is very close to the critical amplitude. Mathematically, this corresponds to $(2\lambda - 4)$ large and $(b_3R^2 - 6b_2)^2$ small. A different expansion and approximation would then be appropriate. Experimental observations showed that the exciting frequency was the critical parameter. The parametrically exciting amplitude was the resonant amplitude of the higher mode. Thus, it is felt that in all cases considered, it is reasonable to assume $\frac{80b_1(2\lambda - 4)}{(b_3R^2 - 6b_2)^2} \ll 1$; and the expression under the square root sign is expanded into powers of $\left(\frac{80\, b_1(2\lambda - 4)}{(b_3R^2 - 6b_2)^2}\right)$ and only the first power term is retained. Using such approximation, a summary of the locations of the singularities under various conditions is given in Table VIII.

Table VIII. LOCATION AND NATURE OF SINGULARITIES WITH DIFFERENT CONDITIONS

| | Conditions on Parametric Excitation | | $\sigma$ | Location of Singularities $B^2$ | Type of Singularities |
|---|---|---|---|---|---|
| | Frequency | Amplitude | | | |
| Case (i) | $2\lambda - 4 > 0$ | $b_3R^2 > 6b_2$ | 0 | $\frac{b_3R^2 - 6b_2}{5b_1}\left[1 + \frac{20b_1(2\lambda - 4)}{(b_3R^2 - 6b_2)^2}\right]$ | center |
| | | | $\pi$ | $\frac{4(2\lambda - 4)}{(b_3R^2 + 6b_2)}$ | saddle pt. |
| Case (ii) | $2\lambda - 4 > 0$ | $b_3R^2 < 6b_2$ | 0 | $\frac{4(2\lambda - 4)}{6b_2 - b_3R^2}$ | center |
| | | | $\pi$ | $\frac{4(2\lambda - 4)}{6b_2 + b_3R^2}$ | saddle pt. |
| Case (iii) | $2\lambda - 4 = 0$ | $b_3R^2 > 6b_2$ | 0 | $\frac{b_3R^2 - 6b_2}{5b_1}$ | center |
| Case (iv) | $2\lambda - 4 = 0$ | $b_3R^2 < 6b_2$ | - | - | - |
| Case (v) | $2\lambda - 4 < 0$ | $b_3R^2 > 6b_2$ | 0 | $\frac{b_3R^2 - 6b_2}{5b_1}\left[1 - \frac{20b_1(4 - 2\lambda)}{(b_3R^2 - 6b_2)^2}\right]$ | center |
| | | | 0 | $\frac{4(4 - 2\lambda)}{b_3R^2 - 6b_2}$ | saddle pt. |
| Case (vi) | $2\lambda - 4 < 0$ | $b_3R^2 < 6b_2$ | - | - | - |

It should be pointed out that the origin $B = 0$ is always a singularity in addition to those shown in Table VIII. When $b_3R^2 - 6b_2 = 0$, all results in Table VIII are no longer valid. The solution can be obtained directly from (VII. 73)

$$B^2 = \left( \frac{4(2\lambda - 4)}{5b_1} \right)^{\frac{1}{2}} \qquad \text{(VII. 76)}$$

In this case, only when $2\lambda - 4 > 0$ can positive real roots exist.

Before the trajectories in the $B - \sigma$ phase plane can be sketched, it is necessary to know the nature of the singularities, i.e., the behavior of the trajectories in the neighborhood of the singularities. Such information can best be obtained by considering the perturbational equations. Let

$$\begin{aligned} B &= B_o + \tilde{B} \\ \sigma &= \sigma_o + \tilde{\sigma} \end{aligned} \qquad \text{(VII. 77)}$$

where $B_o$ and $\sigma_o$ give the location of the singularity and $\tilde{B}$, $\tilde{\sigma}$ are the perturbational variables to describe the trajectories in the neighborhood of the singularity. Substituting (VII. 77) into equations (VII. 66) and (VII. 67) and neglecting higher order terms in $\tilde{B}$ and $\tilde{\sigma}$ the perturbational equations are obtained.

$$\frac{d\tilde{B}}{dt} = \frac{b_3R^2B_o^{n-2}}{2^n} \left[ B_o \cos \sigma_o \tilde{\sigma} + (n-1) \sin \sigma_o \tilde{B} \right] \qquad \text{(VII. 78)}$$

$$B_o \frac{d\tilde{\sigma}}{dt} = (2\lambda - n)\tilde{B} + \frac{nb_3 R^2 B_o^{n-2}}{2^n} \left[ (n-1)\cos \sigma_o \tilde{B} - B_o \sin \sigma_o \tilde{\sigma} \right]$$

$$- \left[ \frac{n(n-1)}{2^{n-1}} b_2 B_o^{n-2} \, {}^{n-1}C_{\frac{n-2}{2}} + \frac{mn}{2^n} b_1 B_o^{m-1} \, {}^{m}C_{\frac{m-1}{2}} \right] \tilde{B} \qquad \text{(VII. 79)}$$

Specializing to the case $m = 5$, $n = 4$, there is obtained

$$\frac{d\tilde{B}}{dt} = \frac{b_3 R^2 B_o^2}{16} \left[ B_o \cos \sigma_o \tilde{\sigma} + 3 \sin \sigma_o \tilde{B} \right] \qquad \text{(VII. 80)}$$

$$B_o \frac{d\tilde{\sigma}}{dt} = (2\lambda - 4)\tilde{B} + \frac{b_3 R^2 B_o^2}{4} \left[ 3 \cos \sigma_o \tilde{B} - B_o \sin \sigma_o \tilde{\sigma} \right]$$

$$- \left[ \frac{9}{2} b_2 B_o^2 + \frac{25}{4} b_1 B_o^4 \right] \tilde{B} \qquad \text{(VII. 81)}$$

To investigate the nature of the singularities, each singularity is examined in turn. For example, in case (i) of Table VIII, one singularity is $\sigma_o = 0$, $B_o^2 = \frac{b_3 R^2 - 6b_2}{5b_1} \left[ 1 + \frac{20\, b_1 (2\lambda - 4)}{(b_3 R^2 - 6b_2)^2} \right]$. From (VII. 80) and (VII. 81), it is found

$$\frac{d\tilde{B}}{dt} = \frac{b_3 R^2 B_o^3}{16} \tilde{\sigma} \qquad \text{(VII. 82)}$$

$$B_o \frac{d\tilde{\sigma}}{dt} = - \left[ \frac{(b_3 R^2 - 6b_2)^2}{10\, b_1} + 6(2\lambda - 4) + O\left((2\lambda - 4)^2\right) \right] \tilde{B} \qquad \text{(VII. 83)}$$

Equations (VII. 82) and (VII. 83) can be written in the form

$$\frac{d\tilde{B}}{d\tilde{\sigma}} = - K \frac{\tilde{\sigma}}{\tilde{B}} \qquad \text{(VII. 84)}$$

where $K$ is a positive constant. Direct integration of (VII. 84) leads

to elliptic trajectories in the neighborhood of the singularity. Therefore, the singularity considered is a center.

Similarly, for the singularity $\sigma_o = \pi$, $B_o^2 = \frac{4(2\lambda-4)}{b_3R^2+6b_2}$, we have

$$\frac{d\tilde{B}}{dt} = -\frac{b_3R^2B_o^3}{16}\tilde{\sigma} \qquad \text{(VII. 85)}$$

$$B_o\frac{d\tilde{\sigma}}{dt} = -\left[2(2\lambda-4) + O\left((2\lambda-4)^2\right)\right]\tilde{B} \qquad \text{(VII. 86)}$$

From (VII. 85) and (VII. 86), there is obtained

$$\frac{d\tilde{B}}{d\tilde{\sigma}} = K\frac{\tilde{\sigma}}{\tilde{B}} \qquad \text{(VII. 87)}$$

where K is a positive constant. Direct integration of (VII. 87) leads to hyperbolic trajectories near the singularity. Thus, the singularity considered is a saddle point.

To complete the consideration of singularities in the case $2\lambda - 4 > 0$, $b_3R^2 > 6b_2$, it is necessary to investigate the singularity at the origin, $B_o = 0$. Substitution of the value of $B_o$ in (VII. 80) and (VII. 81) yields no information. The reason is that the origin happens to be an inherent singularity of the polar coordinate system also. A Van de Pol plot (Cartesian phase plane plot) instead of the polar plot becomes more suitable in this case.

Let $X = B\cos\sigma$, $Y = B\sin\sigma$. Equation (VII. 72) is transformed to

$$\frac{dY}{dX} = \frac{b_3R^2Y^2(X^2+Y^2)^{\frac{1}{2}} + HX}{b_3R^2XY(X^2+Y^2)^{\frac{1}{2}} - HY} \qquad \text{(VII. 85)}$$

where

$$H = 16(2\lambda-4) + 4b_3R^2X(X^2+Y^2)^{\frac{1}{2}} - 24b_2(X^2+Y^2) - 20b_1(X^2+Y^2)^2$$

Let $X = X_o + \tilde{X}$, $Y = Y_o + \tilde{Y}$. The perturbational equations for $\tilde{X}$ and $\tilde{Y}$ can be written in the form

$$\begin{aligned} \frac{d\tilde{Y}}{dt} &= 16(2\lambda-4)\tilde{X} + f_1(X_o, Y_o)\tilde{X} + g_1(X_o, Y_o)\tilde{Y} \\ \frac{d\tilde{X}}{dt} &= -16(2\lambda-4)\tilde{Y} + f_2(X_o, Y_o)\tilde{X} + g_2(X_o, Y_o)\tilde{Y} \end{aligned} \qquad \text{(VII. 86)}$$

where $f_1(0,0) = f_2(0,0) = g_1(0,0) = g_2(0,0) = 0.$ (VII. 87)

The nature of the singularity at the origin can be studied using (VII. 86). At the origin, $X_o = Y_o = 0$. By virtue of (VII. 87), (VII. 86) becomes

$$\frac{d\tilde{Y}}{d\tilde{X}} = \frac{-(2\lambda-4)\tilde{X}}{(2\lambda-4)\tilde{Y}} \qquad \text{(VII. 88)}$$

Direct integration of (VI. 88) gives circular trajectories near the origin. Therefore, the origin is a center for all cases when $2\lambda-4 \neq 0$.

Such a conclusion can also be reached from consideration of the theory of differential equations. It is seen that (VII. 55) satisfies the nonlinearity condition, i.e.,

$$\lim_{a_1 \to 0} \frac{|b_1a_1^m + b_2a_1^{n-1} - b_3R^2a_1^{n-1}\cos 2\lambda t|}{|a_1|} = 0 \qquad \text{(VII. 89)}$$

From theorems on the stability of nonlinear systems[24], it can be

shown that the stability of (VII. 55) is governed by the behavior of its linear parts in the neighborhood of the origin. The linear part of (VII. 55) is marginally stable. Hence (VII. 55) is also marginally stable near the origin. It can then be deduced that the origin is a center.

The other singularities for the different cases are studied in a similar way and their characters are listed in Table VIII. Using (VII. 69) and specializing it to the case $m = 5$, $n = 4$, the equation for the trajectories is given by

$$(2\lambda-4)B^2 - \frac{3}{4} b_2 B^4 + \frac{b_3 R^2 \cos \sigma B^4}{8} - \frac{5 b_1 B^6}{12} = \text{constant} \quad \text{(VII. 90)}$$

Sketches of the trajectories in the phase plane are shown in Figures 26, 27 and 28.

It can be seen that motions in all regions of the phase plane are amplitude stable, but the "phase" $\sigma$ is stable only at the shaded regions. The net change of $\sigma$ in such regions after one cycle is zero while the net change is $2\pi$ in the unshaded regions. $\sigma$ is defined by equation (VII. 62) where $\phi$ is the true phase angle of the motion. Recalling that $|2\lambda - 4|$ is small in all the cases considered, the phase angle $\phi$ is essentially constant when the net change of $\sigma$ over one cycle is zero. From (VII. 56), it is seen that the motion of $a_1(t)$ has a period of $2\pi$ in such regions and hence subharmonic motion is indeed possible. It is interesting to note that the area of the shaded area and also the singularity inside the shaded region is highly dependent on the amplitude of the parametric excitation. For the

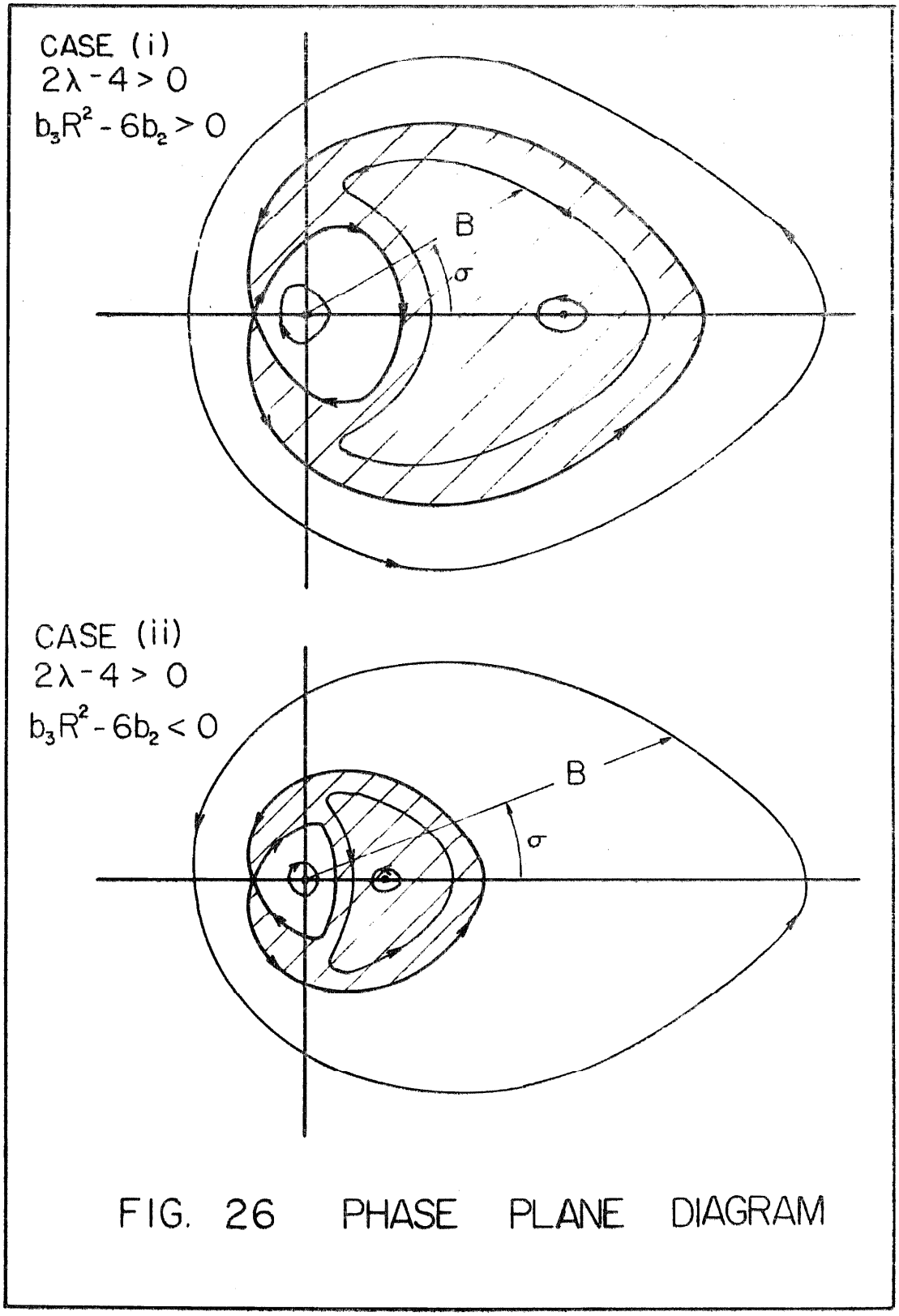


FIG. 26 PHASE PLANE DIAGRAM

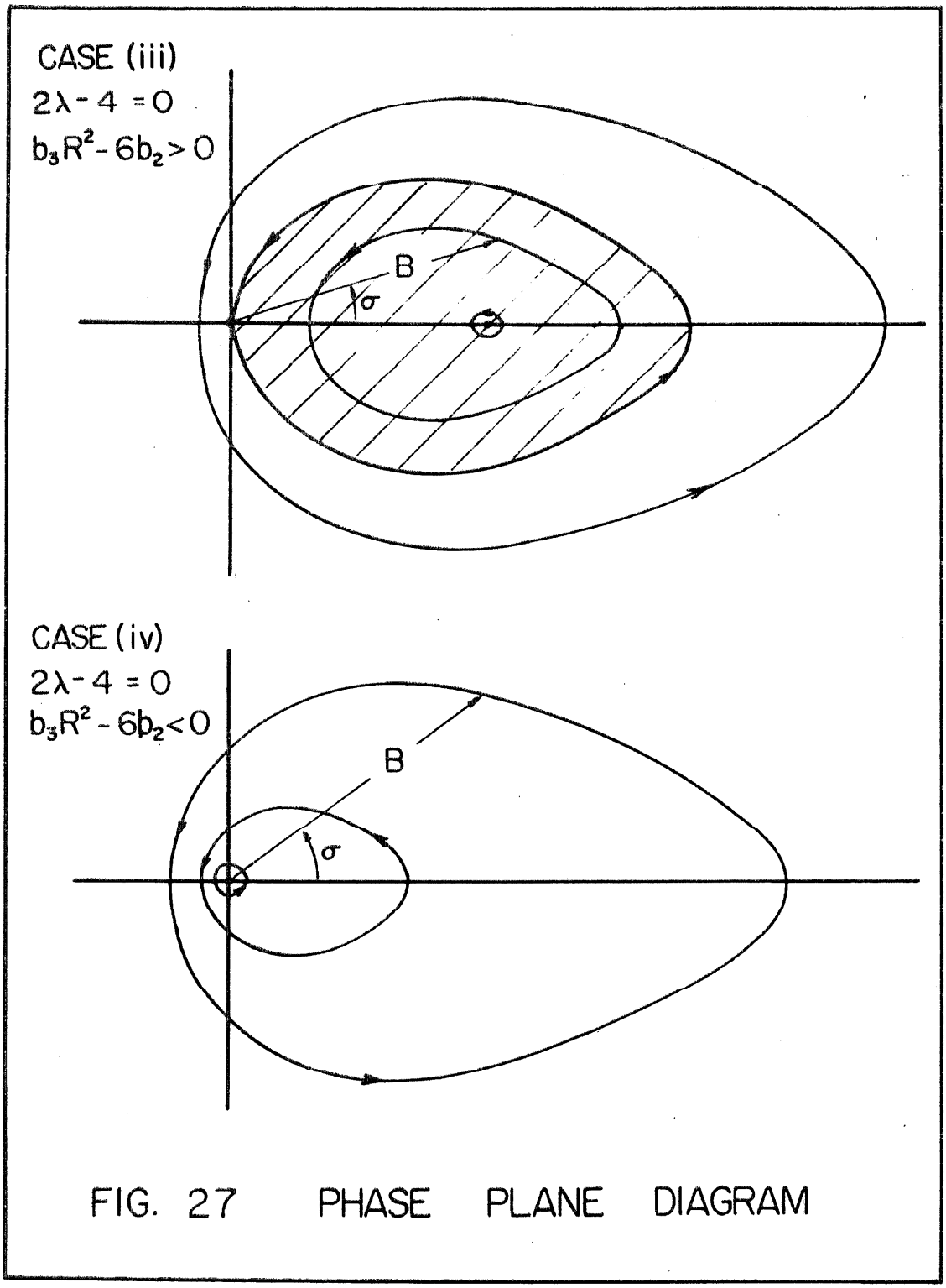


FIG. 27 PHASE PLANE DIAGRAM

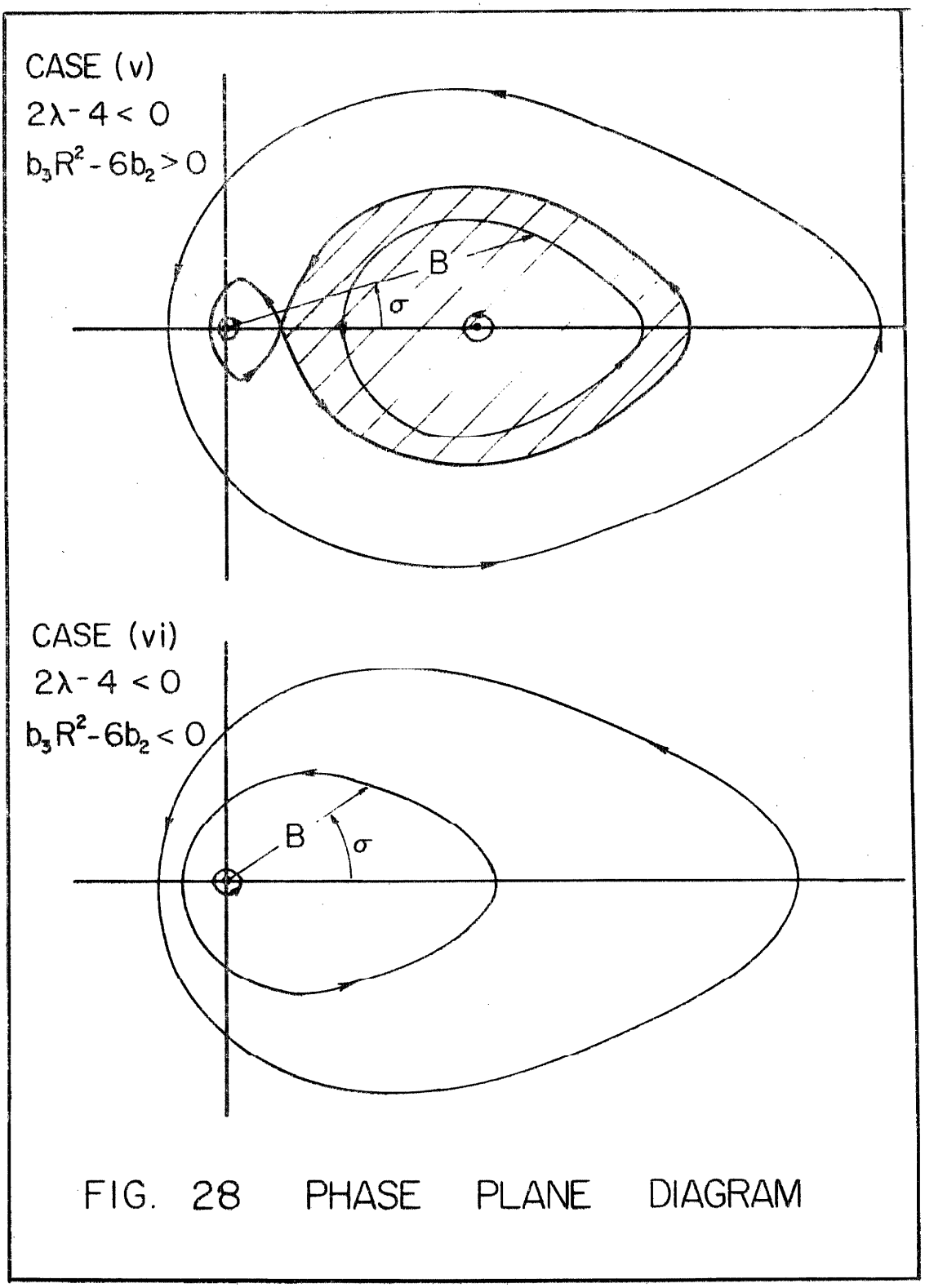


FIG. 28 PHASE PLANE DIAGRAM

exciting amplitude less than a critical value, no shaded area exist in the cases $2\lambda-4 \leq 0$, and the shaded area is small in the case $2\lambda-4 > 0$. The center inside the region is close to the origin in the latter case. On the other hand, when the exciting amplitude exceeds the critical value, shaded areas exist under all three frequency conditions and the distance of the center from the origin is roughly proportional to the exciting amplitude. Large amplitude subharmonic oscillation is possible under such circumstances. This agrees well with experimental observations that the subharmonic behavior was observed only when a higher mode was in resonance and hence the exciting amplitude to the lower mode was large.

The phase plane plots are for the case $m = 5$ and $n = 4$. The corresponding possible subharmonic oscillation is of order $\frac{1}{2}$. In view of Table VII, the distribution of singularities in the general case will be similar and it is reasonable to assume the nature of the singularities will be similar to the case considered also. Then, it is indirectly shown that equation (VII. 55) is capable of producing high order subharmonics under favorable conditions. Equation (VII. 55) is derivable from the equations of elasticity and its solution predicts behavior which agrees well with experimental observations. It is felt that such nonlinear parametric excitation of the lower mode through the resonance of a higher mode is a possible, if not the only mechanism responsible for the observed nonlinear behavior of the beam.

It must be pointed out that there are observed facts not ex-

plained by the proposed model. For example, subharmonic behavior was observed when the beam was excited at the resonant frequency of the higher mode but no ultraharmonic behavior was observed when the beam was excited at the first mode. Perhaps this can be partially argued that the response of the beam in the first mode resonance is of a much more violent nature than the higher modes. Any possible ultraharmonics superposed on the resonant response of the first mode may not be noticeable. Another observed fact was that whenever subharmonic behavior was observed, the two modes involved were the lowest mode and the "second bending predominant mode." The only exception was with a section $\Phi = 120^{\circ}$ at a beam length of 36". A subharmonic of order $\frac{1}{2}$ was observed when the sixth mode (the second bending predominant mode) was excited at 594 cps and subharmonic oscillations occurred at 296 cps, a value close to the resonant frequency of the fourth mode (the third torsion predominant mode).

It is suggested that further research is necessary before such observed facts can be clarified. The analysis in the present case is hampered by the vast number of terms in the governing equations. Various approximations have to be used to simplify the analysis before meaningful results can be obtained. Further research can avoid such difficulty by considering simpler systems. For example, when the section of the beam has two axes of symmetry, the bending and torsional motions are uncoupled. Only the longitudinal and torsional motions are nonlinearly coupled. If there are methods to

excite the specimen torsionally, the response of the specimen will consist only of rotation and longitudinal displacement, but no bending displacements. A system under such conditions is simpler to analyze because the governing equations are a pair of coupled nonlinear equations instead of four coupled equations as in the case of a mono-symmetric section. The difficulty in such an approach lies in the experimentation. It may be difficult to excite the specimen to execute pure torsional motion.

Perhaps a more fruitful approach is to study discrete systems having the characteristics of nonlinear couplings among their generalized coordinates. Such systems are simpler to study because the governing equations will be nonlinear ordinary differential equations instead of nonlinear partial differential equations as in the case of a continuous system. One example of such a system is a beam-pendulum system studied by Sevin[19], Struble and Heinbockel[20]. The system consists of a pinned ended beam supported at the ends of two simple pendulums. The case of free vibration of such a system has been studied. In their analysis, higher order nonlinear coupling terms are neglected and the problem is reduced to a linear parametrically excited system. Under such circumstances, the only subharmonic possible is of order $\frac{1}{2}$. It would be most interesting to extend the analysis to include the higher order nonlinear coupling terms between the pendulum motion and the beam motion to study the necessary and sufficient conditions for higher order subharmonics for such a system.

# Chapter 8

# CONCLUSIONS

The validity of existing theories of the dynamics of thin-walled elastic beams of open cross section has been examined both analytically and experimentally. Analytically, a higher order theory which includes effects of shear strains induced by bending and warping was constructed and compared with the existing elementary theory for different boundary conditions. Experimentally, tests were conducted on beams of two different cross sections and varying lengths. The resonant frequencies were found and compared with the values predicted by the analysis. Although the investigations were confined to specific sections, it is felt that generalizations can be made to extend the results to thin-walled elastic beams of open cross sections in general.

Comparing the experimental results with the calculated curves for the different categories of beam lengths, the following conclusions can be drawn from the investigations:

1. The existing elementary theory gives good predictions of the resonant frequencies of the first few modes of vibration when the beam is long. Recalling the definition of long beam in chapter 6, and that the difference between the higher order theory and the elementary theory is the inclusion of the effect of shear strain due to bending and restraint of warping, it can be concluded that for long beams, the shear strain effect is indeed negligible; and hence both theories give the same result.

2. For medium beam length, the elementary theory is satisfactory in predicting resonant frequencies of the first few torsion predominant modes. It overestimates the natural frequencies for the bending predominant modes. In this range, the higher order theory is preferred for predicting the frequencies of the bending predominant modes.

3. For short beams, the approximate theories are satisfactory in giving the first mode response. Both of them overestimate the frequencies of the higher modes. To estimate the correct values of resonant frequencies of the higher modes, the curves in chapter 6 suggest the following empirical formula,

$$(\text{frequency})_{\text{true}} \approx 2(\text{frequency})_{\text{higher order theory}} - (\text{frequency})_{\text{elementary theory}} \qquad \text{(VIII.1)}$$

4. For very short beams, none of the approximate theories is satisfactory and it is necessary to analyze the system as a shell structure.

Hence, the function of the higher order theory is threefold. Firstly, together with the elementary theory, it serves as a scale to divide up the beam length into the different categories as defined. In this way, the validity of the elementary theory can be estimated. Secondly, it is the theory to use when bending predominant modes are involved since the elementary theory is not adequate in such instances except for very long beams. Thirdly, when the beam is

short, the true frequency of the higher modes can be estimated using the empirical formula (VIII. 1).

The results predicted by the two theories are affected by the geometric shape of the cross section. For a monosymmetric section, it is found that the geometric parameters $\bar{I}_{\omega\omega}$, $\bar{I}_{\omega\omega}/\bar{I}_{hh}$ and $\bar{I}_{cc}$ as defined in (IV. 3) give a good indication of the difference in results predicted by the two theories for a fixed $r/\ell$. When $\bar{I}_{\omega\omega}$, $\bar{I}_{\omega\omega}/\bar{I}_{hh}$ are large and $\bar{I}_{cc}$ is small, the difference in results can be expected to be larger than if the opposite situations occur. Therefore, the useful range of the elementary theory as well as the higher order theory will diminish accordingly.

The occurrence of subharmonic oscillations observed in the experiment indicates that linearization of the governing equations is not valid under certain conditions. The equations for the coupled torsional and bending vibrations are inherently nonlinear because the transformation required to express a rotation in terms of rectilinear displacements is nonlinear. Usually, the transformation may be considered linear for infinitesimal rotations. Whenever such an approximation is used, it is implied that no mechanism exists in the system that will magnify the small nonlinear effects that have been neglected. In the present case, resonance of the lowest mode may act as the magnifying mechanism to render the linear approximation invalid in special circumstances. Since the structural damping for metals is small in general, resonance is a very efficient magnifying mechanism. Thus, the most important conclusion from the nonlinear

analysis is that seemingly insignificant terms can be neglected only when no mechanism exists that may magnify their effects subsequently.

Experimental observations point to the fact that a necessary condition for such subharmonic oscillations is that one of the resonant frequencies of the higher modes being a multiple or near multiple of the resonant frequency of the mode to be excited into subharmonic oscillations. Nonlinear vibrations of large amplitude are generated in the laboratory. Unless it is accounted for in design, such undesirable vibrations may also occur in missiles and submarines where such beams are used.

# REFERENCES


1. Nowinski, J., "Theory of Thin-Walled Bars," Applied Mechanics Review, Vol. 12, No. 4, (April 1959).

2. Gere, J. M., and Lin, Y. K., "Coupled Vibrations of Thin-Walled Beams of Open Cross Section," Journal of Applied Mechanics, (Sept. 1958), pp. 373-378.

3. Gere, J. M., "Bending and Torsional Vibrations of Thin-Walled Bars of Open Cross Section," Ph. D. Thesis, Stanford University, (1954).

4. Vlasov, V. Z., Thin Walled Elastic Beams, second edition, translated from Russian; published by Israel Programme for Scientific Translations, Jerusalem, (1961).

5. Mindlin, R. D., and Goodman, L. E., "Bending Vibration with Time Dependent Boundary Condition," Journal of Applied Mechanics, (1950), pp. 377-380.

6. Dolph, C. L., "Normal Modes of Oscillations in Beams," Report UMM 79, Willow Run Research Center, University of Michigan, (1951).

7. Dzanelidze, G. J., "Variational Formulation of the Vlasov Theory of Thin Walled Rods," (in Russian), Prikl. Math. Mekh., Vol. 7, No. 6, (1943), pp. 455-462.

8. Goldstein, H., Classical Mechanics, Addison-Wesley Publishing Co., Inc., (1959), Chapter 2.

9. Love, A. E. H., The Mathematical Theory of Elasticity, 4th edition, Dover Publication, (1944), Chapter 14.

10. Koiter, W. T., "A Consistent First Approximation in the General Theory of Thin Elastic Shell," Proceedings of Symposium on the Theory of Thin Elastic Shells, (I. U. T. A. M.), North-Holland Publishing Company, (1959).

11. Courant, R. and Hilbert, D., Methods of Mathematical Physics, Vol. 1, Interscience Publishers Inc., (1953).

12. Anderson, R. A., "Flexural Vibrations of a Uniform Beam According to the Timoshenko Theory," Journal of Applied Mechanics, (Dec. 1953), pp. 504-510.

13. Gere, J. M., "Torsional Vibration of Beams of Thin-Walled Open Sections," Journal of Applied Mechanics, (1954), pp. 381-387.

14. Barr, A. D. S., "Torsional Waves in Uniform Rods of Non-Circular Sections," Journal of Mechanical Engineering Science, Vol. 4, No. 2, (1962).

15. Temple, G., and Bickley, W. G., Rayleigh's Principle, Dover Publication Inc., (1956).

16. Timoshenko, S. P., Vibrational Problems in Engineering, second edition, Van Nostrand Company Inc., (1937), pp. 337-338.

17. Friedman, B., Principles and Techniques of Applied Mathematics, John Wiley and Son Inc., (1960), pp. 207-213.

18. Cullimore, M. S. G., "The Shortening Effect: A Nonlinear Feature of Pure Torsion," Research, Engineering Structures Supplement, London (1949).

19. Sevin, E., "On the Parametric Excitation of Pendulum Type Vibration Absorber," Journal of Applied Mechanics, (Sept. 1961).

20. Struble, R. A., and Heinbockel, J. H., "Resonant Oscillations of a Beam-Pendulum System," Journal of Applied Mechanics, (June 1963).

21. Hsu, C. S., "On the Parametric Excitation of a Dynamic System Having Multiple Degrees of Freedom," Journal of Applied Mechanics, (Sept. 1963).

22. Stoker, J. J., Nonlinear Vibrations, Interscience Publishers Inc., (1950).

23. McLachlan, N. W., Theory of Mathieu Functions, Oxford University Press, (1947).

24. Struble, R. A., Nonlinear Differential Equations, McGraw-Hill Series in Pure and Applied Mathematics, McGraw Hill Book Company, (1962).

## Appendix I

## CALCULATIONS OF THE GEOMETRIC PROPERTIES OF A SPLIT RING SECTION

A circular split ring section is completely defined geometrically by three quantities: the radius a, the thickness c, and the semi-central angle $\Phi$ as shown in Figure 3. The origin of the axes is at the centroid of the section and let OY be the axis of symmetry. Let the coordinates of the geometric center of the section B be (O, L), and $\phi$ be the angle measured from the axis of symmetry as shown. It is noted in chapter 3 that the origin of the coordinate s for a monosymmetric section is at the point where the axis of symmetry cuts the section. From the geometric properties of a circle, the following relations are obtained.

$$s = a\phi \tag{1}$$

$$x = a \sin \phi \tag{2}$$

$$y = L - a \cos \phi \tag{3}$$

$$\psi = \phi \tag{4}$$

The value of L is found by noting $\int_s yc\, ds = 0$, giving

$$L = \frac{a \sin \Phi}{\Phi} \tag{5}$$

$$I_{xx} = \int_s x^2 c\, ds = a^3 c \int_{-\Phi}^{\Phi} \sin^2\phi\, d\phi$$

$$= a^3 c(\Phi - \sin \Phi \cos \Phi) \tag{6}$$

The next step is to determine the shear center C, $(a_x, a_y)$.

From symmetry, $a_x = 0$. It can be shown[4] that

$$a_y = L - \frac{1}{I_{xx}} \int_s x \omega_B c \, ds$$

where

$$\omega_B(s) = a^2 \phi$$

= twice the area swept by the radius moving along the section starting at $s = 0$

Therefore,

$$a_y = L - \frac{1}{I_{xx}} \int_{-\Phi}^{\Phi} a^4 c \phi \sin \phi \, d\phi$$

$$= \frac{a \sin \Phi}{\Phi} - \frac{2a(\sin \Phi - \Phi \cos \Phi)}{\Phi - \sin \Phi \cos \Phi}$$

$$= \frac{-a(\Phi \sin \Phi + \sin^2 \Phi \cos \Phi + 2\Phi^2 \cos \Phi)}{(\Phi - \sin \Phi \cos \Phi)} \qquad (7)$$

From (III. 7), the expressions for $h(s)$ and $n(s)$ are determined.

$$h(s) = (x - a_x) \sin \psi - (y - a_y) \cos \psi$$

$$= a - \frac{2a(\sin \Phi - \Phi \cos \Phi)}{(\Phi - \sin \Phi \cos \Phi)} \cos \phi \qquad (8)$$

and

$$n(s) = (x - a_x) \cos \psi + (y - a_y) \sin \psi$$

$$= \frac{2a(\sin \Phi - \Phi \cos \Phi)}{(\Phi - \sin \Phi \cos \Phi)} \sin \phi \qquad (9)$$

$$\omega(s) = \int_0^s h \, ds$$

$$= a^2 \left[ \phi - \frac{2(\sin \Phi - \Phi \cos \Phi)}{(\Phi - \sin \Phi \cos \Phi)} \sin \phi \right] \qquad (10)$$

With the expressions for $h(s)$, $n(s)$ and $\omega(s)$ given, all the remaining sectional properties can be calculated.

$$I_p = \int_s (h^2 + n^2)c \, ds$$

$$= 2a^3c \left[ \Phi + \frac{4\Phi(\sin\Phi - \Phi\cos\Phi)^2}{(\Phi - \sin\Phi\cos\Phi)^2} - \frac{4\sin\Phi(\sin\Phi - \Phi\cos\Phi)}{\Phi - \sin\Phi\cos\Phi} \right] \quad (11)$$

$$I_{\omega\omega} = \int_s \omega^2 c \, ds$$

$$= \frac{2}{3} a^5 c \left[ \Phi^3 - \frac{6(\sin\Phi - \Phi\cos\Phi)^2}{\Phi - \sin\Phi\cos\Phi} \right] \quad (12)$$

$$I_{hh} = \int_s h^2 c \, ds$$

$$= 2a^3c \left[ \Phi + \frac{2\Phi(\sin\Phi - \Phi\cos\Phi)^2}{(\Phi - \sin\Phi\cos\Phi)^2} - \frac{4\sin\Phi(\sin\Phi - \Phi\cos\Phi)}{(\Phi - \sin\Phi\cos\Phi)} + \frac{\sin 2\Phi(\sin\Phi - \Phi\cos\Phi)^2}{\Phi - \sin\Phi\cos\Phi} \right] \quad (13)$$

$$I_{hc} = \int_s h\cos\psi \, c \, ds$$

$$= 2a^2c \left[ \sin\Phi - \frac{(\sin\Phi - \Phi\cos\Phi)(\Phi + \sin\Phi\cos\Phi)}{(\Phi - \sin\Phi\cos\Phi)} \right] \quad (14)$$

$$I_{cc} = \int_s \cos^2\psi \, c \, ds$$

$$= ac(\Phi + \sin\Phi\cos\Phi) \quad (15)$$

# SUMMARY OF SYMBOLS

Most symbols used are defined. The following list is a summary of those appearing more frequently in the thesis.

$A$ = Area of the cross section

$E$ = Modulus of elasticity

$G$ = Shear modulus

$a_x, a_y$ = Coordinates of the shear center $C$

$c$ = Wall thickness of the beam

$\ell$ = Length of the beam

$r$ = Radius of gyration in the $X$ direction

$t$ = Time

$x, y, z$ = Cartesian coordinates along the principle directions of the cross section and along the axis of the beam

$\nu$ = Poisson's ratio (taken to be 0.33 in all calculations)

$\theta$ = Rotation of the section about the shear center

$\xi$ = Displacement of the shear center in the $X$ direction

$\eta$ = Displacement of the shear center in the $Y$ direction

$\rho$ = Density

$\lambda$ = Frequency

$O(\mu^2)$ = Of the order of $\mu^2$